ION-SPECIFIC AND WATER-MEDIATED EFFECTS ON PROTEIN PHYSICAL STABILITY

A Thesis
Presented to
The Academic Faculty

by

Jonathan Rubin

In Partial Fulfillment
of the Requirements for the Degree
Doctor of Philosophy in the
School of Chemical and Biomolecular Engineering

Georgia Institute of Technology
May 2013

ION-SPECIFIC AND WATER-MEDIATED EFFECTS ON PROTEIN PHYSICAL STABILITY

Approved by:

Dr. Andreas S. Bommarius, Advisor
School of Chemical and Biomolecular Engineering
Georgia Institute of Technology

Dr. Sven H. Behrens, Advisor
School of Chemical and Biomolecular Engineering
Georgia Institute of Technology

Dr. Yury O. Chernoff, Advisor
School of Biology
Georgia Institute of Technology

Dr. Victor Breedveld
School of Chemical and Biomolecular Engineering
Georgia Institute of Technology

Dr. Nicholas V. Hud
School of Chemistry and Biochemistry
Georgia Institute of Technology

Date Approved: February 22, 2013

To Ema, and Abba,
Gabe and Ben.

Long live the Rubins!

ACKNOWLEDGEMENTS

I'd like to begin by thanking the three individuals who've had the most profound impact on my academic career: Dr. Gabriel Rubin, Dr. Mélanie Hall, and Peter Ziemendorf. I often struggled to articulate how they helped me, but I recognized their influence made me better in some intangible way. Robert Prisig's notion of *Quality* put it best.[1] These three have *Quality* and imparted it to me. As Prisig explains, *Quality* or *areté* [in Greek] means excellence or virtue in all aspects of life. It "implies a respect for the wholeness or oneness of life" and can be seen in the *Quality* of one's work. I am grateful to Peter, Gabe, and Mélanie for imparting their *Quality* in academics, research, and character to me, without which I would not have succeed as I have.

My eldest brother, Gabe, has always been the Rubin family's gold standard. From his academic success at MIT, to his sardonic humor, to his light-hearted and beautiful family (Ariel, Shai, and Talya), Gabe has always been a 'sibling upon a hill.' His *excellence* in all aspects of his life (with exception to anything requiring physical abilities, i.e. basketball or workmanship) has inspired me to do better, reach higher, and try to keep up.

Peter, my dear friend from McGill University, exudes *Quality.* I entered McGill a lazy whelp, and left an efficient, accomplished, top-flight engineer mainly through his influence. Peter's exceptional work ethic taught me to excel though meticulous

---

[1] Prisig, Robert M., 1974. *Zen and the Art of Motorcycle Maintenance*. New York, NY, Bantam New Age/William Morrow and Company Inc.,.

workmanship and a deeper understanding of engineering principles. He truly embodies *excellence* in work and character.

Cette bonne vieille Mélanie is easily the most efficient person I have ever met. Not a minute of the day was wasted or unaccounted for. Mélanie has "a much higher idea of efficiency, an efficiency which exists not in one department of life but in life itself" (Prisig 1974). Mélanie taught me to be an effective, skeptical researcher; a swift distance runner; and a boisterous, yet courteous partier. Thank you.

Next I'd like to thank my trio of advisors: Andy Bommarius, Sven Behrens, and Yury Chernoff. Andy was always in my corner. He was optimistic when things were going wrong and questioning when progress was too rapid. Andy was always there to offer expert advice when I got stuck or sound criticism when I overlooked details. He gave me free rein to discover and reigned me in when I wandered too far. Andy's buoyant, enthusiastic personality made him an agreeable and highly-entertaining advisor that I'm very thankful to have studied under. Sven is the consummate advisor. His immense knowledge, adept guidance, assiduousness, and excellence in research and writing are nicely paired with an easy-going demeanor and a genuine desire to help his students excel. I am very grateful to have adopted such a wonderful advisor. I thank Yury for helping with the biological aspects of my work. Yury's command of every piece of literature on prions astounded me. His expertise and ability to design logical and definitive experiments time and again got me unstuck when I hit dead-ends. I am grateful to my three advisors for giving breadth that few chemical engineers have.

I thank my committee members Dr. Victor Breedveld and Dr. Nicholas Hud for their valuable feedback during the course of my doctorate. Specifically, I thank Dr.

Breedveld for always asking tough, probing questions that really tested my understanding, and Dr. Hud for discussing the nature of Hofmeister effects with me and his indispensable assistance interpreting CD data.

I extend thanks to everyone in the Bommarius, Behrens, and Chernoff research group [past and present] who have helped me along the way. Jonathan T. Park for struggling though everything with me: late nights, advisors, multiple desk relocations, fantasy basketball injuries, student center food, SOs, confounding research, and Travian alliances. Jon, thanks for being an excellent friend I could always count on, I can't imagine what graduate school would've been like without you. Ryan Clairmont for cooking tips, mental stimulation, analytic advice, immensely fruitful discussions, and help directing my writing. I thank Michael Abrahamson for being the life of the Bommarius party, providing in-depth investment analysis, and always being cheerful and agreeable. Katy Bruce, my yeast expert, for assistance with all things biology. Katy, Gary Newnam, and Denis Kiktev all were of great help when Dr. Chernoff would ask me to do something biological which I had no idea how to do. I thank other group members who made graduate school a pleasure: Yanto Yanto, Michael Rood, Yuzhi Kang, Thomas Rogers, Janna Blum, Sam Au, Hongzhi Wang, Joohyung Lee, Abiola Shitta, and Russell Vegh.

I'd also like to thank my closest friends who may be unaware, but helped me through grad school by distracting me, giving me perspective, and stimulating the right-side of my brain: Justin Vaughn, Peter Winter, Jake Smith, Meghan Claiborne, Laura Mislan, Erin Redmond, Brendan McLaughlin, Steph Didas, Asher Levinthal, Ismael Gomez, Max Margolius, Dan Noga, Special K, and Matt Kollman. Thank you all!

Finally, I'd like to thank my *mishpacha* for their unwavering support and love during my academic career. I could not have been blessed with more caring, amusing, wiser, generous, and wonderful parents. Without their emphasis on education and strong work ethic I would not have my PhD today. Thank you *Ema* and *Abba*! My older brothers Gabe and Ben and my sisters-in-law Ariel and Allison thank you for your continual support and regular interrogations regarding what actually goes on in Atlanta. Ben, thank you for handling all family events for Gabe and me, engaging me in pseudo-scientific discourse, and being the most passionate and compassionate Rubin of all. Only recently did I realize that you're an amazing role model - overflowing with heart, humor, and professionalism. I wish you, Allison, and Maya only the best. For Shai: you should like this thesis better than your *Abba*'s (see appendix D).

TABLE OF CONTENTS

LIST OF TABLES

Page

LIST OF FIGURES

Page

SUMMARY

Protein aggregation and physical stability are perpetual concerns in medicine and industry. Misfolded protein can form ordered protein aggregates, amyloids, which are associated with a host of neurodegenerative diseases in mammals and control heritable traits in fungi and yeast. Industrially, amorphous aggregates reduce the efficacy of protein-based therapeutics and activity of enzymes during production and storage. This work studies ion-specific and solvent-based effects on protein physical stability. We show that ion-specificity significantly affects amyloid formation kinetics, aggregate morphology, thermostability, frangibility, and, most intriguingly, prion infectivity *in vivo*. Forming amyloid in chaotropic or kosmotropic solutions generates predominately weak or strong prion variants, respectively. Ion-specific effects also influenced amorphous aggregation of model proteins and antibodies. To quantify protein – protein stability/affinity, we developed a rapid and reliable diffusion-based technique. Our technique was able to resolve relative differences in colloidal stability between various saline and saccharide solutions. In all, this dissertation expands our understanding of ion-specific and water-mediated interactions with prion proteins and protein dispersions.

CHAPTER 1

INTRODUCTION

This dissertation studies ion-specificity and water-mediated effects on protein physical stability in the contexts of prions, therapeutic proteins, and a biofuel producing enzyme. The main goal of this thesis is to further understanding and characterize ion-specific (Hofmeister) effects on prion nucleation and therapeutic protein formulations.

1.1 Protein Function and Folding

Proteins are one of the four major classes of biomacromolecules essential for life. They function as catalysts, transporters, structural stabilizers, hormones, signaling molecules, storage units, and pathogen identifiers/neutralizers.[1] In addition to being present in every living system, proteins are widely used in industry because of their exceptional specificity and extensive range of chemistries. Protein catalysts, known as enzymes, are a $2.5+ billion industry[2] and are used in detergents, wine and beer making, baking, biofuel production, cosmetics, personal care, and the pulp and paper industry, among many other applications (for review on industrial enzymes see Kirk *et al.* (2002) or for a more extensive read on biocatalysts see textbook by Bommarius and Riebel-Bommarius (2004)).[3, 4] Therapeutic proteins, namely antibodies, represent a $52+ billion market[5] and treat a wide variety of cancers, autoimmune diseases, and inflammatory disorders.[6, 7] All proteins, no matter their function, require proper folding and maintenance of their native folding state to be efficacious.

Proteins are amino acid polymers, synthesized in a cell's ribosome using a DNA blueprint.[1] As the newly minted proteins exit the ribosome, they are disordered or "unfolded." These polymers have high free energy because all amino acid residues, be they hydro-phobic or –philic, charged or neutral, are solvent exposed. The nascent peptide chains subsequently undergo a series of rapid conformational changes to 'hide' hydrophobic residues, reduce their solvent exposed area, and access the most thermodynamically favorable conformation, known as the native state.[8] This process takes tens of milliseconds to a few seconds to complete, depending on the size of the molecule (for a more detailed discussion on protein folding see chapter 6 of Brandon and Tooze (1999)).[8, 9] Only in the native state are proteins functional and active.

Despite being the most thermodynamically favorable conformation, the native state is only marginally stable.[10, 11] Small perturbations during or after folding can degrade or deactivate proteins chemically[12] or physically[10, 11, 13] (for reviews see Cleland *et al.*[12] or Chi *et al.*[13]). Chemical degradation of proteins may occur by deamidation [of asparagines or glutamine residues], oxidation [of methionine, histidine, cysteine, tyrosine, or tryptophan residues], di-sulfide bond scrambling, hydrolysis, proteolysis, or fragmentation.[14, 15] Physical instability occurs *via* self-association, aggregation, and/or denaturation.[6, 12, 13, 16] This thesis will focus entirely on protein physical stability.

1.2 Protein Aggregation and Physical Stability

Two types of protein aggregates can form: (i) disordered, amorphous aggregates or (ii) ordered, fibrillar aggregates, known as amyloids.[17] Figure 1.1 depicts a simplified sequence of protein folding and aggregation.

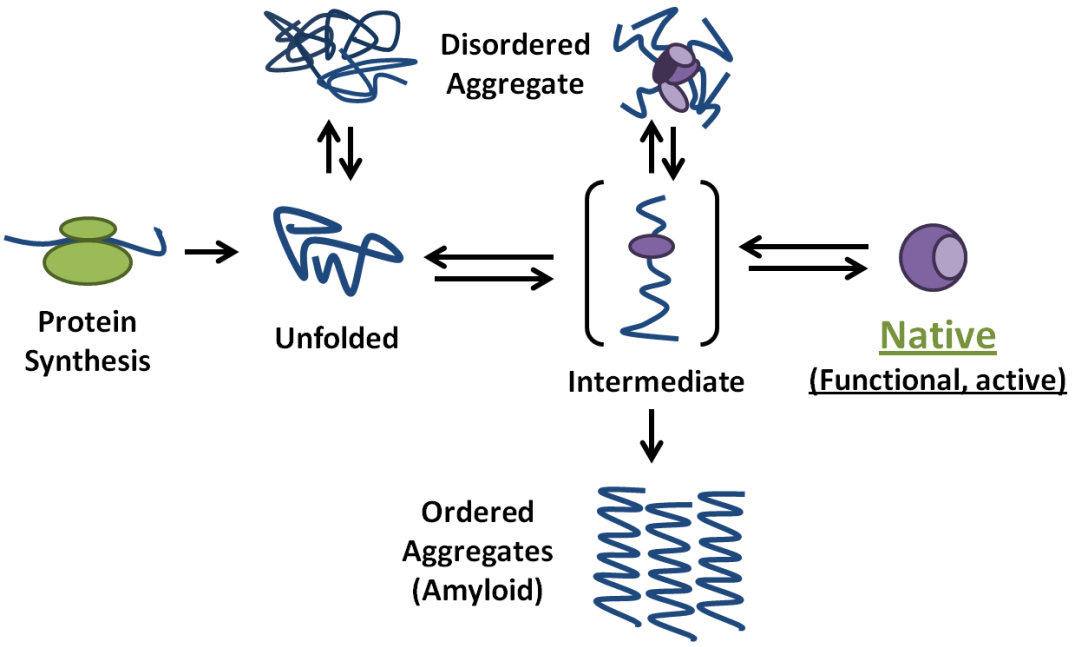

Figure 1.1: Scheme of protein folding and aggregation pathways

1.2.1 Amorphous Aggregation

Native or denatured proteins may form amorphous aggregates. Aggregates made of native proteins form when proteins are either salted-out, isoelectrically precipitated, self-associate, or are over-produced *in vivo*.[13, 18] Native aggregation is generally a reversible phenomenon and is often induced intentionally as part of a purification procedure (i.e. ammonium sulfate precipitation). Formation of amorphous aggregates from denatured proteins, in contrast, is almost always and unwelcome occurrence. These aggregates form when proteins denature due to some stress (to be discussed later this chapter) and previously 'hidden' hydrophobic residues become solvent exposed. A denatured protein may remain monomeric if stabilized by an appropriate concentration of surfactants, reducing agents, or strong denaturants.[19] However, in the absence of a

stabilizer, hydrophobic patches associate inter-molecularly with one another forming globular, amorphous aggregates.[20] Although hydrophobic interactions are not covalent, such aggregation and denaturation is often irreversible.[13]

This type of aggregation commonly afflicts biopharmaceutical production. Irreversible aggregation is a familiar and adverse occurrence during fermentation, purification, formulation, and storage. In addition to being aesthetically undesirable and reducing product yield and efficacy, aggregates can incite an immune response within a patient.[21-23] For industrial biocatalytic processes, aggregation is harmful because it destroys valuable catalyst and decreases or may even halt production.[24]

1.2.2 Ordered Aggregation

A class of proteins known as prions can misfold and aggregate to form ordered, fibrous, self-seeding structures, known as amyloids.[25] Amyloids are associated with a host of terminal diseases in mammals, such as Creutzfeldt-Jakob disease, scrapies in sheep, "mad cow" disease, Parkinson's disease, kuru, Chronic Wasting disease in deer and elk, and fatal familial insomnia, to name a few.[25-27] Prions also exist in fungi and yeast, but are not terminal; rather, they control heritable, epigenetic traits.[28] Most yeast prions are not considered to be toxic and are thought to be evolutionarily conserved because they may aid the organism under extreme or mercurial conditions.[28, 29] However, controversy exists over the physiological effect of Sup35p, the most extensively studied yeast prion and subject of Chapters 2 and 3, as to whether Sup35p is a disease or potential life-saver.[29, 30]

Amyloids form when a naturally occurring, native protein undergoes a conformational change (spontaneously or when stressed) to a β-sheet rich conformer. Through favorable sterics and hydrogen-bonding opportunities, the 'misfolded' conformers aggregate along their β-sheets. The amyloid nuclei then induce other native protein of the *same* amino acid sequence to misfold and add onto one of the aggregate's fiber ends.[31] Once aggregates get long enough they fragment, forming two fibers, each of which perpetuates aggregation and may fragment further.[28, 32, 33] *In vitro* fragmentation is likely due to a physical effect, such as shear or tensile stresses. *In vivo* fragmentation occurs when certain chaperones (heat shock proteins) attempt to un-aggregate amyloids. At normal chaperone expression levels, amyloid aggregation proceeds faster than the chaperones are able to un-aggregate; this results in the chaperones actually accelerating aggregation because they produce more chain ends. A series of works by Chernoff *et al.* elucidated this mechanism.[32-35]

1.2.3 Influencing Aggregation

Since aggregation is such a destructive phenomenon both medicinally and industrially, much research has been dedicated to understanding which factors govern and contribute to it.[12-14, 16, 18, 20, 24] The physical stability of proteins is mainly dictated by amino acid sequence and environmental conditions.[16, 17] Increasing protein stability through structure-guided mutagenesis can be highly-effective and is often necessary to optimize enzymes for specific applications; however, it is also an arduous and non-linear

process.[24, 36-38] Environmental conditions are more easily altered and can have profound effects on protein stability, as will be chronicled in the chapters to come.

1.3 Environmental Conditions and Physical Stability

Every protein is unique in its amino acid composition and, as a result, has distinct stability behavior. The extent to which a given environmental condition affects a protein is protein-specific; however, certain factors have been identified as being significant in affecting the physical stability of all proteins. These factors include, but are not limited to: solution pH, temperature, surfactants, relative humidity, oxygen content, shear or shaking, co-solutes, preservatives, salt type and concentration, and light/irradiation.[13, 18] This thesis studies in detail the effects of salt type and concentration, temperature, and co-solutes (namely, sugars). pH is often considered to be one of the most important determinants of stability[18] and is studied tangentially in this work. The optimal pH for the proteins studied in this work was known *a priori*, thus further study was not necessary. Potential future work regarding pH is discussed in the final chapter.

1.3.1 Salt Effects

Salts are present in every living system and pharmaceutical formulation. They are used as buffering, tonicity, acidifying, and stabilizing agents.[39] Salts exert both non-specific and ion-specific (Hofmeister) effects on proteins; consequently, both the salt concentration and salt type are crucial factors in protein stability/aggregation.[13, 18, 40-45]

Salt concentration controls the strength of electrostatic interactions between charged groups intra- and inter-molecularly in a non-specific manner.[13] Low salt concentrations are necessary for maintaining pH, ensuring tonicity, and stabilizing proteins. As ionic strength increases, Debye lengths decrease and charges become screened, which reduces electrostatic repulsion between proteins. How charge screening affects aggregation depends strongly on the pH of the solution, which dictates the charged state of a protein. If addition of salt tends toward neutralizing the protein surface, then unfolding is likely to occur; otherwise, stability will likely increase.[18, 46, 47] Generally, some level of salt is requite for stability, but high ionic strengths will cause denaturation and/or aggregation.

The importance of salt type was first described by Franz Hofmeister (1888). He found that hen egg white lyzosyme (HEWL) precipitated at different ionic strengths depending on which ion was present in solution. He ranked the ions according to how readily they would precipitate HEWL;[48] this ranking is now known as the Hofmeister series (for review see Zhang and Cremer[49]):[50]

$$SCN^- > I^- > ClO_4^- > NO_3^- > Br^- > Cl^- > HCO^- > F^- > SO_4^{-2} > CH_3CO_2^-$$

$$Cs^+ > Rb^+ > NH_4^+ > K^+ > Na^+ > Li^+ > Ba^+ > Ca^{+2} > Mg^{+2}$$

Hofmeister divided salts into two major groups, chaotropes and kosmotropes, according to how they interacted with protein. Chaotropes (*khaos*, Greek for chaos or disorder) are ions that decrease surface tension, increase protein solubility, and cause denaturation.[49, 50] Chaotropic ions are those to the left of, and including, chloride and potassium. Extreme chaotropic agents include urea and guanidine hydrochloride, which

are used to break up inclusion bodies and cleanse chromatography columns. Ions to the right of chloride and potassium are known as kosmotropes (*kosmos* being Greek for order). These ions increase surface tension, decrease protein solubility, and stabilize the native state.[49, 50] Many osmolytes, such as sugars and amino acids, act as kosmotropic agents.[51] Hofmeister's finding that kosmotropes (namely sulfates) caused native precipitation was a major discovery in biochemistry. Sulfate precipitation was one of the first method of protein purification[52] and is still commonly used because it is one of the most economical and easiest purification techniques.[53, 54]

The origin of ion-specific or Hofmeister effects is not fully understood, but the hydration state of ions is thought to play a major role. Ions can be thought of as spheres with a point charge at the center. As the sphere gets larger (as you go down the period table e.g. F^- to Cl^- to I^-) the distance between the point charge and water gets larger. At some distance, water has a stronger interaction with itself than with the ion; this distance marks the difference between chaotropes and kosmotropes (~1.78 Å and ~1.06 Å ionic radii for monovalent anions and cations, respectively).[55] The larger, poorly-hydrated ions are chaotropes; whereas the smaller, well-hydrated ions are kosmotropes.[50, 55] As a result of differences in water affinity, chaotropes will accumulate at hydrophobic interfaces, such as an air-water or protein-water interface; kosmotropes will preferentially interact with each other and the bulk water, rather than those interfaces.[41, 50, 56-58]

Arakawa and Timasheff[51, 59] proposed the preferential interaction model to explain why kosmotropes [and osmolytes, such as sugars,] stabilize proteins. The model states that exclusion of kosmotropes from the protein-water interface creates a layer of pure water around the protein. This *exclusion volume* is thermodynamically unfavorable

because the solvent prefers to interact with itself rather than the protein, elevating the interfacial tension. Thus, the system works to minimize the high energy interfacial area. The added interfacial tension makes protein expansion (i.e. denaturation) more energy intensive; as a result, protein is forced into its most compact conformation: the native state.[49, 51, 55, 60] In concentrated salt solutions, the driving force to minimize interfacial area is large enough to cause native aggregation and/or amorphous precipitation through the coalescence of excluded volumes.[59]

The molecular mechanism of why chaotropes denature proteins is still somewhat murky; however, a few theories attempt to rationalize it.[55, 60, 61] As chaotropes have lower affinity for water, they tend to accumulate at hydrophobic surfaces, such as that of a protein.[55] As the concentration of chaotrope in solution increases, more ions remain in the bulk solution, making the bulk overall more amenable to hydrophobic residues because of potentially favorable hydrogen-bonding and van der Waals interactions. Kita *et al.*[60] suggest that denaturation then occurs because protein – solvent interactions become more thermodynamically favorable than existing *intra*-molecular interactions. In such a case, proteins then maximize their solvent exposed area and become denatured. Muller[61] adds that protein solubility is increased in chaotropic solutions because of the favorable solvent – protein interactions.

Denaturation in chaotropes is highly concentration dependent. At low concentrations (<300 mM), chaotropes are actually seen to stabilize protein; at intermediate concentrations, they denature proteins, but the driving force for amorphous aggregation is greater than the protein – solvent interactions; at high concentrations (8 M urea or 6 M guanidine HCl), proteins denature and remain monomeric.[62]

1.3.2 Temperature

Proteins operate in a narrow temperature window and slight perturbations can derail an industrial process or cause a therapeutic protein is irreversibly aggregate. Enzymes are most active at elevated temperatures; hence industrial processes try to maximize the operating temperature without thermally denaturing their catalyst.[24, 63-65] Such considerations will be discussed in a case study on a biofuels producing enzyme, Cel7A, in chapter 7. For further reading on temperature considerations and biocatalysts see reviews by Polizzi *et al.*[24] and Bommarius and Broering.[64] For therapeutic proteins, high thermal tolerance is advantageous because processing, transportation, and storage are more economical and straight-froward when performed at ambient temperature, as opposed to under refrigerated conditions.[39]

Temperature is often considered to be the most important factor contributing to protein stability, or lack thereof.[13, 18, 64] The thermodynamic stability of the native state is typically characterized by the free energy of unfolding ΔG_{unfold}, as shown in Figure 1.2. As temperature increases, a protein will expand and ultimately unfold as it reaches its melting temperature T_m at $\Delta G_{unfold} = 0$. By convention, the melting temperature is defined as the temperature at which the protein is half way through the unfolding process.[18, 24] Irreversible aggregation often accompanies unfolding at high temperatures.[13]

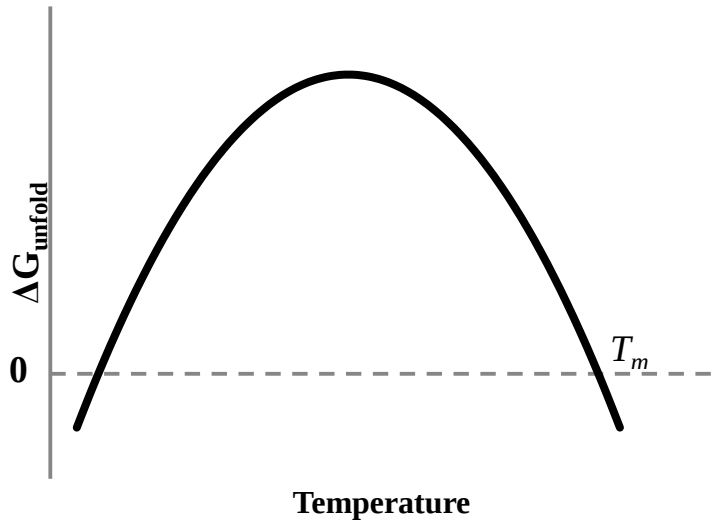

Figure 1.2: Relation between temperature and protein thermodynamic stability

Proteins can also unfold when temperature is decreased. Aggregates can and do form due to cold denaturation; however, it is not uncommon for such denaturation and aggregation to be reversible because the hydrophobic interactions that cohere aggregates are dulled at lower temperatures.[18] Rees and Robertson give a more detailed account of the molecular origins of thermal denaturation.[66]

1.3.3 Sugars

Sugars and other osmolytes are often used to stabilize proteins in solution or during lyophilization.[6, 67, 68] The mechanism of sugar stabilization in solution is thought to derive from the preferential hydration of proteins and exclusion of sugar from the protein – water interface; this is known as the preferential interaction model and is the same as was discussed earlier in the context of kosmotropic ions.[51, 59, 67, 69] The exclusion of sugars

causes elevated interfacial tension and, by Le Chatelier's principle, the system will minimize the unfavorable water – protein interface. Protein is then forced into its most compact conformation, which is the native state.[51]

Sugars are often added to protein solution to prevent cold denaturation during lyophilization. As temperature rapidly decreases, sugars become vitrified and create a glassy matrix. Proteins are evenly dispersed throughout this matrix and are stabilized because their conformational mobility is restricted.[70-73] Sucrose, glucose, and trehalose are the most frequently used sugars to stabilize protein during spray drying and lyophilization.[73]

Sugars are also used to stabilize proteins *in vivo* (for review see Davis-Searles *et al.* [74]). The most marked effects are in organisms that may undergo anhydrobiotic stress (Greek for *life without water*), such as brine shrimp, fungal spores, baker's yeast, tardigrades, and certain desert plants.[75-77] During anhydrobiosis, these organisms are in a cryptobiotic state (Greek for *hidden life*), which is a kind of suspended animation, due to extreme dehydration. Under such desiccating conditions, these organisms accumulate large stores of disaccharides, such as sucrose or trehalose. The disaccharides become vitrified and stabilize the organisms' cell membranes and proteins through hydrogen-bonding to polar residues and restricting mobility.[74-76]

1.4 Proteins in this Study

This thesis will study the physical stability of a yeast prion protein (Sup35p), two model proteins (lysozyme and bovine serum albumin), a pair of human immunoglobulin G1 antibodies (hIgG1), and a cellulase (Cel7A). Sup35p is a translation termination sub-unit

in yeast, capable of forming ordered aggregates. This yeast prion is often used as a proxy for mammalian prions because it is easier to express and safer to handle. Lysozyme is 14.3 kDa muramidase that hydrolyzes bacterial cell walls. It is often used as a model protein because it is relatively inexpensive, available at high purity, and can be approximated well as a sphere. Bovine serum albumin (BSA) is another model protein. It is a 66.8 kDa protein that is used as a nutrient, enzyme stabilizer, and as non-specific binding molecule.[43] The two hIgG1s studied are 145 kDa antibodies and only differ in that one is glycosylated and the other is not. The pair was provided by Bayer Pharma and their function is unknown.[44] Cel7A is a 52 kDa enzyme that assists in the hydrolysis of cellulose en route to making glucose for biofuels applications.[78]

1.5 Map of Dissertation

This thesis is organized in the following manner. Chapters 2 and 3 study salt-effects on Sup35p. Chapter 2 looks at salt-specific effects on Sup35NM (a truncated version of Sup35p) nucleation kinetics *in vitro* and how infectious those amyloids are *in vivo*. Chapter 3 investigates aggregation kinetics of Sup35NM from three closely related *Saccharomyces* species in different saline conditions. Cross-species seeding experiments are then studied with and without the influence of salts. Chapters 4 through 6 study the effect of anions and sugars on protein – protein interactions and if they can be quantified through diffusivity measurements. Chapter 4 is a proof-of-concept paper, which relates fast diffusivity measurements in low salt conditions to long-term, high salt aggregation experiments using two model proteins. Chapter 5 tests and expands on the technique outlined in Chapter 4 using a pair of hIgG1 antibodies. This chapter investigates the

effects of temperature, ion-specificity, and glycosylation on the stable protein – protein interactions and aggregation. Chapter 6 examines whether protein diffusivity correlates well to aggregation and protein melting temperature in saccharide solutions. The aglycosylated hIgG1 used in Chapter 5 was the focus of this study. Chapter 7 investigates the thermostability of Cel7A from *Trichoderma reesei* and its two domains. Chapter 8 is the final chapter which summarizes the previous seven chapters and offers suggestions for further research.

1.4 References

1. Madigan, M. T.; Martinko, J. M., *Brock Biology of Microorganisms*. 11th ed.; Pearson Education, Inc.: Upper Saddle River, NJ, 2006.

2. Demain, A. L.; Vaishnav, P., Production of recombinant proteins by microbes and higher organisms, *Biotechnology Advances* **2009,** *27*, 297-306.

3. Kirk, O.; Borchert, T. V.; Fuglsang, C. C., Industrial enzyme applications, *Current Opinion in Biotechnology* **2002,** *13*, 345-51.

4. Bommarius, A. S.; Riebel-Bommarius, B. R., *Biocatalysis: Fundementals and Applications*. Wiley Vch: New York, 2004.

5. Mullard, A., Can next-generation antibodies offset biosimilar competition?, *Nature Reviews Drug Discovery* **2012,** *11*, 426-28.

6. Wang, W.; Singh, S.; Zeng, D. L.; King, K.; Nema, S., Antibody structure, instability, and formulation, *Journal of Pharmaceutical Sciences* **2007,** *96*, 1-26.

7. Carter, P. J., Potent antibody therapeutics by design, *Nature Reviews Immunology* **2006,** *6*, 343-57.

8. Brandon, C.; Tooze, J., *Introduction to Protein Structure*. 2nd ed.; Garland Publishing, Inc.: New York, NY, 1999.

9. Cabrita, L. D.; Dobson, C. M.; Christodoulou, J., Protein folding on the ribosome, *Current Opinions Structructral Biology* **2010,** *20*, 33-45.

10. Manning, M. C.; Chou, D. K.; Murphy, B. M.; Payne, R. W.; Katayama, D. S., Stability of protein pharmaceuticals: An update, *Pharmaceutical Research* **2010,** *27*, 544-75.

11. Brange, J., Physical stability of proteins. In *Pharmaceutical Formulation and Development of Peptides and Proteins*, Frokjaer, S.; Hovgaards, L., Eds. Taylor and Francis: London, UK, 2000; pp 89-112.

12. Cleland, J. L.; Powell, M. F.; Shire, S. J., The development of stable protein formulations - a close look at protein aggregation, deamidation, and oxidation, *Critical Reviews in Therapeutic Drug Carrier Systems* **1993,** *10*, 307-77.

13. Chi, E. Y.; Krishnan, S.; Randolph, T. W.; Carpenter, J. F., Physical stability of proteins in aqueous solution: Mechanism and driving forces in nonnative protein aggregation, *Pharmaceutical Research* **2003,** *20*, 1325-36.

14. Li, S. H.; Schoneich, C.; Borchardt, R. T., Chemical-instability of protein pharmaceuticals - mechanisms of oxidation and strategies for stabilization, *Biotechnology and Bioengineering* **1995,** *48*, 490-500.

15. Ganan-Jimenez, A.; Brake, B., Q5C -stability testing of biotechnological / biological products. ICH, Ed. 1995.

16. Wei, W., Instability, stabilization, and formulation of liquid protein pharmaceuticals, *International Journal of Pharmaceutics* **1999,** *185*, 129-88.

17. Stefani, M.; Dobson, C. M., Protein aggregation and aggregate toxicity: New insights into protein folding, misfolding diseases and biological evolution, *Journal of Molecular Medicine-Jmm* **2003,** *81*, 678-99.

18. Wang, W.; Nema, S.; Teagarden, D., Protein aggregation-pathways and influencing factors, *International Journal of Pharmaceutics* **2010,** *390*, 89-99.

19. Randolph, T. W.; Jones, L. S., Surfactant–protein interactions. In *Rational design of stable protein formulations, theory and practice*, Carpenter, J. F.; Mannings, M. C., Eds. Kluwer Academic/Plenum Publishers: New York, NY, 2002; p 198.

20. Fink, A. L., Protein aggregation: Folding aggregates, inclusion bodies and amyloid, *Folding & Design* **1998,** *3*, R9-R23.

21. Hermeling, S.; Crommelin, D. J. A.; Schellekens, H.; Jiskoot, W., Structure-immunogenicity relationships of therapeutic proteins, *Pharmaceutical Research* **2004,** *21*, 897-903.

22. Rosenberg, A. S., Effects of protein aggregates: An immunologic perspective, *Aaps Journal* **2006,** *8*, E501-E07.

23. Wang, W.; Singh, S. K.; Li, N.; Toler, M. R.; King, K. R.; Nema, S., Immunogenicity of protein aggregates-concerns and realities, *International Journal of Pharmaceutics* **2012,** *431*, 1-11.

24. Polizzi, K. M.; Bommarius, A. S.; Broering, J. M.; Chaparro-Riggers, J. F., Stability of biocatalysts, *Current Opinion in Chemical Biology* **2007,** *11*, 220-25.

25. Prusiner, S. B., Prions, *Proceedings of the National Academy of Sciences of the United States of America* **1998,** *95*, 13363-83.

26. Eisenberg, D.; Jucker, M., The amyloid state of proteins in human diseases, *Cell* **2012,** *148*, 1188-203.

27. Jackson, G. S.; Clarke, A. R., Mammalian prion proteins, *Current Opinions Structructral Biology* **2000,** *10*, 69-74.

28. Liebman, S. W.; Chernoff, Y. O., Prions in yeast, *Genetics* **2012,** *191*, 1041-72.

29. Halfmann, R.; Jarosz, D. F.; Jones, S. K.; Chang, A.; Lancaster, A. K.; Lindquist, S., Prions are a common mechanism for phenotypic inheritance in wild yeasts, *Nature* **2012,** *482*, 363-8.

30. McGlinchey, R. P.; Kryndushkin, D.; Wickner, R. B., Suicidal [psi+] is a lethal yeast prion, *Proceedings of the National Academy of Science of the United States of America* **2011,** *108*, 5337-41.

31. Shorter, J.; Lindquist, S., Prions as adaptive conduits of memory and inheritance, *Nature Reviews Genetics* **2005,** *6*, 435-50.

32. Chernoff, Y. O.; Lindquist, S. L.; Ono, B.; Inge-Vechtomov, S. G.; Liebman, S. W., Role of the chaperone protein hsp104 in propagation of the yeast prion-like factor [psi+], *Science* **1995,** *268*, 880-4.

33. Chernoff, Y. O.; Newnam, G. P.; Kumar, J.; Allen, K.; Zink, A. D., Evidence for a protein mutator in yeast: Role of the hsp70-related chaperone ssb in formation, stability, and toxicity of the [psi] prion, *Molecular Cell Biology* **1999,** *19*, 8103-12.

34. Newnam, G. P.; Birchmore, J. L.; Chernoff, Y. O., Destabilization and recovery of a yeast prion after mild heat shock, *Journal of Molecular Biology* **2011,** *408*, 432-48.

35. Newnam, G. P.; Wegrzyn, R. D.; Lindquist, S. L.; Chernoff, Y. O., Antagonistic interactions between yeast chaperones hsp104 and hsp70 in prion curing, *Molocular Cell Biology* **1999,** *19*, 1325-33.

36. Vazquez-Figueroa, E.; Chaparro-Riggers, J.; Bommarius, A. S., Development of a thermostable glucose dehydrogenase by a structure-guided consensus concept, *Chembiochem* **2007,** *8*, 2295-301.

37. Tokuriki, N.; Tawfik, D. S., Stability effects of mutations and protein evolvability, *Current Opinion in Structural Biology* **2009,** *19*, 596-604.

38. Bommarius, A. S.; Blum, J. K.; Abrahamson, M. J., Status of protein engineering for biocatalysts: How to design an industrially useful biocatalyst, *Current Opinion in Chemical Biology* **2011,** *15*, 194-200.

39. Allen, L. V.; Popovich, N. G.; Ansel, H. C., *Ansel's pharmaceutical dosage forms and drug delivery systems*. 9th ed.; Lippincott, Williams & Wilkins: Philadelphia, Pennsylvania, 2010.

40. Broering, J. M.; Bommarius, A. S., Evaluation of hofmeister effects on the kinetic stability of proteins, *Journal of Physical Chemistry B* **2005,** *109*, 20612-19.

41. Pegram, L. M.; Wendorff, T.; Erdmann, R.; Shkel, I.; Bellissimo, D.; Felitsky, D. J.; Record, M. T., Why hofmeister effects of many salts favor protein folding but not DNA helix formation, *Proceedings of the National Academy of Sciences of the United States of America* **2010,** *107*, 7716-21.

42. Yeh, V.; Broering, J. M.; Romanyuk, A.; Chen, B. X.; Chernoff, Y. O.; Bommarius, A. S., The hofmeister effect on amyloid formation using yeast prion protein, *Protein Science* **2010,** *19*, 47-56.

43. Rubin, J.; San Miguel, A.; Bommarius, A. S.; Behrens, S. H., Correlating aggregation kinetics and stationary diffusion in protein-sodium salt systems observed with dynamic light scattering, *Journal of Physical Chemistry B* **2010,** *114*, 4383-87.

44. Rubin, J.; Linden, L.; Coco, W. M.; Bommarius, A. S.; Behrens, S. H., Salt-induced aggregation of a monoclonal human immunoglobulin g1, *Journal of Pharmaceutical Science* **2013,** *2*, 377-86.

45. Yamasaki, M.; Yano, H.; Aoki, K., Differential scanning calorimetric studies on bovine serum-albumin .2. Effects of neutral salts and urea, *International Journal of Biological Macromolecules* **1991,** *13*, 322-28.

46. Saluja, A.; Kalonia, D. S., Nature and consequences of protein-protein interactions in high protein concentration solutions, *International Journal of Pharmaceutics* **2008,** *358*, 1-15.

47. Saluja, A.; Badkar, A. V.; Zeng, D. L.; Kalonia, D. S., Ultrasonic rheology of a monoclonal antibody (igg(2)) solution: Implications for physical stability of proteins in high concentration formulations, *Journal of Pharmaceutical Sciences* **2007,** *96*, 3181-95.

48. Hofmeister, F., On the understanding of the effects of salts, *Arch. Exp. Pathol. Pharmakol* **1888,** *24*, 247-60.

49. Zhang, Y. J.; Cremer, P. S., Interactions between macromolecules and ions: The hofmeister series, *Current Opinion in Chemical Biology* **2006,** *10*, 658-63.

50. Collins, K. D., Ions from the hofmeister series and osmolytes: Effects on proteins in solution and in the crystallization process, *Methods* **2004,** *34*, 300-11.

51. Arakawa, T.; Timasheff, S. N., The stabilization of proteins by osmolytes, *Biophysical Journal* **1985,** *47*, 411-4.

52. Dixon, M.; Webb, E. C., Enzyme fractionation by salting out. In *Advances in protein chemistry*, Acedemic Press: New York, NY, 1961; Vol. 16, p 216.

53. Abernethy, J. L., Franz hofmeister. The impact of his life and research on chemistry, *Journal of Chemical Education* **1967,** *44*, 177-80.

54. Mirica, K. A.; Lockett, M. R.; Snyder, P. W.; Shapiro, N. D.; Mack, E. T.; Nam, S.; Whitesides, G. M., Selective precipitation and purification of monovalent proteins using oligovalent ligands and ammonium sulfate, *Bioconjug Chem* **2012,** *23*, 293-9.

55. Collins, K. D., Sticky ions in biological systems, *Proceddings of the National Academy of Science of the United States of America* **1995,** *92*, 5553-7.

56. Pegram, L. M.; Record, M. T., Jr., Thermodynamic origin of hofmeister ion effects, *Journal of Physical Chemistry B* **2008,** *112*, 9428-36.

57. Cheng, J.; Hoffmann, M. R.; Colussi, A. J., Anion fractionation and reactivity at air/water:Methanol interfaces. Implications for the origin of hofmeister effects, *Journal of Physical Chemistry B* **2008,** *112*, 7157-61.

58. Gokarn, Y. R.; Fesinmeyer, R. M.; Saluja, A.; Razinkov, V.; Chase, S. F.; Laue, T. M.; Brems, D. N., Effective charge measurements reveal selective and preferential accumulation of anions, but not cations, at the protein surface in dilute salt solutions, *Protein Science* **2011,** *20*, 580-7.

59. Arakawa, T.; Timasheff, S. N., Preferential interactions of proteins with salts in concentrated solutions, *Biochemistry* **1982,** *21*, 6545-52.

60. Kita, Y.; Arakawa, T.; Lin, T. Y.; Timasheff, S. N., Contribution of the surface free energy perturbation to protein-solvent interactions, *Biochemistry* **1994,** *33*, 15178-89.

61. Muller, N., Model for the partial reversal of hydrophobic hydration by addition of a urea, *Journal of Phyical Chemistry* **1990,** *94*, 3856-59.

62. Bostrom, M.; Parsons, D. F.; Salis, A.; Ninham, B. W.; Monduzzi, M., Possible origin of the inverse and direct hofmeister series for lysozyme at low and high salt concentrations, *Langmuir* **2011,** *27*, 9504-11.

63. Aymard, C.; Belarbi, A., Kinetics of thermal deactivation of enzymes: A simple three parameters phenomenological model can describe the decay of enzyme activity, irrespectively of the mechanism, *Enzyme Microbial Technology* **2000,** *27*, 612-18.

64. Bommarius, A. S.; Broering, J. M., Established and novel tools to investigate biocatalyst stability, *Biocatalysis and Biotransformation* **2005,** *23*, 125-39.

65. Rogers, T. A.; Daniel, R. M.; Bommarius, A. S., Deactivation of tem-1 beta-lactamase investigated by isothermal batch and non-isothermal continuous enzyme membrane reactor methods, *ChemCatChem* **2009,** *1*, 131-37.

66. Rees, D. C.; Robertson, A. D., Some thermodynamic implications for the thermostability of proteins, *Protein Science* **2001,** *10*, 1187-94.

67. Chang, L. Q.; Shepherd, D.; Sun, J.; Ouellette, D.; Grant, K. L.; Tang, X. L.; Pikal, M. J., Mechanism of protein stabilization by sugars during freeze-drying and storage: Native structure preservation, specific interaction, and/or immobilization in a glassy matrix?, *Journal of Pharmaceutical Sciences* **2005,** *94*, 1427-44.

68. Cleland, J. L.; Lam, X.; Kendrick, B.; Yang, J.; Yang, T. H.; Overcashier, D.; Brooks, D.; Hsu, C.; Carpenter, J. F., A specific molar ratio of stabilizer to protein is required for storage stability of a lyophilized monoclonal antibody, *Journal of Pharmaceutical Sciences* **2001,** *90*, 310-21.

69. Kaushik, J. K.; Bhat, R., Thermal stability of proteins in aqueous polyol solutions: Role of the surface tension of water in the stabilizing effect of polyols, *Journal of Physical Chemistry B* **1998,** *102*, 7058-66.

70. Wang, B.; Tchessalov, S.; Warne, N. W.; Pikal, M. J., Impact of sucrose level on storage stability of proteins in freeze-dried solids: I. Correlation of protein-sugar interaction with native structure preservation, *Journal of Pharmaceutical Sciences* **2009,** *98*, 3131-44.

71. Allison, S. D.; Chang, B.; Randolph, T. W.; Carpenter, J. F., Hydrogen bonding between sugar and protein is responsible for inhibition of dehydration-induced protein unfolding, *Archives of Biochemistry and Biophysics* **1999,** *365*, 289-98.

72. Franks, F.; Hatley, R. H. M.; Mathias, S. F., Materials science and the production of shelf-stable biologicals, *Biopharm-the Technology & Business of Biopharmaceuticals* **1991,** *4*, 38-&.

73. Kaushik, J. K.; Bhat, R., Why is trehalose an exceptional protein stabilizer? An analysis of the thermal stability of proteins in the presence of the compatible osmolyte trehalose, *Journal of Biological Chemistry* **2003,** *278*, 26458-65.

74. Davis-Searles, P. R.; Saunders, A. J.; Erie, D. A.; Winzor, D. J.; Pielak, G. J., Interpreting the effects of small uncharged solutes on protein-folding equilibria, *Annual Review of Biophysics and Biomolecular Structure* **2001,** *30*, 271-306.

75. Crowe, J. H.; Carpenter, J. F.; Crowe, L. M., The role of vitrification in anhydrobiosis, *Annual Review of Physiology* **1998,** *60*, 73-103.

76. Crowe, J. H.; Crowe, L. M.; Chapman, D., Preservation of membranes in anhydrobiotic organisms - the role of trehalose, *Science* **1984,** *223*, 701-03.

77. Welnicz, W.; Grohme, M. A.; Kaczmarek, L.; Schill, R. O.; Frohme, M., Anhydrobiosis in tardigrades-the last decade, *Journal of Insect Physiology* **2011,** *57*, 577-83.

78. Hall, M.; Rubin, J.; Behrens, S. H.; Bommarius, A. S., The cellulose-binding domain of cellobiohydrolase cel7a from trichoderma reesei is also a thermostabilizing domain, *Journal of Biotechnol* **2011,** *155*, 370-6.

CHAPTER 2

ION-SPECIFIC EFFECTS ON PRION NUCLEATION AND STRAIN FORMATION

This chapter is adapted from a research article bearing the same title submitted for publication in March 2013. Hasan Khosravi, Kathryn Bruce, Megan Lydon, Sven Behrens, Yury Chernoff, and Andreas Bommarius contributed to this work.

2.1 Abstract

Ordered, fibrous, self-seeding aggregates of misfolded proteins known as amyloids (and their transmissible versions, prions) are associated with uniformly terminal mammalian diseases. In fungi, amyloids control phenotypic traits. Curiously, a given protein may adopt multiple distinct amyloid conformations, known as "variants" or "strains," each of which leads to a distinct disease pattern or phenotype. In mammals and fungi, the growth of amyloid fibers follows a two-step pattern of initial nucleation followed by fiber elongation. The kinetics of nucleation is thought to critically influence amyloid conformation and strain properties. In this work, we study the effect of Hofmeister ions on nucleation and strain generation by the prion-domain-containing fragment (Sup35NM) of a yeast protein Sup35p, the [PSI^+] prion determinant. We show that strongly hydrated anions (kosmotropes) initiate nucleation quickly and cause rapid fiber elongation, whereas poorly hydrated anions (chaotropes) delay nucleation and do not greatly affect the elongation rate. Amyloids formed in kosmotropes are less thermostable, shorter, and propagated [PSI^+] more effectively *in vivo* compared to amyloids formed in chaotropes. We suggest that these phenomena result from differences in the biochemistry of

Hofmeister ions: chaotropic anions adsorbs to the prion recognition domain, inhibiting sequence recognition and amyloidogenesis; whereas kosmotropic anions do not affect sequence recognition and may accelerate amyloid formation by inducing a depletion attraction between the templating aggregate surfaces and not aggregated protein. Our work shows that the ionic composition of a solution not only influences the kinetics of amyloid nucleation but also determines the amyloid strain that is preferentially formed.

2.2 Introduction

Amyloidoses are disorders marked by the deposition of fibrous protein aggregates (amyloids) within an organism.[1, 2] In mammals, these disorders include widespread, sporadic, or familial neurodegenerative diseases such as Alzheimer's and Parkinson's disease. Infectious amyloids, termed "prions", cause transmissible spongiform encephalopathies or prion diseases, which include Creutzfeldt-Jakob disease in humans and "mad cow" disease in cattle (for review see refs.[1, 3, 4]). Not all amyloidoses are pathological, however, as in the case of the mammalian melanocyte Pmel17 which is biologically beneficial [5]. In yeast and fungi, there is an ever-growing list of prions which control specific phenotypic traits and may have pathological effects [6-9]. Amyloids are also formed spontaneously in the preparations of protein- or peptide-based drugs upon storage which decreases drug efficiency and may increase immunogenicity [10].

2.2.1 How Amyloids Form

The basic scheme of amyloid formation appears to be the same for all amyloidogenic proteins, mammalian or fungal. The process typically originates with a morphological change in the protein's secondary structure, resulting in an increased proportion of β-

sheets [11]. For many, maybe most [12] proteins, such a conversion can occur *in vitro* under extreme solution conditions (high temperature and low pH), as in the cases of lysozyme, transthyretin, and insulin [13-16]. Prion proteins, however, spontaneously misfold under physiological conditions. Regardless of how the conformers were induced, the β-sheet-rich peptides aggregate to form nuclei. Solution conditions play a great role in determining the rate of nucleation and the structure of the nucleus [17-19]; however, this relationship is not yet clearly understood. After nucleation, other peptides of the *same* amino acid sequence are recruited to the aggregate in a unidirectional manner, analogous to "one-dimensional crystallization" (Figure 2.1).

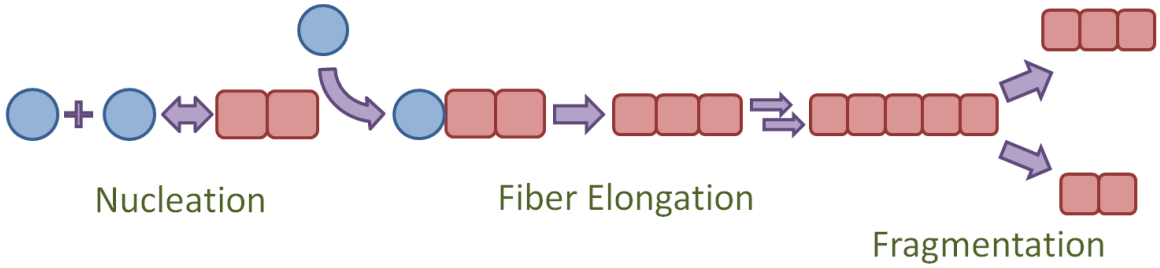

Figure 2.1: Basic scheme of amyloid nucleation and propagation

2.2.2 Sup35p

Yeast prions are often used as a model for mammalian prions because yeast prions aggregate through the same mechanism, are easier to express, are inexpensive, and, most importantly, do not pose a biohazard threat to the experimenter. The most extensively studied yeast prion is Sup35p. Sup35p, also known as eukaryotic release factor 3, is a translation terminal subunit in yeast composed of three domains (Figure 2.2):[20]

Non-polar (%)	30.9	31.5	48.6
Uncharged, polar (%)	**65**	26.2	22.7
Charged, polar (%)	4.1	**42.3**	28.7

Figure 2.2: Domains of Sup35p and their amino acid (aa) composition

The C-terminal domain is responsible for the protein's biological function; the middle (M) domain's function is unknown; the N-proximal domain is prion domain. The glutamine (glu) and aspargine (asn) rich N domain can misfold and form aggregates by aligning glu and asn residues inter-molecularly, forming a steric zipper (Figure 2.3):[6, 21] Since only the N domain is required for amyloid formation, a truncated version of Sup35p composed of just the N and M regions, known as Sup35NM, is often used for *in vitro* experimentation, as is done in this thesis. The N domain alone is difficult to express, is not very water soluble, and aggregates too rapidly to study; addition of the M domain resolves all these issues.

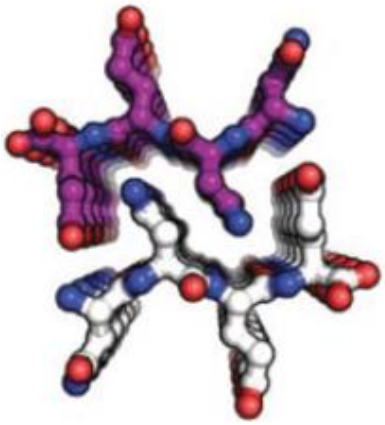

Figure 2.3: Steric zipper between β-sheets from aggregating Sup35p molecules. Image is taken from Tessier and Lindquist (2009).[22]

Sup35p is the protein determinant of the [*PSI*$^+$] trait. Cells containing the prion form of Sup35p are said to be [*PSI*$^+$]; those without the prion form are denoted [*psi*$^-$]. A nonsense mutation *ade1-14* (UGA) in the *ADE1* gene allows for a simple phenotypic test for [*PSI*$^+$].[6] If Sup35p is not aggregated ([*psi*$^-$] cells), it continues to function as a translation termination co-factor and will stop translation of the Ade1 protein prematurely [because the nonsense mutation introduced a stop codon in the middle that gene] (Fig. 2.4c). Ade1p allows for the biosynthesis of adenine; hence in media devoid of adenine (-ade media), cells cannot grow. Additionally, cells grown on non-selective YPD media will attempt to produce adenine, but the biosynthesis will not go to completion [because Ade1p is not present] and a red intermediate accumulates in the cells (Fig. 2.4a). If Sup35p is inactivated in aggregates ([*PSI*$^+$] cells), then read-through of the nonsense mutation occurs and Ade1p is properly translated (Fig. 2.4c). Cells can now grow on –ade media. On YPD media, cells can process the red intermediate that would form in [*psi*$^-$] cells, making them phenotypically white (Fig 2.4b).[6, 21]

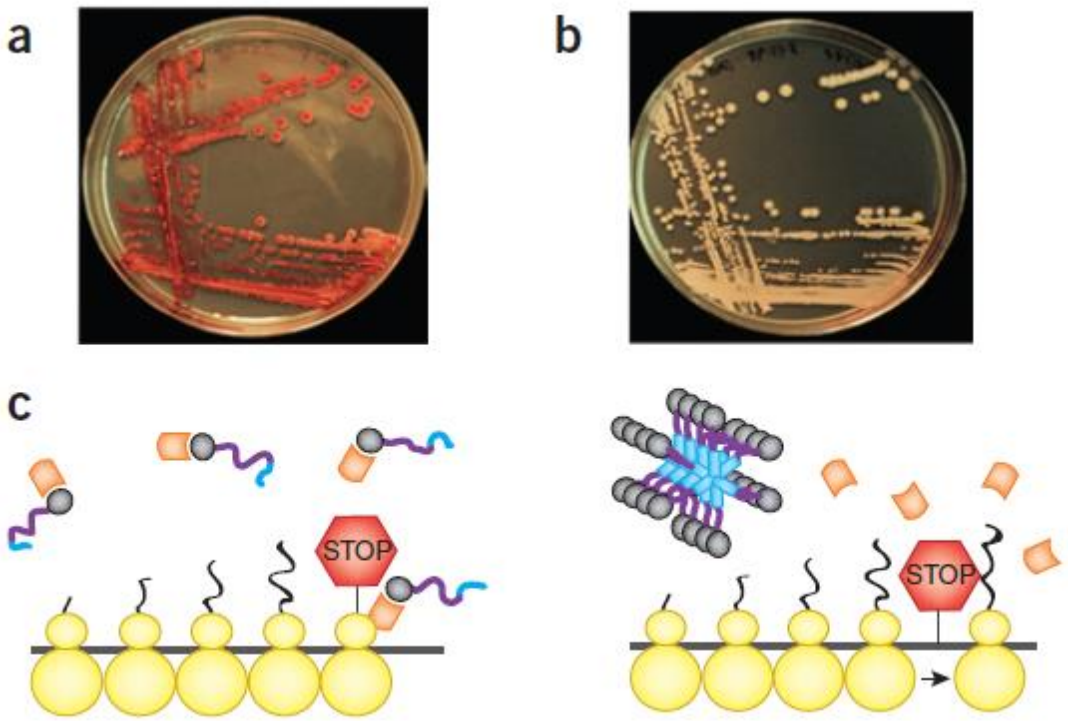

Figure 2.4: Characteristically (a) red [*psi*$^{-}$] cells and (b) white [*PSI*$^{+}$] cells. (c) Sup35p is soluble and functional when not aggregated (left). When Sup35p is sequestered in aggregates (right), the protein cannot perform its function and read-through of the nonsense mutation in the Ade1-14 gene occurs. This image is taken from Tessier and Lindquist (2009).[22]

2.2.3 Environmental Factors and Strains

Two main factors dictate the folding state, nucleation, and aggregation propensity of proteins: the primary sequence and environmental conditions [23-25]. The high primary sequence specificity of amyloid propagation has been clearly demonstrated through mutational studies, construction of synthetic prion, and species barrier studies [26-31] ; however, the mechanism of a curious phenomenon in prion biology where a given peptide can misfold into a variety of distinct amyloid structures, each leading to a distinct transmissible or inheritable phenotype [22, 32, 33], remains unclear. The question arises as to whether environmental factors, such as pH, co-solutes, shear, temperature, and ionic

strength, can elicit these different aggregation states giving rise to different prion "strains" or "variants."

Prion strains have been extensively studied for the yeast prion protein Sup35p, the protein determinate of the [*PSI*$^+$] prion [11, 22, 34-38]. *In vitro* studies typically employ a 253-residue, amyloid-forming fragment of Sup35p, called Sup35NM. Sup35NM has been shown to predominantly form different strains of [*PSI*$^+$] when nucleation occurs at different temperatures [17, 39-42]. Amyloids formed *in vitro* at 4 ^{0}C (Sc4) and 37 ^{0}C (Sc37) preferentially induced "strong" and "weak" [*PSI*$^+$] strains, respectively, when transfected into *Saccharomyces cerevisiae* [39]. These different [*PSI*$^+$] strains were shown to form at different rates [40], through different pathways [17], and create distinct structures [41]. Notably, phenotypically "strong" strains are characterized by less stable physical structure and shorter amyloid core region, as quantified by SDD-AGE and solid state NMR; the opposite is true of phenotypically "weak" strains. This is due to the fact that efficient prion propagation *in vivo* occurs via a chaperone-mediated fragmentation of aggregates that generates new seeds. Amyloids that are physically more stable are less efficiently fragmented and therefore are phenotypically weak [6].

Similar to temperature, the ionic composition of the solution has been shown to affect aggregation kinetics in a number of amyloid forming proteins, including α-synuclein [43], mouse PrP [44, 45], PABPN1 [46], and Sup35NM [18]; however, the effect of solution composition on amyloid structures and biological effects was not studied in detail. The present work relates the differences in aggregation kinetics of Sup35NM caused by different salts to the structures and propagation parameters of amyloids formed in respective conditions. We find striking differences between aggregates formed in the

presence of kosmotropes (well-hydrated anions) versus chaotropes (poorly hydrated anions). Overall, our data show for the first time that the ionic composition of the solution modulates the structural patterns of nucleated amyloids.

2.3 Materials and Methods

2.3.1 Sup35NM Purification and Polymerization

Sup35NM was heterologously produced in HMS174 (pLysS) *E.coli* (Novagen) using a pET20b-SUP35NM-$(His)_6$ expression vector as previously published [47]. Ni-NTA purification was performed as previously described [18]. Sup35NM was resuspended in PBS (pH 7.4) containing 0.5 M of a given sodium salt to a final concentration of 10 μM and allowed to rotate at 20 rpm at room temperature for 48 hours to polymerize. Samples were frozen at -80 ^{0}C until used.

2.3.2 Kinetic Assay

Solutions of thioflavin T (Sigma Aldrich) were prepared daily in PBS. Aggregation experiments were conducted in quadruplicate with final ThT and Sup35NM concentrations of 100 μM and 10 μM, respectively, and containing a sodium salt. Polymerization was initiated by shaking samples at 18 Hz linearly at 27 ^{0}C in a BioTek Instruments Synergy H4 Hybrid Multi-Mode Microplate Reader (Winooski, VT). Fluorescent readings were taken every 15 minutes for 12 hours using an excitation wavelength of 440 nm and emission wavelength of 480 nm. Data was modeled using a

non-linear MATLAB sigmoidal curve fitting program (available at http://bommarius.chbe.gatech.edu/research).

2.3.3 Thermostability Assays

Amyloid samples were centrifuged and washed to remove residual salt. Amyloids were resuspended in 100x diluted PBS. For SDS-PAGE gel-entry assay, aggregates were held for 15 minutes in a pre-heated thermal block, then run on an acrylamide gel. Densitometry analysis was performed using ImageJ software. For the DLS technique, resuspended amyloids were sonicated, then covered with silicon oil (to prevent solvent evaporation), and subjected to a temperature ramp protocol in a Malvern Zetasizer Nano ZS90 (Worcestershire, UK). The protocol increased the temperature by $1^{\mathbf{0}}$C, equilibrated the sample for 2 minutes, and then took a single size measurement for 1 minute. For these size measurements, the z-average of the amyloid diffusion coefficients was obtained from a second-order cumulant fit to the scattering intensity autocorrelation function, and translated into a hydrodynamic diameter *via* the Stokes-Einstein relation.

2.3.4 Imaging

Aggregates were first washed and resuspended in DI water. For TEM images, aggregates were adsorbed on formvar carbon coated 200 mesh copper grids by dropping 5 μL of protein solution onto the grid. Fibers were negatively stained using 2 μL of a 3% (w/v) uranyl acetate solution. After 60 seconds of staining, the sample was washed with deionized water and dried at 40 °C overnight. Images were acquired with a JEOL JEM 100CX II electron microscope operating at 100 kV. The microscope was equipped with a

LaB6 filament and side-mounted 4.2 megapixel FLI CCD camera. Bright-field images were acquired at magnifications of 14,000-80,000 x with a 300 μm second condenser aperture, 40 μm objective aperture, and "spot size" of 2. MaxIm DL software was used for imaging.

For AFM samples, 20 μL of aggregate solution was allowed to adsorb onto freshly cleaved mica for 20 minutes. The sample was then washed and dried at room temperature overnight. Images were acquired using a Veeco Dimension 3100 AFM (Plainview, NY) with a >10 nm AppNano silicon tip in tapping mode. Measurement of individual fibers was conducted manually offline using NanoScope Analysis software.

2.3.5 Semi-Denaturing Detergent Agarose Gel Electrophoresis (SDD-AGE)

SDD-AGE experiments were conducted on amyloid formed *in vitro* in either perchlorate or sulfate as previously published [48], except 0.1 % SDS added to the transfer buffer.

2.3.6 Electrophoretic Mobility

Electrophoretic mobility measurements were conducted using a Malvern ZS90 Zetasizer. Monomeric Sup35NM was suspended in water and pH'd using very dilute NaOH or HCl solutions. The isoelectric points (pI or IEP) was determined by finding the pH at which the electrophoretic mobility was zero (i.e. the protein carried no charge).

2.3.7 Transfection

S. cerevisiae strain GT17 (*MAT***a** *ade1-14* (UGA) *his3 leu2 trp1 ura3* [*psi*$^-$] [*pin*$^-$]) was used for all experiments [49]. GT17 contains a nonsense mutation *ade1-14* (UGA) in the

ADE1 gene, which causes premature translational termination of Ade1 protein synthesis in [*psi*$^-$] cells, as described above. Again, [*psi*$^-$] cells cannot grow on media lacking adenine and appear red on YPD media; [*PSI*$^+$] cells do grow on –ade media and appear white on YPD.[6]

In vitro generated amyloid was washed with DI water, sonicated, and then transfected into yeast along with a *URA3*-marker plasmid using a protocol described by Tanaka *et al*. [39] with the following modifications: SCE buffer did not contain dithiothreitol (it was added separately to the sphereoplasting solution); PEG buffer was prepared with (44% w/v PEG 3350); top agar concentration was 0.8%, and it was incubated at 42°C to prevent solidification.

Transfectants were transferred to *–ura* selective media then velveteened onto YPD and -ade for phenotypic determination of strain.

2.4 Results

2.4.1 Ion-specificity and Sup35NM Aggregation Kinetics.

We first examined the effects of salt type and salt concentration on Sup35NM amyloid formation *in vitro* via a fluorescence assay using the amyloid-binding dye thioflavin T (ThT) [50]. A typical aggregation profile is presented in the inset of Figure 2.6A. The classical sigmoidal-shape of these data is indicative of nucleation-dependent (ND) aggregation. ND aggregation is characterized by three phases: lag phase, fiber elongation, and mature fibril [11]. This behavior can be modeled empirically using a sigmoidal curve [51-53]:

$$F(t) = \frac{A}{1+\exp\left[-k(t-t_{1/2})\right]} + Offset\,, \qquad \text{(Eqn. 2.1)}$$

where A is the normalized amplitude, k is the fiber elongation rate constant, t is time, $t_{1/2}$ is the time at 50% fluorescence. The lag time t_{lag} is given by:

$$t_{lag} = t_{1/2} - \frac{2}{k}, \qquad \text{(Eqn. 2.2)}$$

The duration of the lag and fiber elongation phases varied significantly between ions and salt concentrations (Fig. 2.5). The rate of fiber elongation (Fig. 2.6A) was increased and the lag time (Fig. 2.6B) diminished in the presence of kosmotropes (shown in blue) in an ion-specific and concentration-dependent manner. Chaotropes (shown in orange) dramatically lengthened the lag time in an ion-specific and concentration-dependent manner (Fig. 2.6B). Strong chaotropes or kosmotropes (shown as darkness of hue) accentuated these effects.

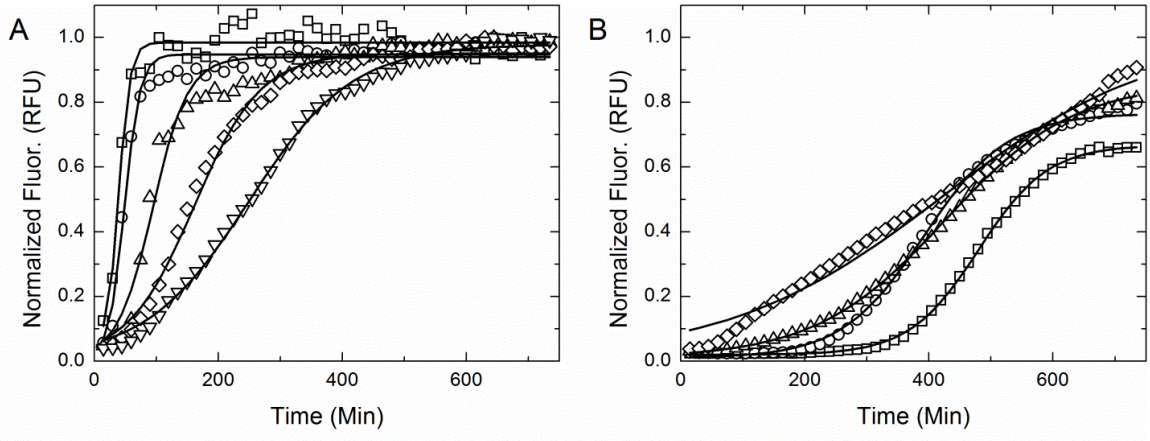

Figure 2.5: Examples of thioflavine T aggregation kinetic data and model fits for a strong kosmotrope, sulfate (A), and a strong chaotrope, perchlorate (B), at the following salt molarities: 0.4 (□), 0.3 (○), 0.2 (Δ), 0.1 (◊), and 0.025 (upside-down triangle). MATLAB non-linear regression models are shown in solid black line (Eqn. 2.1).

Ostensibly, chaotropes stabilized the monomeric form of Sup35NM while kosmotropes promoted formation of the polymeric (aggregated) form, confirming the "inverse" Hofmeister trend previously observed[18]. Having confirmed that ion-specific effects greatly affect aggregation rate, we examined the structural and biological effects of these differing rates.

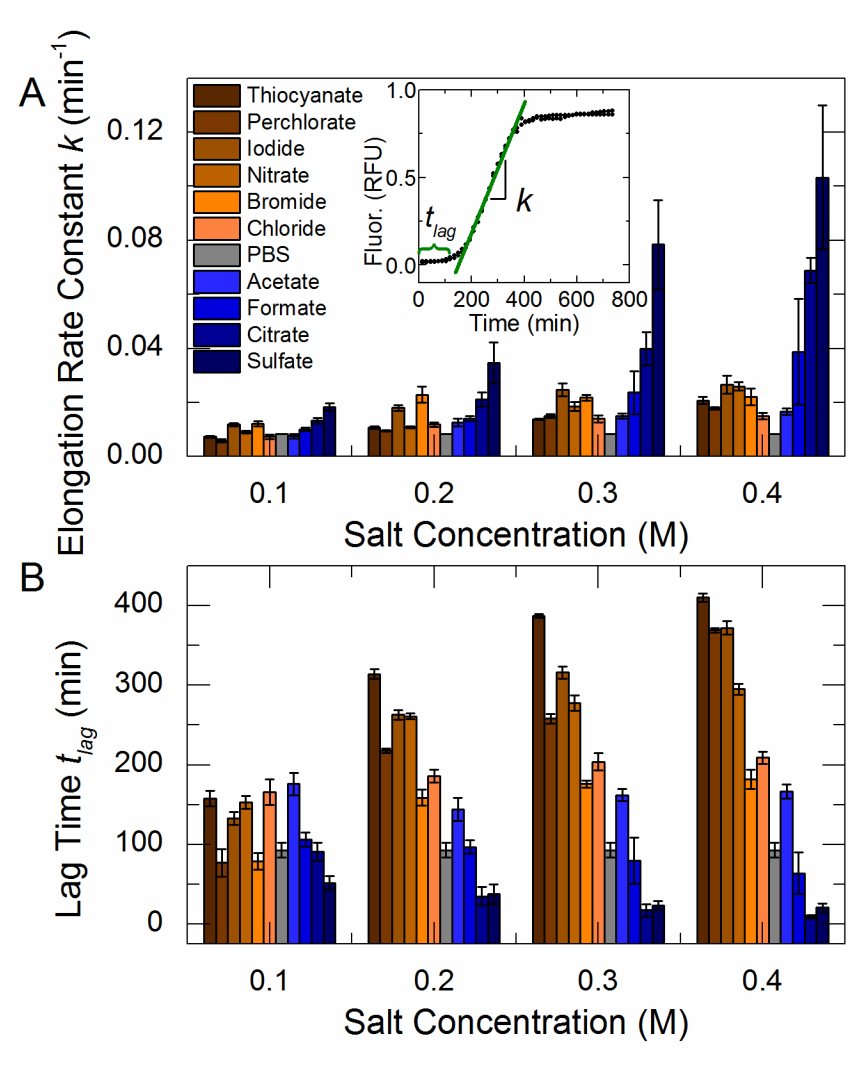

Figure 2.6: *In vitro* Sup35NM aggregation kinetics determined using thioflavine T fluorescence. A characteristic aggregation experiment and model parameter determination is shown in the inset to (A). Chaotropes are shown in orange and kosmotropes are shown in blue. The background buffer, PBS, without added salt is shown in grey. The elongation rate constants (A) and lag times (B) are shown over four salt concentrations.

2.4.2 Temperature Stability and Frangibility

We hypothesized that a correlation exists between the time aggregates take to form in different salt solutions and the compactness and stability of the resulting aggregate structure. This hypothesis is motivated by an analogous kinetics-structure relation known from the aggregation of isotropically interacting colloidal particles [54] and by the general notion that slower aggregation kinetics allows for the exploration of a larger configuration space and the realization of lower energy aggregate states. According to this expectation, a faster forming amyloid would contain more imperfect intermolecular bonds and have a smaller amyloid core, similar to Sup35NM amyloids preferentially formed at low temperature. On the other hand, a slow forming amyloid would create a compact structure with well-formed intermolecular bonds, allowing for a larger, more robust amyloid core, as in Sup35NM amyloids preferentially formed at high temperature [39]. We tested this prediction using two different techniques, both applied to amyloids produced in the presence of various salts (Fig. 2.7C). In both cases, amyloids were subjected to a temperature ramp and either particle size was measured using dynamic light scattering (DLS) or the proportion of non-aggregated (monomeric) protein was determined based on its ability to enter the SDS-PAGE gel (gel entry assay). The temperature of disaggregation T_D as determined by DLS correlates (Fig. 2.7B) well with that determined by gel entry assay (Fig. 2.7A). Despite slight differences in T_D caused by qualitative differences in the two techniques, both assays indicated that amyloids created in the presence of kosmotropes had lower thermostability than those formed more slowly in chaotropic conditions.

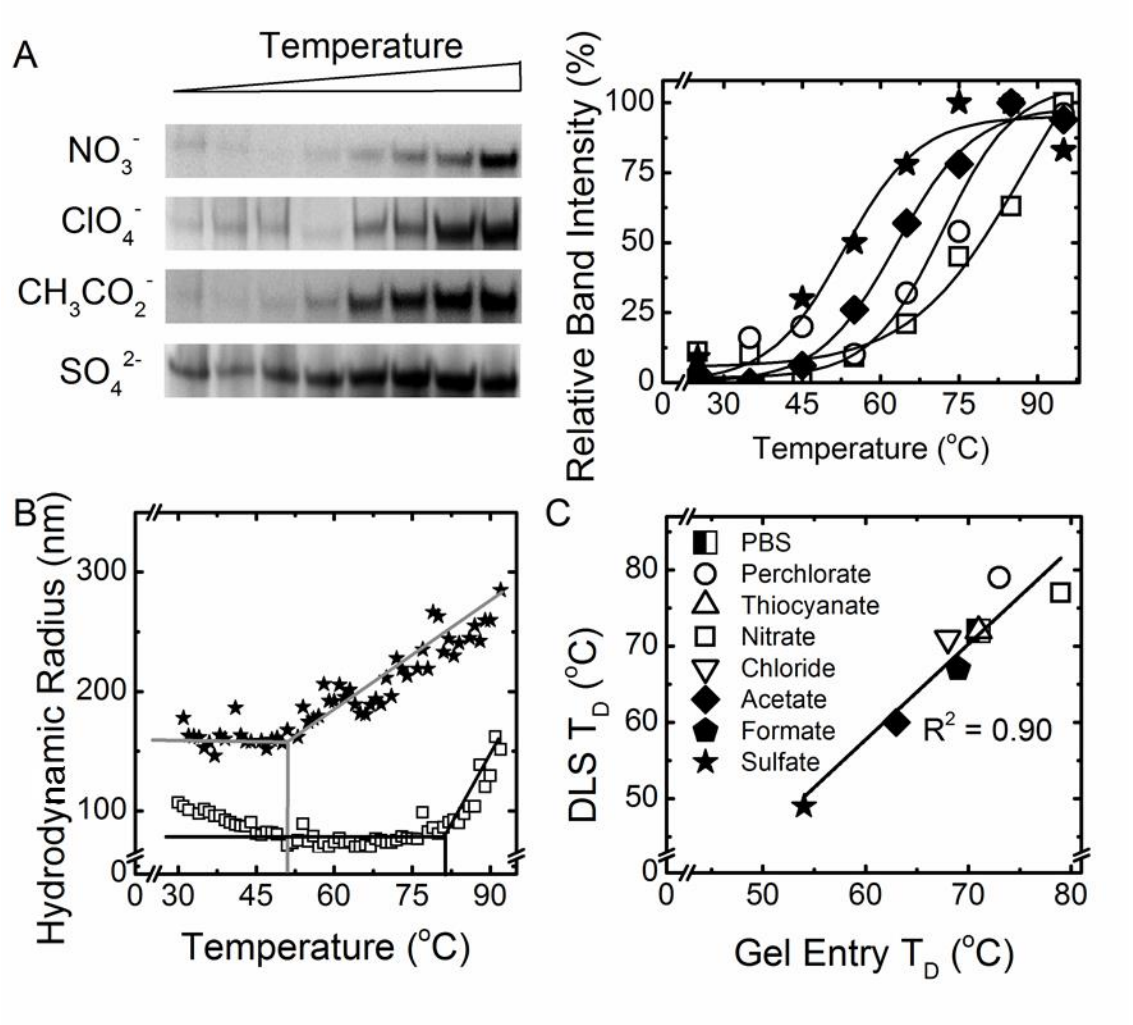

Figure 2.7. Analysis of the amyloid thermostability. Examples of the gel entry assay are shown in (A) and DLS disaggregation temperature ramp in (B). Gel entry assay and DLS determined thermostability of amyloids (C). Chaotropes are shown with open icons, kosmotropes are shown with closed icons.

Amyloid frangibility was assessed by fractionating polymers by sizes using semi-denaturing detergent agarose gel electrophoresis (SDD-AGE) after sonication. Amyloids formed in the presence of sulfate (ScS), a strong kosmotrope, were more readily fragmented by sonication than amyloids formed in perchlorate (ScP), a strong chaotrope (Fig. 2.8A). This result also confirms that ScS is physically less stable than ScP. Notably,

non-sonicated ScP fibers could not enter the gel whereas ScS fibers could, indicating that ScP fibers are larger than ScS fibers (Fig. 2.8B).

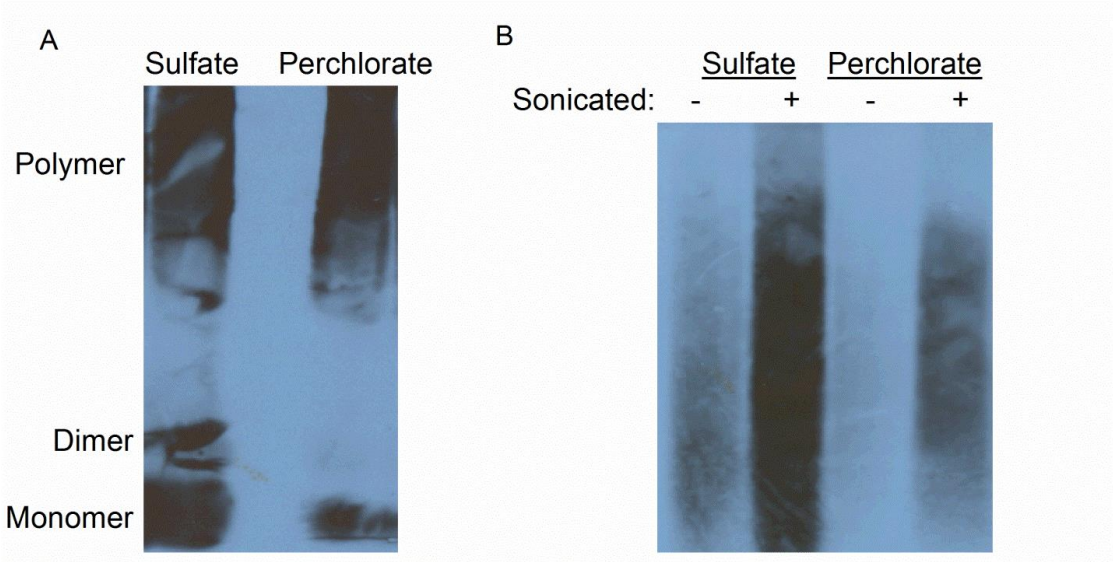

Figure 2.8: SDD-AGE gels comparing ScS and ScP susceptibility to sonication (A) and size (B). Both lanes in (A) are sonicated. Size is compared in (B) by what is able to enter the gel.

The differences in stability, like differences in kinetics (Fig. 2.6), between amyloids formed in the presence of intermediate Hofmeister ions were less pronounced than for ScS and ScP (Fig. 2.7C). Ion-specific effects are more apparent when comparing ions at the extremes of the Hofmeister series, as exemplified by comparing ScS and ScP.

2.4.3 Microscopy Analysis of Amyloids Produced in the Presence of Various Salts

Transmission electron microscopy (TEM) of Sup35NM amyloids formed in the presence of different salts revealed a systematic structural variation that follows an inverse Hofmeister trend. Amyloids formed in chaotropes were visibly most ordered compared to those formed in kosmotropes (Fig. 2.9A-E). The most pronounced difference is seen by

comparing the highly-ordered, helical fiber bundles of ScP aggregates (Fig. 2.9A) to the grainy ScS aggregates (Fig. 2.9E). The strong contrast between amyloids formed in chaotropes (Fig. 2.6F) and kosmotropes (Fig. 2.10G) was also confirmed by using atomic force microscopy (AFM).

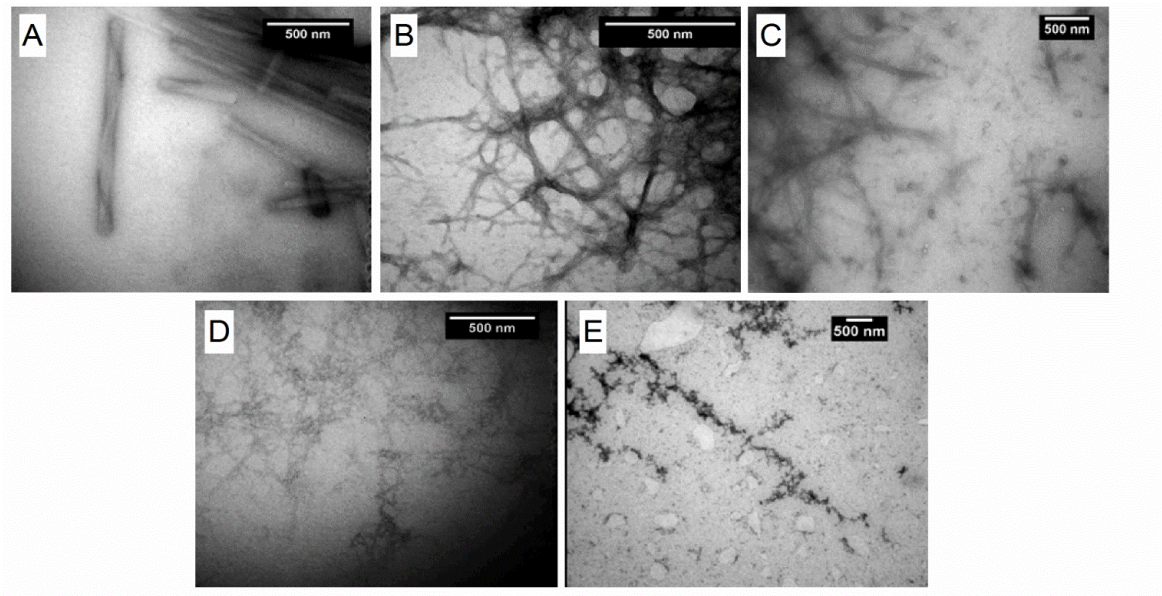

Figure 2.9: Bright-field TEM images of negatively stained amyloid fibers. Amyloids were formed in the presence of the following salts: perchlorate (A), nitrate (B), chloride (C), acetate (D), and sulfate (E).

AFM was employed to measure average fiber lengths. All conditions produced log-normal fiber length distributions. The difference in lengths as determined by AFM follows an inverse Hofmeister trend. Fibers formed in chaotropes, such as perchlorate and nitrate (Fig. 2.10, A and B), were markedly longer than fibers formed in kosmotropes, such as acetate and sulfate (Fig. 2.10, C and D); these findings agree with SDD-AGE data.

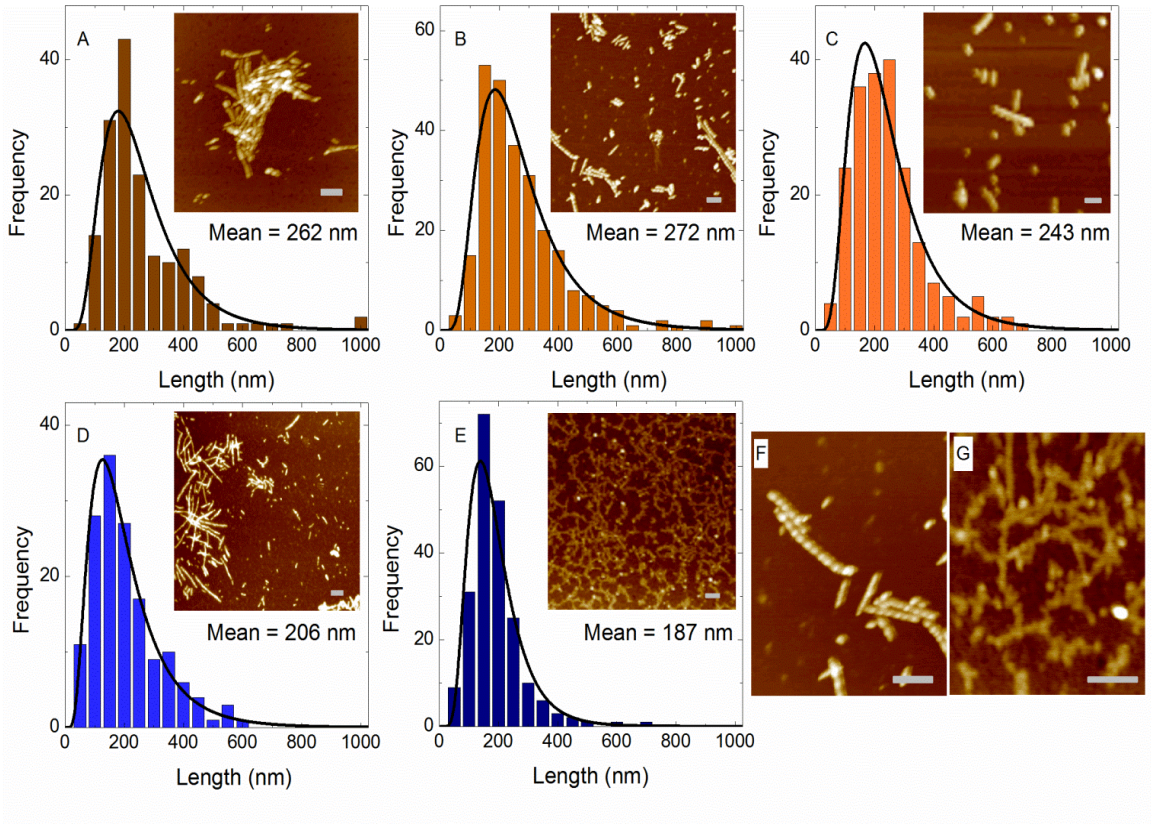

Figure 2.10: AFM analysis of the Sup35NM amyloids formed in perchlorate (A), nitrate (B), chloride (C), acetate (D), and sulfate (E). Scale bar = 200 nm. Length distributions were fit to a log-normal probability density function, shown as black curve $f(L,\mu,\sigma)=\frac{1}{L\sigma\sqrt{2\pi}}\exp\left(-\frac{[\ln(L)-\mu]^2}{2\sigma^2}\right)$ where L, μ, and σ are fiber length, mean, and standard deviation, respectively (44). Close-up images of amyloid formed in nitrate (F), a chaotrope, and sulfate (G), a kosmotrope, are shown to contrast their structures.

2.4.4 Phenotypic Characterization of Prion Variants Produced in the Presence of Different Salts

Next, we investigated if the different amyloid structures formed in different salts would lead to different strains of the [PSI^+] prion upon transfection into the yeast cells. Conversion of Sup35p into a prion ([PSI^+]) form results in a defect of translation termination. The degree of Sup35p inactivation depends on the prion variant or strain and

leads to a spectrum of [*PSI*$^+$] phenotypes ranging from white (strong [*PSI*$^+$]) to dark pink (weak [*PSI*$^+$]) [6].

Notably, phenotypically strong [*PSI*$^+$] strains typically correspond to the physically less stable amyloids; the opposite is true of weak variants [40, 41]. This is rationalized by the ability of frangible, fast aggregating fibers to break and create more fiber ends at which soluble Sup35p can be quickly recruited to the fiber; conversely, more robust, slowly aggregating fibers create fewer fiber ends and therefore cannot immobilize and inactivate soluble Sup35p as efficiently *in vivo*. Thus, we hypothesized that smaller, frangible, more rapidly aggregating fibers, such as ScS, would lead to phenotypically strong [*PSI*$^+$], whereas larger, more stable, slowly aggregating fibers, such as ScP, would lead to phenotypically weak [*PSI*$^+$].

This hypothesis was tested by transfecting *in vitro* formed Sup35NM amyloids into *S. cerevisiae* cells (Fig. 2.11A). For simplicity, [*PSI*$^+$] strains were divided into three classes - "strong", "intermediate," and "weak" (Fig. 2.11B). All three classes were curable by three passages on YPD medium containing 5 mM GuHCl, as typical of [*PSI*$^+$] [55]. In line with our hypothesis, the slowly forming, stable ScP amyloids predominantly induced weak [*PSI*$^+$] (Fig. 2.11C & D); whereas the fast-forming, frangible ScS aggregates primarily induced strong [*PSI*$^+$] (Fig. 2.11C & E). A strain continuum was produced by transfected amyloid formed in anions that fall between perchlorate and sulfate (Fig. 2.11C). A summary of the transfection results along with tranfection efficiencies is presented in Table 2.1. These results resemble data obtained for Sup35NM amyloids formed at different temperatures [39]. We have repeated Sup35NM aggregation at different temperatures (4^0C and 37^0C) followed by transfection and confirmed that a variety of

prion variants was generated at each temperature, with stronger strains more prevalent at lower temperature and weaker strains more prevalent at higher temperature. Therefore, both Sc4/ScS and Sc37/ScP samples produce an array of strain phenotypes, the predominant, (but not exclusive), of which are strong and weak, respectively. Non-homogeneity of each sample apparently originates from the fact that in vitro aggregation is initiated by multiple nucleation events in each case.

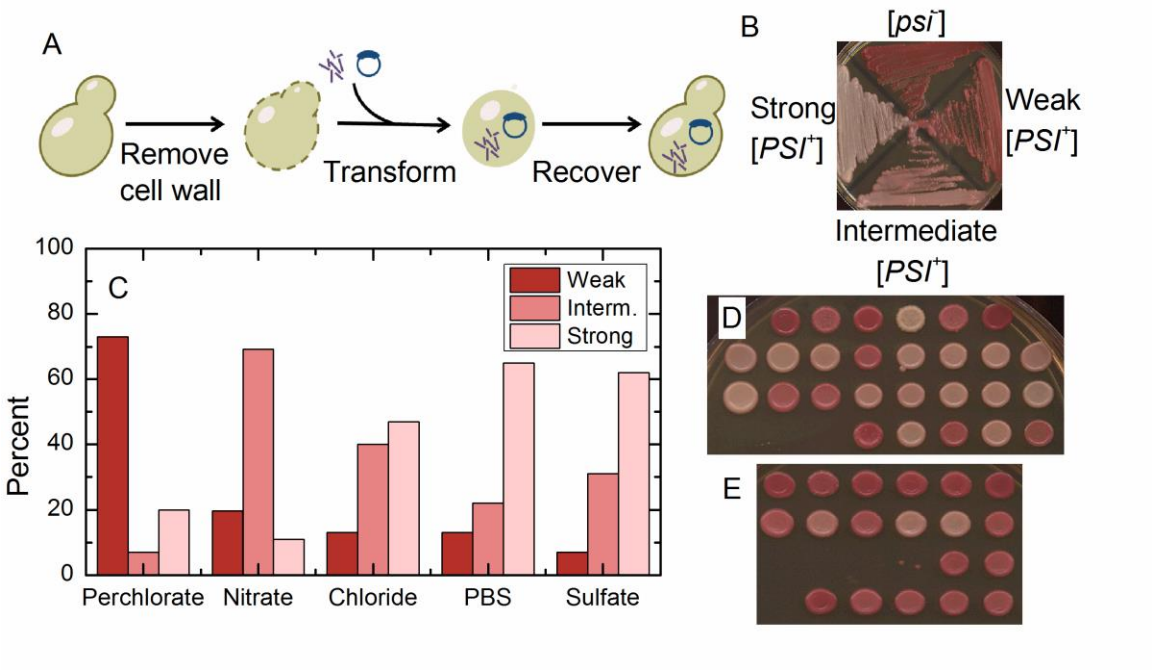

Figure 2.11: *In vivo* testing study. Transfection experiments are conducted by enzymatically stripping the yeasts' cell walls, then simultaneously transforming a marker plasmid and amyloid material. The yeast is then regrown in stabilizing media (A). Classification of strains (B) and transfection results (C). Patches from transfection of ScP (D) and ScS (E) are shown to illustrate the most divergent phenotype distributions. Data corresponding to the percentages shown in (C) are presented in the SI, as well as statistical analysis comparing the ScS and ScP sample populations.

Table 2.1: Transfection results. The frequency of [*PSI*$^+$] phenotypes and percent transfection efficiency is presented.

	Perchlorate	Nitrate	Chloride	PBS	Sulfate
Weak [*PSI*$^+$]	11	16	4	3	2
Intermediate [*PSI*$^+$]	1	47	12	5	9
Strong [*PSI*$^+$]	3	6	14	15	18
Total [*PSI*$^+$] colonies	15	69	30	23	29
Total transformants checked	49	242	150	76	142
Transfection efficiency (%)	30.6	28.5	20	30.3	20.4

2.5 Discussion

Our data confirm an inverse Hofmeister effect on Sup35NM aggregation, which agrees with our previous work [18] and with observations for other amyloidogenic proteins that allow this conclusion while not explicitly stating it [43, 44, 46]. An "inverse" Hofmeister trend arises when a colloidal particle is positively charged and hydrophilic or when a particle is negatively charged and hydrophobic [56]. We probably observe this trend because unfolded proteins are inherently hydrophobic [57] and at our operating pH, 7.4, Sup35NM carries a negative charge (pI = 5.3, Fig. 2.12).

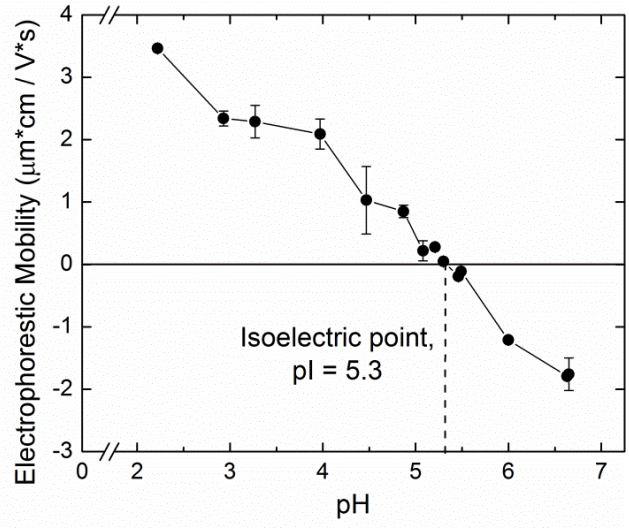

Figure 2.12: Determination of Sup35NM's isoelectric point.

We hypothesize that the structural and biological differences observed between amyloids produced in kosmotropes versus chaotropes stem from their contrasting amyloid formation kinetics. Although the theory on why and how Hofmeister effects exist is still evolving, the notion that chaotropes adsorb onto the protein surface and kosmotropes preferentially interact with bulk water is generally accepted [56-58]. The adsorption of chaotropes to the proteins' surface changes the proteins' topography and electrostatic landscape and, given that amyloid formation is a site-specific, recognition-based process [26-30], such steric or electrostatic alterations likely hinder aggregation; however, these aggregates are characterized by a higher degree of order and more rigid structure. Apparently, the more robust amyloids form due to a selection pressure requiring more stringent intermolecular interactions to overcome the anti-aggregation effect of chaotropic ions. This means that fewer collisions result in an aggregation event (Fig. 2.6) and that the aggregates that ultimately do form are compact and stable (Figs. 2.7 and 2.9). Even though chaotropes produce more compact aggregates, as we

hypothesized, their fiber lengths are generally longer than fibers formed in kosmotropes. One might have expected the inverse to be true; however, the number of fibers formed in kosmotropes is likely larger than the number of fibers formed in chaotropes due to differences in frangibility, resulting in shorter fibers.

For aggregation in the presence of kosmotropes, we hypothesize that depletion interactions accelerate aggregation [59, 60]. Depletion interaction arises when a solute molecule (a hydrated kosmotrope in this case) cannot fit between two colloidal particles (proteins). The absence or depletion of kosmotrope from the gap between colliding particles means that the unbalanced osmotic pressure associated with the solute effectively pushes the two particles together. The more hydrated the ion and the higher the salt concentration, the greater the range and strength of this effect become (Fig. 2.6). As kosmotropes do not alter a protein's surface but can be depleted from the gap, aggregates form faster, and intermolecular bonds need not be as precise and energetically favorable as in the case of aggregation in chaotropes. This leads to aggregates that nucleate rapidly, elongate quickly (Fig. 2.6), and are less compact and less stable by comparison (Figs. 2.7 and 2.9).

Transfection experiments confirm that amyloids formed in chaotropes and kosmotropes indeed produce different [PSI^+] strains. Both thermostability and transfection assays reveal a clear analogy between amyloids produced in different salts (this present work) and at different temperatures [39-41]. As low temperature, strong kosmotropes induce amyloids that are poorly thermostable, frangible, and preferentially generate the phenotypically strong [PSI^+] variants upon transfection. The opposite is true for amyloids produced in strong chaotropes or at high temperature. As this and previous

works have shown [61, 62], Sup35NM is able to create a number of distinct fiber types, which alludes to fiber conformations as the determinant of strains [39].

We hypothesize that chaotropic anions sterically alter the prion-recognition domain, slowing aggregation and forcing the most energetically favorable inter-molecular bonds to be selected, and kosmotropes accelerate aggregation through structural forces (depletion interactions, crowding). The disparate kinetics gave rise to varied fiber morphologies, as observed using TEM and AFM imaging. Thermostability tests showed fibers differ biochemically as well; and finally, transfection experiments proved that the varied structures induce different strains. To conclude, our work demonstrates that ion composition of the solution determines the amyloid formation rate, which in turn has a strong bearing on fiber morphology, prion strains, and infectivity. We further corroborate the assertion that form and function in regards to prion aggregates are closely associated. More generally, this work supports the supposition that environmental conditions are a strong driver of prion variants. The rate of fiber formation, whether it is influenced by temperature or ion composition, is the salient determinant of aggregate size, compactness/order, stability, and infectivity. Our data may be relevant to understanding amyloid formation both *in vivo* (as local gradients of ions exist in living systems) and *in vitro* (e. g. in the preparations of protein- or peptide-based drugs).

2.6 References

1. Eisenberg, D.; Jucker, M., The amyloid state of proteins in human diseases, *Cell* **2012,** *148,* 1188-203.

2. Prusiner, S. B., Molecular-biology of prion diseases, *Science* **1991,** *252,* 1515-22.

3. Prusiner, S. B., Prions, *Proceedings of the National Academy of Sciences of the United States of America* **1998,** *95,* 13363-83.

4. Weissmann, C., The state of the prion, *Nature Reviews Microbiology* **2004,** *2*, 861-71.

5. Fowler, D. M.; Koulov, A. V.; Alory-Jost, C.; Marks, M. S.; Balch, W. E.; Kelly, J. W., Functional amyloid formation within mammalian tissue, *Plos Biology* **2006,** *4*, 100-07.

6. Liebman, S. W.; Chernoff, Y. O., Prions in yeast, *Genetics* **2012,** *191*, 1041-72.

7. McGlinchey, R. P.; Kryndushkin, D.; Wickner, R. B., Suicidal [psi+] is a lethal yeast prion, *Proceedings of the National Academy of Sciences of the United States of America* **2011,** *108*, 5337-41.

8. Wickner, R. B.; Edskes, H. K.; Bateman, D.; Kelly, A. C.; Gorkovskiy, A., The yeast prions [psi+] and [ure3] are molecular degenerative diseases, *Prion* **2011,** *5*, 258-62.

9. Wickner, R. B.; Edskes, H. K.; Shewmaker, F.; Nakayashiki, T.; Engel, A.; McCann, L.; Kryndushkin, D., Yeast prions evolution of the prion concept, *Prion* **2007,** *1*, 94-100.

10. Chiti, F.; Dobson, C. M., Protein misfolding, functional amyloid, and human disease, *Annual Review of Biochemistry* **2006,** *75*, 333-66.

11. Shorter, J.; Lindquist, S., Prions as adaptive conduits of memory and inheritance, *Nature Reviews Genetics* **2005,** *6*, 435-50.

12. Dobson, C. M., Protein-misfolding diseases: Getting out of shape, *Nature* **2002,** *418*, 729-30.

13. Chiti, F.; Webster, P.; Taddei, N.; Clark, A.; Stefani, M.; Ramponi, G.; Dobson, C. M., Designing conditions for in vitro formation of amyloid protofilaments and fibrils, *Proceedings of the National Academy of Sciences of the United States of America* **1999,** *96*, 3590-94.

14. Bouchard, M.; Zurdo, J.; Nettleton, E. J.; Dobson, C. M.; Robinson, C. V., Formation of insulin amyloid fibrils followed by ftir simultaneously with cd and electron microscopy, *Protein Science* **2000,** *9*, 1960-67.

15. Booth, D. R.; Sunde, M.; Bellotti, V.; Robinson, C. V.; Hutchinson, W. L.; Fraser, P. E.; Hawkins, P. N.; Dobson, C. M.; Radford, S. E.; Blake, C. C.; Pepys, M. B., Instability, unfolding and aggregation of human lysozyme variants underlying amyloid fibrillogenesis, *Nature* **1997,** *385*, 787-93.

16. Chiti, F.; Taddei, N.; Bucciantini, M.; White, P.; Ramponi, G.; Dobson, C. M., Mutational analysis of the propensity for amyloid formation by a globular protein, *Embo Journal* **2000,** *19*, 1441-49.

17. Ohhashi, Y.; Ito, K.; Toyama, B. H.; Weissman, J. S.; Tanaka, M., Differences in prion strain conformations result from non-native interactions in a nucleus, *Nature Chemical Biology* **2010,** *6*, 225-30.

18. Yeh, V.; Broering, J. M.; Romanyuk, A.; Chen, B. X.; Chernoff, Y. O.; Bommarius, A. S., The hofmeister effect on amyloid formation using yeast prion protein, *Protein Science* **2010,** *19*, 47-56.

19. Walters, R. H.; Jacobson, K. H.; Pedersen, J. A.; Murphy, R. M., Elongation kinetics of polyglutamine peptide fibrils: A quartz crystal microbalance with dissipation study, *Journal of Molecular Biology* **2012,** *421*, 329-47.

20. Tuite, M. F.; Cox, B. S., Propagation of yeast prions, *Nature Reviews Molecular Cell Biology* **2003,** *4*, 878-90.

21. Tessier, P. M.; Lindquist, S., Unraveling infectious structures, strain variants and species barriers for the yeast prion [psi+], *Nature Structural & Molecular Biology* **2009,** *16*, 598-605.

22. Tessier, P. M.; Lindquist, S., Unraveling infectious structures, strain variants and species barriers for the yeast prion [psi+], *Nature Structural & Molecular Biology* **2009,** *16*, 598-605.

23. Chi, E. Y.; Krishnan, S.; Randolph, T. W.; Carpenter, J. F., Physical stability of proteins in aqueous solution: Mechanism and driving forces in nonnative protein aggregation, *Pharmaceutical Research* **2003,** *20*, 1325-36.

24. Fink, A. L., Protein aggregation: Folding aggregates, inclusion bodies and amyloid, *Folding & Design* **1998,** *3*, R9-R23.

25. Rubin, J.; San Miguel, A.; Bommarius, A. S.; Behrens, S. H., Correlating aggregation kinetics and stationary diffusion in protein-sodium salt systems observed with dynamic light scattering, *Journal of Physical Chemistry B* **2010,** *114*, 4383-87.

26. Bruce, K. L.; Chernoff, Y. O., Sequence specificity and fidelity of prion transmission in yeast, *Seminars in Cell & Developmental Biology* **2011,** *22*, 444-51.

27. Chen, B.; Newnam, G. P.; Chernoff, Y. O., Prion species barrier between the closely related yeast proteins is detected despite coaggregation, *Proceedings of the National Academy of Science of the United States of America* **2007,** *104*, 2791-6.

28. Chen, B. X.; Bruce, K. L.; Newnam, G. P.; Gyoneva, S.; Romanyuk, A. V.; Chernoff, Y. O., Genetic and epigenetic control of the efficiency and fidelity of cross-species prion transmission, *Molecular Microbiology* **2010,** *76*, 1483-99.

29. Ross, E. D.; Toombs, J. A., The effects of amino acid composition on yeast prion formation and prion domain interactions, *Prion* **2010,** *4*.

30. Toombs, J. A.; Petri, M.; Paul, K. R.; Kan, G. Y.; Ben-Hur, A.; Ross, E. D., De novo design of synthetic prion domains, *Proceedings of the National Academy of Sciences of the United States of America* **2012,** *109*, 6519-24.

31. Tessier, P. M.; Lindquist, S., Prion recognition elements govern nucleation, strain specificity and species barriers, *Nature* **2007,** *447*, 556-+.

32. Chien, P.; Weissman, J. S.; DePace, A. H., Emerging principles of conformation based prion inheritance, *Annual Review of Biochemistry* **2004,** *73*, 617-56.

33. Caughey, B.; Lansbury, P. T., Protofibrils, pores, fibrils, and neurodegeneration: Separating the responsible protein aggregates from the innocent bystanders, *Annual Review of Neuroscience* **2003,** *26*, 267-98.

34. Tuite, M. F.; Cox, B. S., The [psi+] prion of yeast: A problem of inheritance, *Methods* **2006,** *39*, 9-22.

35. Derkatch, I. L.; Chernoff, Y. O.; Kushnirov, V. V.; IngeVechtomov, S. G.; Liebman, S. W., Genesis and variability of [psi] prion factors in saccharomyces cerevisiae, *Genetics* **1996,** *144*, 1375-86.

36. King, C. Y.; Diaz-Avalos, R., Protein-only transmission of three yeast prion strains, *Nature* **2004,** *428*, 319-23.

37. Toyama, B. H.; Weissman, J. S., Amyloid structure: Conformational diversity and consequences, *Annual Review of Biochemistry, Vol 80* **2011,** *80*, 557-85.

38. Uptain, S. M.; Lindquist, S., Prions as protein-based genetic elements, *Annual Review of Microbiology* **2002,** *56*, 703-41.

39. Tanaka, M.; Chien, P.; Naber, N.; Cooke, R.; Weissman, J. S., Conformational variations in an infectious protein determine prion strain differences, *Nature* **2004,** *428*, 323-28.

40. Tanaka, M.; Collins, S. R.; Toyama, B. H.; Weissman, J. S., The physical basis of how prion conformations determine strain phenotypes, *Nature* **2006,** *442*, 585-89.

41. Toyama, B. H.; Kelly, M. J. S.; Gross, J. D.; Weissman, J. S., The structural basis of yeast prion strain variants, *Nature* **2007,** *449*, 233-U8.

42. Verges, K. J.; Smith, M. H.; Toyama, B. H.; Weissman, J. S., Strain conformation, primary structure and the propagation of the yeast prion [psi+], *Nature Structural & Molecular Biology* **2011,** *18*, 493-U135.

43. Munishkina, L. A.; Henriques, J.; Uversky, V. N.; Fink, A. L., Role of protein-water interactions and electrostatics in alpha-synuclein fibril formation, *Biochemistry* **2004,** *43*, 3289-300.

44. Jain, S.; Udgaonkar, J. B., Salt-induced modulation of the pathway of amyloid fibril formation by the mouse prion protein, *Biochemistry* **2010,** *49*, 7615-24.

45. Diaz-Espinoza, R.; Mukherjee, A.; Soto, C., Kosmotropic anions promote conversion of recombinant prion protein into a prpsc-like misfolded form, *Plos One* **2012,** *7*.

46. Lodderstedt, G.; Sachs, R.; Faust, J.; Bordusa, F.; Kuhn, U.; Golbik, R.; Kerth, A.; Wahle, E.; Balbach, J.; Schwarz, E., Hofmeister salts and potential therapeutic compounds accelerate in vitro fibril formation of the n-terminal domain of pabpn1 containing a disease-causing alanine extension, *Biochemistry* **2008,** *47*, 2181-89.

47. Allen, K. D.; Wegrzyn, R. D.; Chernova, T. A.; Muller, S.; Newnam, G. P.; Winslett, P. A.; Wittich, K. B.; Wilkinson, K. D.; Chernoff, Y. O., Hsp70 chaperones as modulators of prion life cycle: Novel effects of ssa and ssb on the sacharomyces cerevisiae prion [psi+], *Genetics* **2005,** *169*, 1227-42.

48. Halfmann, R.; Lindquist, S., Screening for amyloid aggregation by semi-denaturing detergent-agarose gel electrophoresis, *Journal of Visualized Experiments* **2008**.

49. Bailleul, P. A.; Newnam, G. P.; Steenbergen, J. N.; Chernoff, Y. O., Genetic study of interactions between the cytoskeletal assembly protein sla1 and prion-forming domain of the release factor sup35 (erf3) in saccharomyces cerevisiae, *Genetics* **1999,** *153*, 81-94.

50. Wolfe, L. S.; Calabrese, M. F.; Nath, A.; Blaho, D. V.; Miranker, A. D.; Xiong, Y., Protein-induced photophysical changes to the amyloid indicator dye thioflavin t, *Proceedings of the National Academy of Sciences of the United States of America* **2010,** *107*, 16863-68.

51. Hellstrand, E.; Boland, B.; Walsh, D. M.; Linse, S., Amyloid beta-protein aggregation produces highly reproducible kinetic data and occurs by a two-phase process, *Acs Chemical Neuroscience* **2010,** *1*, 13-18.

52. Nielsen, L.; Khurana, R.; Coats, A.; Frokjaer, S.; Brange, J.; Vyas, S.; Uversky, V. N.; Fink, A. L., Effect of environmental factors on the kinetics of insulin fibril formation: Elucidation of the molecular mechanism, *Biochemistry* **2001,** *40*, 6036-46.

53. Sorci, M.; Grassucci, R. A.; Hahn, I.; Frank, J.; Belfort, G., Time-dependent insulin oligomer reaction pathway prior to fibril formation: Cooling and seeding, *Proteins-Structure Function and Bioinformatics* **2009,** *77*, 62-73.

54. Kim, A. Y.; Berg, J. C., Fractal aggregation: Scaling of fractal dimension with stability ratio, *Langmuir* **2000,** *16*, 2101-04.

55. Chernoff, Y. O.; Uptain, S. M.; Lindquist, S. L., Analysis of prion factors in yeast, *Methods Enzymol* **2002,** *351*, 499-538.

56. Peula-Garcia, J. M.; Ortega-Vinuesa, J. L.; Bastos-Gonzalez, D., Inversion of hofmeister series by changing the surface of colloidal particles from hydrophobic to hydrophilic, *Journal of Physical Chemistry C* **2010,** *114*, 11133-39.

57. Pegram, L. M.; Wendorff, T.; Erdmann, R.; Shkel, I.; Bellissimo, D.; Felitsky, D. J.; Record, M. T., Why hofmeister effects of many salts favor protein folding but not DNA helix formation, *Proceedings of the National Academy of Sciences of the United States of America* **2010,** *107*, 7716-21.

58. Pegram, L. M.; Record, M. T., Jr., Thermodynamic origin of hofmeister ion effects, *Journal of Physical Chemistry B* **2008,** *112*, 9428-36.

59. Asakura, S.; Oosawa, F., On interaction between 2 bodies immersed in a solution of macromolecules, *Journal of Chemical Physics* **1954,** *22*, 1255-56.

60. Baynes, B. M.; Trout, B. L., Rational design of solution additives for the prevention of protein aggregation, *Biophysical Journal* **2004,** *87*, 1631-39.

61. Glover, J. R.; Kowal, A. S.; Schirmer, E. C.; Patino, M. M.; Liu, J. J.; Lindquist, S., Self-seeded fibers formed by sup35, the protein determinant of [psi+], a heritable prion-like factor of s-cerevisiae, *Cell* **1997,** *89*, 811-19.

62. DePace, A. H.; Weissman, J. S., Origins and kinetic consequences of diversity in sup35 yeast prion fibers, *Nature Structural Biology* **2002,** *9*, 389-96.

CHAPTER 3

HOFMEISTER AND PRION STRAIN EFFECTS ON THE CROSS-SPECIES NUCLEATION OF YEAST PRION

This chapter is a portion of an on-going collaboration between the Chernoff, Bommarius, and Behrens groups. Kathryn Bruce and Aditi Sharma will continue this work in the future. Their data will be amalgamated with this chapter and submitted for publication.

3.1 Summary

In Chapter 2, we showed that forming amyloid in strong kosmotrope or chaotrope produced predominately strong or weak prion variants, respectively. Recent work by the Chernoff group has shown that prion variant strength has a bearing on prion transmission between closely related yeast species. In this chapter, we ask whether the different variants produced in salts and having Hofmeister salts in solution effects *inter*-species transmission of [*PSI*$^{+}$]. Pre-formed amyloid was used to seed to monomer from each of the three species examined. Consistent with Chapter 2 and Chernoff's findings, amyloid formed in sulfate was more effective in cross-species seeding and behaved as a strong prion would; amyloid formed in perchlorate was ineffective or inhibited co-aggregation and acted as a weak prion would. The presence of chaotropic anions in the aggregation buffer poisoned amyloid propagation; whereas, addition of kosmotropes accelerated amyloid formation when a mild species barrier existed.

3.2 Introduction

Amyloidogenic proteins are associated with a myriad of protein misfolding diseases in mammals, such as Alzheimer's, Parkinson's, and "mad cow" disease. In fungi and yeast,

amyloid proteins control heritable, epigenetic traits.[1, 2] These proteins, including a transmissible subset known as prions, undergo a conformational change in their secondary structure to form β-sheet rich conformers (Fig. 3.1). The misfolded proteins then aggregate along their β-sheets through favorable sterics and hydrogen-bonding opportunities to form ordered, insoluble, fibrillar aggregates, known as amyloids (Fig. 2.1).[3]

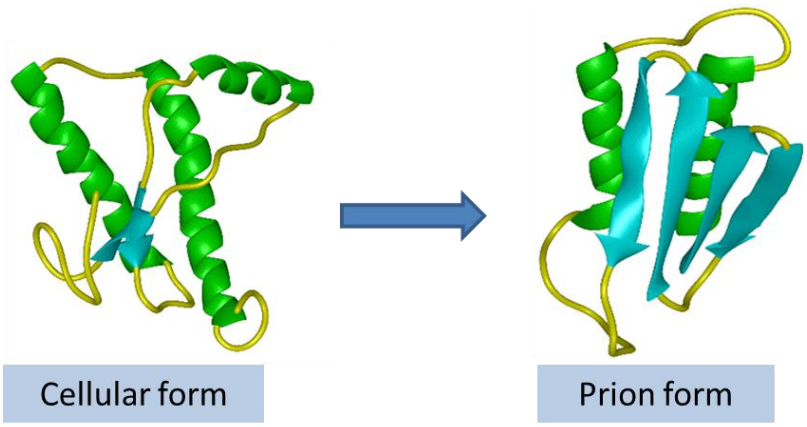

Figure 3.1: Hypothetical conformational change in the scrapies protein from its properly folded cellular form to its infectious, β-sheet rich prion form. This image was adapted from an image obtained at <http://www.bio.davidson.edu/Courses/Molbio/MolStudents/spring2003/WilsonE/home.prions.html>, accessed on January 27, 2013.

As shown in Figure 2.1 and discussed in Chapters 1 and 2, misfolded proteins recruit native protein of the *same* amino acid sequence into amyloids by altering the previously soluble protein's structure.[3] A high degree of sequence recognition is required between the amyloid fiber end and the soluble monomer for amyloid elongation to occur. Protein mutants and prion strains which alter the amyloid templating surface can seed analogous proteins from different species that have *different* (albeit very similar) amino acid sequences.[1, 4-6] For example, both mice and hamsters contain the 'prion protein' PrP and both proteins have similar (but not the same) sequence. Despite sequence differences, mouse PrP's prion form has been shown to be transmitted to hamsters, though at low

efficiency.[7] This phenomenon, where prion transmission between species occurs and is markedly less efficient than *intra*-species transmission, is known as the 'species barrier' (for review see Collinge and Clark (2007)).[4] A species barrier is said to be "high" if transmission efficiency between two species is very low or non-existent; a "low" species barrier exists if inter-species transmission is as efficient as *intra*-species transmission.[1]

3.1.1 Mad cow epidemic

The great significance of the species barrier became apparent during the infamous bovine spongiform encephalopathy (BSE or "mad cow" disease) epidemic in the United Kingdom (1985-96).[8] Incidents of BSE quickly ballooned from a single case in 1985 to ~3,000 new cases of BSE per month from 1992-93.[8] Although 180,000 cases were confirmed in total, it is estimated that over one million cattle were infected during the decade long outbreak.[4, 9] Along with mass cattle slaughters, import bans on UK-produced beef, and a severe decline in UK-produced beef prices, the gravest consequence of the mad cow outbreak was the serious public health risk. BSE is able to cross the species barrier and manifest itself in humans as a variant of Creutzfeldt-Jakob disease (vCJD).[1, 4, 10-15] In all, 24 cases of vCJD in humans were diagnosed in the UK and one in France during the epidemic.[1]

Although, BSE and vCJD are enormously impactful medicinally and economically, little is known about the molecular mechanism of transmission because studies involving cattle are exceedingly long and complex, and human studies are confined to epidemiological studies. To probe the species barrier, other models, such as yeast and transgenic (Tg) mice, have been developed.[7, 16] This chapter will focus on yeast models, although a significant amount of impactful literature is available on Tg mice studies (see works by Prusiner and Collinge and references within).[1, 4, 9-11, 13, 17, 18]

3.1.2 Yeast species barrier models

Yeast systems are ideal for studying the species barrier because yeast are easily genetically manipulated, have relatively short doubling times, and have a variety of prion-like proteins and species to choose from. The species barrier between yeast species was first identified when researchers attempted to pass the [*PSI*$^+$] trait, determined by Sup35p, from *Saccharomyces cerevisiae* to other yeast species (e.g. *Picha methanolica*, *Candida albicans*, and *Kluyveromyces lactis*) that also contained Sup35p.[6, 19, 20] These yeast species are highly divergent and the species barrier between them is considered "long-distance."[21] The prion domains (PrDs) between *S. cerevisiae* Sup35p and the other species' Sup35ps were only 30-40% identical, but all Sup35ps were known to form amyloids. Co-aggregation of Sup35p from different species was not observed, likely because of sequence divergence between the PrDs;[6] however, *C. albians* did show some "promiscuous" aggregation behavior.[2, 22]

As would be expected, "short distance" species barriers between more closely related yeast species show less of a barrier.[21] In a pair of recent publications, the Chernoff group studied the transmission of [*PSI*$^+$] between three very closely related *Saccharomyces* species.[16, 23] All three yeast species naturally contain Sup35p; however, the sequences of Sup35p, especially in the PrD, are slightly different (Fig. 3.2). Amyloid efficiently seeds and accelerates aggregation of monomer in solution if the amyloid and monomer are of the same species (i.e. homologous seeding). Chernoff found that cross-species seeding was notably less effective and asymmetric.[16] That is, for example, [*PSI*$^+$] from *S. paradoxus* (SP) was faithfully transmitted to *S. cerevisiae* (SC), but a high barrier was encountered when SC was the donor and SP the recipient.[16] This may be due to the amyloid template, as the prion strain donor also has a strong bearing on transmission efficiency.[1, 23]

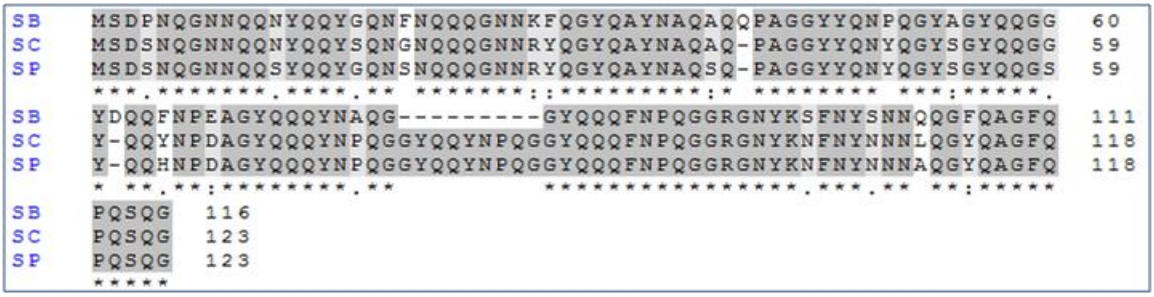

Figure 3.2: Sequence alignments of Sup35N from *S. bayanus* (SB), *S. cerevisiae* (SC), and *S. paradoxus SP).* The percent identity and similarity between: SC and SB are 80 and 86.4, respectively; SC and SP are 94.3 and 96.7, respectively; SB and SP are 77.6 and 85.6, respectively.

As discussed in Chapter 2, polymerizing Sup35NM in different electrolyte solutions produces different prion strains. In this chapter, we combine that notion with Chen *et al.*'s[23] finding that prion strains affect interspecies prion transmission. In this chapter we examine how amyloid seeds produced in strongly chaotropic or kosmotropic solutions from three closely related yeast species from the *Saccharomyces senso stricto* group affect polymerization kinetics of monomer from each of those three species *in vitro*. We also study how salts in the aggregation buffer effect cross-species aggregation. This work is meant to probe how prion strains and salts affect inter-species [PSI^+] transmission *in vitro*. Future transfection experiments, like those in Chapter 2, will be conducted to corroborate these findings *in vivo*. Plasmid shuffle experiments (as published previously[23]) will augment our transfection and *in vitro* kinetic data.

3.3 Materials and Methods

3.3.1 Sup35NM Expression, Purification, and Polymerization

Sup35NM from *S. cerevisiae* (SC), *S. bayanus* (SB), and *S. paradoxus* (SP) was heterologously produced in HMS174 (pLysS) *E.coli* (Novagen) using a pET20b-SUP35NM-$(His)_6$ expression vector as previously published.[24] Ni-NTA purification was

performed as described in Chapter 2. Purified protein was precipitated in 100% methanol and stored at -80 °C in 80% methanol.

To polymerize, Sup35NM was prepped as in Chapter 2 and resuspended in PBS (pH 7.4) containing 0.5 M of a sodium salt to a final concentration of 10 μM protein. The protein salt solution was rotated at 20 rpm at room temperature for 48 hours then stored at -80 °C.

3.3.2 Kinetic Assays

Solutions of thioflavin T (Sigma Aldrich) were prepared daily in PBS. Aggregation experiments were conducted in at least duplicate with final ThT and Sup35NM concentrations of 100 μM and 10 μM, respectively, and containing a sodium salt. In non-seeded experiments, polymerization was initiated by shaking samples at 18 Hz linearly at 25 °C in a BioTek Instruments Synergy H4 Hybrid Multi-Mode Microplate Reader (Winooski, VT). Fluorescent readings were taken every 15 minutes for 16 hours using an excitation wavelength of 440 nm and emission wavelength of 480 nm. Data was modeled using a non-linear MATLAB sigmoidal curve fitting program (Appendix A).

For seeded experiments, seeds were first sonicated then added to monomer at 5% (v/v), as previously published.[16] The ThT kinetic data and modeling were performed as the non-seeded experiments were.

3.4 Results and Discussion

3.4.1 Non-Seeded Aggregation Kinetics in High Salt Conditions

Aggregation kinetics with SC, SB, and SP monomer were run in solutions containing a strong kosmotrope (sulfate), a strong chaotrope (perchlorate), a neutral salt (chloride), or in PBS with no added salt (Figure 3.3). Figures 3.3A-C show kinetic runs with SC, SB, and SP, respectively, in different salt solutions. Figure 3.3D presents the lag times from the kinetic runs in Figures 3.3A-C as determined by the sigmoidal curve model presented in Chapter 2. The same trend in ion-specificity was apparent for all three yeast species, which agrees with results in Chapter 2 and previously published work on $Sup35NM_{SC}$.[24] For all species, the lag time was shortest in sulfate, longest in perchlorate, and in between in chloride. The duration of the lag phase was also salt concentration dependent, with added sulfate decreasing the lag time and additional perchlorate increasing the lag time, again consistent with $Sup35NM_{SC}$ results in Chapter 2.

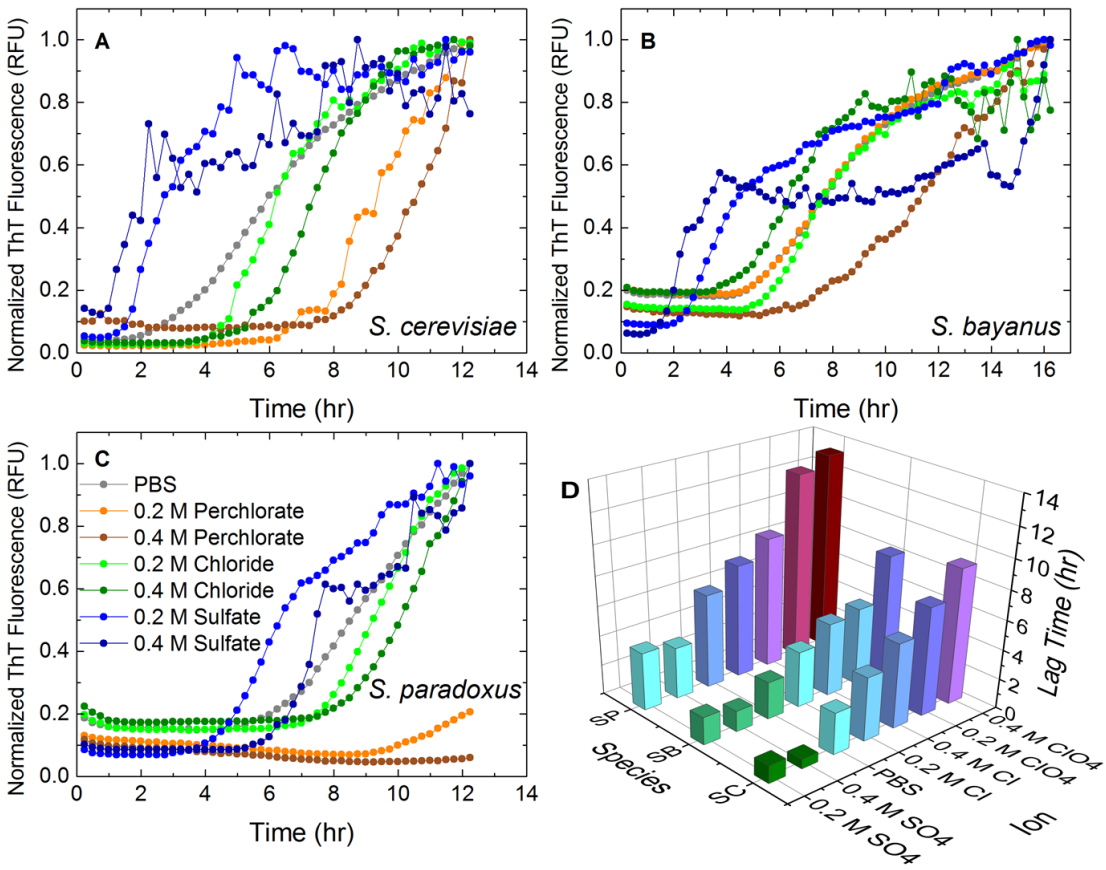

Figure 3.3: Non-seeded kinetic experiments in sulfate, chloride, and perchlorate for (A) SC, (B) SB, and (C) SP. The kinetic curves presented are averages of three experiments run in parallel. The averages were normalized to unity. (D) The lag times from each kinetic curve were obtained using the kinetic model present in Chapter 2. The color scale from green to red aids in visualizing short to long lag.

Figure 3.3 establishes that ion-specific interactions are the same for Sup35NM from all three yeast species. Notably, the duration of the lag time between species differed. SC and SB show similar lag times in all salts, but SP has considerably longer lag times in all conditions. This is a species specific finding and is in agreement with anecdotal, unpublished evidence from the Chernoff group.

3.4.2 Self- and Cross-Seeded Aggregation Kinetics

Homologous and heterologous kinetic seeding experiments were carried out in PBS (Figures 3.4). As expected, seeding a monomer with amyloid from the same species

(homologous) was very efficient and accelerated aggregation.[16, 23, 24] Figure 3.4A presents a representative comparison between non-seed and homologously seeded SP monomer. Aggregation was initiated in 51 minutes in the seeded case, whereas the non-seeded experiment took over 300 minutes to begin aggregating.

Similar decreases in lag time were seen for every homologous combination of seed and monomer compare to the 'no seed' control (Figs. 3.4B-D). Homologous seeding using the SC and SB amyloids formed in perchlorate were not as efficient as seeds formed sulfate or chloride. Chen *et al.* (2010) previously showed that weak prion variants (such as those formed in perchlorate) from SC are more poorly transmitted to SC *in vivo* than strong variants (such as those formed in sulfate),[23] which agrees with our results.

A species barrier was apparent for heterologous seeding experiments; however, the barrier's stringency varied. SP seeds formed in sulfate seeded SC monomer effectively; however, all SB seeds slowed or *poisoned* SC monomer aggregation (Fig. 3.4B). Amyloid poisoning is a phenomenon where heterologous amyloid poorly templates monomer and hinders amyloid propagation. Poisoning can lead to "curing" or loss of the prion *in vivo* (for review on amyloid poisoning see Bruce and Chernoff and references within).[21] SB monomer showed a high species barrier with both SC and SP seeds (Fig. 3.4C). SP monomer was seeded well by SC amyloid formed in sulfate, but nothing else. SB seeds poisoned SP monomer aggregation (Fig. 3.4D). Poisoning with SB seeds may be derived from $Sup35NM_{SB}$ being seven amino acids shorter than $Sup35NM_{SC}$ or $Sup35NM_{SP}$ (Fig. 3.2). The shorter protein length may account for why SB seeds are an ineffective template heterologously. From our data it is unclear whether strains effect poisoning or not in this case.

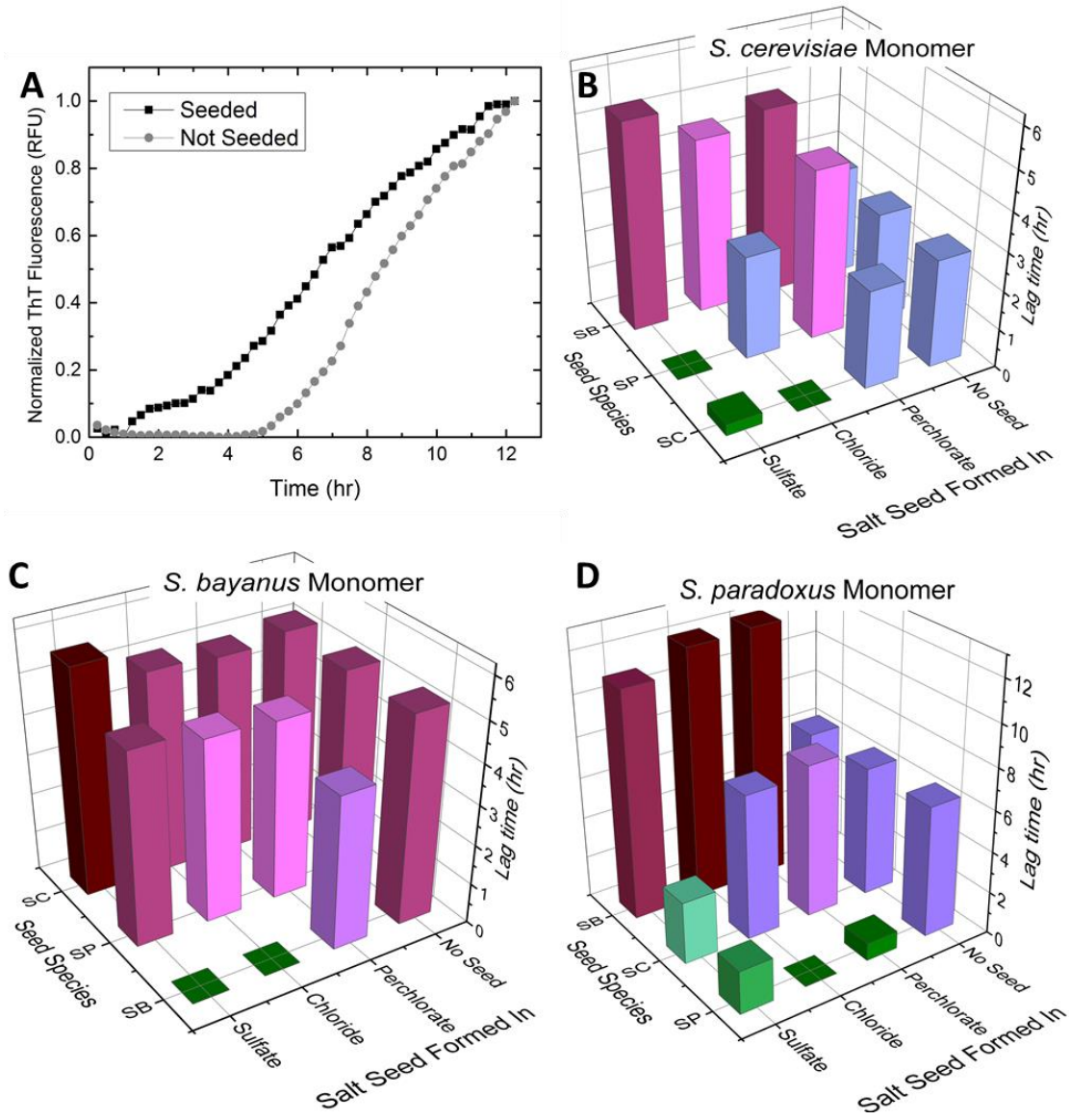

Figure 3.4: Homologous and heterologous seeding lag times. (A) Comparison between SP aggregation kinetics in PBS (not seeded) and SP monomer with SP seed formed in perchlorate. Homologous and heterologous seeding lag times for (B) SC monomer, (C) SB monomer, and (D) SP monomer are presented. The color scale from green to red is the same as in Figure 3.3. NOTE: the species axis is **NOT** the same for figures B-D; this was done to aid in visualizing all data.

To compare seeded to non-seeded aggregation, the change in lag time was calculated as follows:

$$\Delta Lag = \left(\frac{Seed_{Chloride} - Nonseeded}{Nonseeded} \right) * 100\% \qquad \text{(Eqn. 3.1)}$$

The chloride seeded aggregation experiments were used in this calculation because chloride is the most neutral Hofmeister salt and produces amyloid of all strains. Negative *ΔLag* suggests effective seeding and positive *ΔLag* indicates that seeding slowed aggregation. The magnitude of *ΔLag* describes how high or low the species barrier is. Our *ΔLag* values are generally in agreement with *in vivo* cytoduction and plasmid shuffle experiments performed by Chen *et al.*[16, 23] All except one heterologous combination of seed and monomer agree with Chen *et al.*'s (2007) cytoduction experiments (Table 3.1). Chen *et al*. found that SC monomer was seeded well by SB polymer,[16] but our *in vitro* experiments showed the opposite behavior.

In 2010, Chen *et al.* investigated how prion strains affected heterologous seeding using SC seeds. Their cytoduction and plasmid shuffle results showed that strong SC seeds were effectively transmitted to SC and SP, but not to SB,[23] just as our SC sulfate seeds were. Weak SC seeds were transmitted to SB and SP at notably lower efficiencies than strong seeds were. Our results agree with both trends for strong and weak seeds, given that sulfate seeds are strong and perchlorate seeds are weak (see Chapter 2).

Table 3.1: Comparison between previously published work by Chen *et al.* and current work. The transmission efficiency data is taken from Chen *et al*..[4] The change in lag time shows the reduction in lag between seed and non-seeded aggregation.

[*PSI*$^+$] donor	[*psi*$^-$] recipient	Transmission Efficiency (%)	Δ Lag Time (%)
SC	SC	100	-100
	SB	2.1	61.2
	SP	13	-4.4
SB	SC	76.7	9.2
	SB	97.5	-100
	SP	6.9	-7.4
SP	SC	95.6	-53.1
	SB	3.8	75.1
	SP	97.5	-67.6

3.4.3 Sup35NM$_{SC}$ Amyloid Cross-Species Seeding in High Salt Solutions

Since fibril formation is recognition dependent process, the presences of chaotropes or kosmotropes in a seeded solution may have a bearing on whether a monomer can conform to an amyloid template successfully or not. Chaotropes adsorb to both the amyloid surface and monomer. The additional surface changes and changes in template topography potentially slowing the already slow inter-species transmission. Kosmotropes, by the preferential interaction model,[25] would force amyloid and monomer together and accelerate aggregation. In this set of experiments we use seeds from *S. cerevisiae* and monomer from SB or SP (just as we did in section 3.4.3) with 0.4 M of salt added to the aggregation solution. These experiments were meant to test if salts had an effect on the species barrier. From the section 3.4.2, we observed a high species barrier when SB monomer was seeded with SC and a mild barrier when SP monomer was seeded by SC.

Seeding the presence of sulfate was the most efficient (Figs. 3.5A, B). The lag time observed for SB monomer with SC seeds in sulfate (Fig. 3.5A) was very similar to the lag time observed for non-seeded SB monomer in sulfate (Fig. 3.3B). This suggests that the high species barrier (ΔLag = 61.2) was not overcome; rather, the strong kosmotrope caused the SB monomer to aggregate rapidly on its own. Future experiments

could be conducted to ascertain whether co-aggregation was occurring or not. The lag times for SP monomer in sulfate were decreased compared to heterologous seeding without salt (Fig. 3.5B) or non-seeded SP in sulfate (Fig. 3.3C). This result suggests that sulfate aided in overcoming the species barrier. With no salt added, SC seeds could template SP, but not very effectively (ΔLag = -4.4). The addition of kosmotrope likely forced greater SP monomer - SC seeds interactions, as per the preferential interaction model. This theory could be further tested by examining if sulfate increases seeding of SP monomer with SB seeds since we see a mild species barrier between that pair (Table 3.1, ΔLag = -7.4).

The presence of chaotrope in solution poisoned inter-species transmission. The large red bars in Figures 3.5 A and B indicate that no aggregation was detected during the 15 hour experiments. It is possible that aggregation may occur after a longer period of time. Perchlorate, and chloride to a lesser extent, greatly slowed or completely inhibited aggregation. The high species barrier observed for SB monomer – SC seed systems in solutions without salt is exacerbated by the addition of chaotrope. The mild species barrier for SP monomer – SC seed systems became high in chaotropic solutions (Fig. 3.5B). Addition of chaotrope stymied co-aggregation in all combinations tested, regardless of the strain of the seed. Strong [PSI^+] seeds did have lower lag times in chaotropic solutions than weak [PSI^+] seeds, but both were slower than solutions without chaotrope.

From these data and Figures 3.4, it is apparent that the strain variant of the [PSI^+] donor has an impact on the efficacy of transmission, as was seen in Chen *et al.* (2010).[23] We can also see that salts in solutions do effect inter-species transmission. Kosmotropes can assist in overcoming a moderate species barrier and chaotropes inhibit any co-aggregation.

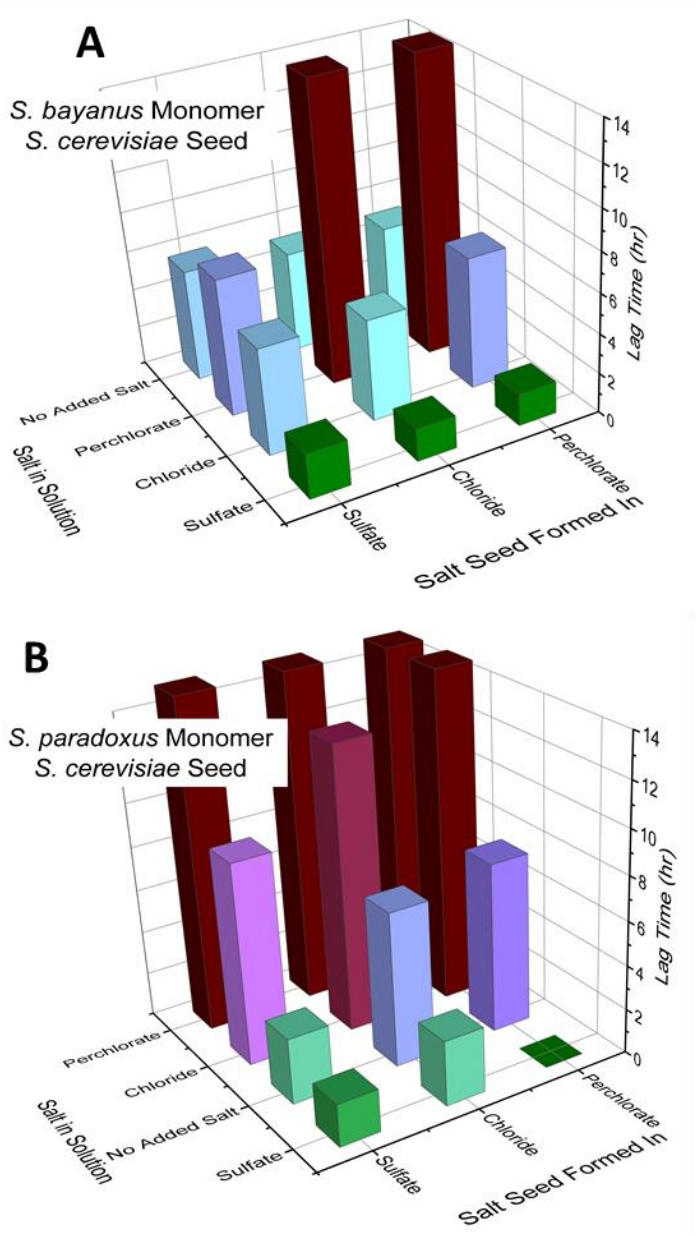

Figure 3.5: Seeding experiments in 0.4 M salt. SC seeds were used for all experiments. (A) SB monomer, (B) SP monomer lag times. The no salt added data is heterologous seeding data taken from Figure 3.4.

3.5 Conclusion and Future Work

This chapter studied the effect of ion-specificity on the species barrier between three closely related yeast species. All three species showed the same trend in ion-specificity in non-seeded experiments. Homologous seeding experiments for all species were

expectedly efficient; however, a species barrier was observed during heterologous seeding. As shown in Chapter 2, seeds formed in sulfate are predominantly strong and seeds formed in perchlorate are predominately weak. The cross-species transmission of [*PSI*$^{+}$] was strain-dependent, when the barrier could be overcome. Additional kosmotropic anions in the seeded aggregation solution accelerated co-aggregation if the species barrier was mild. Chaotropic anions poisoned amyloid propagation. These results reveal the dichotomous behavior salts have with the species barrier and provide another example of how chaotropes and kosmotropes interact inversely with proteins.

Future work on this topic will include *in vivo* tranfection experiments to prove more conclusively that the strains formed *in vitro* are in fact strong for sulfate and weak for perchlorate, as indicated in this chapter. Other solution additives could be tested to see if the behavior observed is ion-specific or a result of differences in surface tension. The crowding effect kosmotropes have on polymer and monomer alike should arise in solutions of other osmolytes as well. Sucrose could be added to non-seeded or seeded solutions to see if kinetics were similar to sulfate. The poisoning effect chaotropes have may be reproduced in solutions containing surfactants (SDS) or other surface tension reducing agents. These results should look similar to kinetics with perchlorate.

3.6 References

1. Prusiner, S. B., Prions, *Proc Natl Acad Sci U S A* **1998,** *95*, 13363-83.

2. Liebman, S. W.; Chernoff, Y. O., Prions in yeast, *Genetics* **2012,** *191*, 1041-72.

3. Shorter, J.; Lindquist, S., Prions as adaptive conduits of memory and inheritance, *Nature Reviews Genetics* **2005,** *6*, 435-50.

4. Collinge, J.; Clarke, A. R., A general model of prion strains and their pathogenicity, *Science* **2007,** *318*, 930-6.

5. Wickner, R. B.; Edskes, H. K.; Shewmaker, F.; Kryndushkin, D.; Nemecek, J., Prion variants, species barriers, generation and propagation, *Journal of Biology* **2009,** *8*, 47.

6. Santoso, A.; Chien, P.; Osherovich, L. Z.; Weissman, J. S., Molecular basis of a yeast prion species barrier, *Cell* **2000,** *100*, 277-88.

7. Kimberlin, R. H.; Cole, S.; Walker, C. A., Temporary and permanent modifications to a single strain of mouse scrapie on transmission to rats and hamsters, *Journal of Genetic Virology* **1987,** *68 (Pt 7)*, 1875-81.

8. Collee, J. G.; Bradley, R., Bse: A decade on--part i, *Lancet* **1997,** *349*, 636-41.

9. Collinge, J., Prion diseases of humans and animals: Their causes and molecular basis, *Annual Review of Neuroscience* **2001,** *24*, 519-50.

10. Collinge, J.; Palmer, M. S.; Sidle, K. C.; Hill, A. F.; Gowland, I.; Meads, J.; Asante, E.; Bradley, R.; Doey, L. J.; Lantos, P. L., Unaltered susceptibility to bse in transgenic mice expressing human prion protein, *Nature* **1995,** *378*, 779-83.

11. Prusiner, S. B., Prion diseases and the bse crisis, *Science* **1997,** *278*, 245-51.

12. Hill, A. F.; Desbruslais, M.; Joiner, S.; Sidle, K. C.; Gowland, I.; Collinge, J.; Doey, L. J.; Lantos, P., The same prion strain causes vcjd and bse, *Nature* **1997,** *389*, 448-50, 526.

13. Collinge, J.; Sidle, K. C.; Meads, J.; Ironside, J.; Hill, A. F., Molecular analysis of prion strain variation and the aetiology of 'new variant' cjd, *Nature* **1996,** *383*, 685-90.

14. Bruce, M. E.; Will, R. G.; Ironside, J. W.; McConnell, I.; Drummond, D.; Suttie, A.; McCardle, L.; Chree, A.; Hope, J.; Birkett, C.; Cousens, S.; Fraser, H.; Bostock, C. J., Transmissions to mice indicate that 'new variant' cjd is caused by the bse agent, *Nature* **1997,** *389*, 498-501.

15. Bruce, M.; Chree, A.; McConnell, I.; Foster, J.; Pearson, G.; Fraser, H., Transmission of bovine spongiform encephalopathy and scrapie to mice: Strain variation and the species barrier, *Philosophical Transactions of the Royal Society London: B Biology* **1994,** *343*, 405-11.

16. Chen, B.; Newnam, G. P.; Chernoff, Y. O., Prion species barrier between the closely related yeast proteins is detected despite coaggregation, *Proceedings of the National Academy of Science of the United States of America* **2007,** *104*, 2791-6.

17. Prusiner, S. B., Molecular biology of prion diseases, *Science* **1991,** *252*, 1515-22.

18. Prusiner, S. B., Genetic and infectious prion diseases, *Archives of Neurology* **1993,** *50*, 1129-53.

19. Chernoff, Y. O.; Galkin, A. P.; Lewitin, E.; Chernova, T. A.; Newnam, G. P.; Belenkiy, S. M., Evolutionary conservation of prion-forming abilities of the yeast sup35 protein, *Molecular Microbiology* **2000,** *35*, 865-76.

20. Kushnirov, V. V.; Kochneva-Pervukhova, N. V.; Chechenova, M. B.; Frolova, N. S.; Ter-Avanesyan, M. D., Prion properties of the sup35 protein of yeast pichia methanolica, *EMBO J* **2000,** *19,* 324-31.

21. Bruce, K. L.; Chernoff, Y. O., Sequence specificity and fidelity of prion transmission in yeast, *Seminars in Cell & Developmental Biology* **2011,** *22*, 444-51.

22. Tessier, P. M.; Lindquist, S., Unraveling infectious structures, strain variants and species barriers for the yeast prion [psi+], *Nature Structural & Molecular Biology* **2009,** *16*, 598-605.

23. Chen, B.; Bruce, K. L.; Newnam, G. P.; Gyoneva, S.; Romanyuk, A. V.; Chernoff, Y. O., Genetic and epigenetic control of the efficiency and fidelity of cross-species prion transmission, *Molecular Microbiology* **2010,** *76*, 1483-99.

24. Yeh, V.; Broering, J. M.; Romanyuk, A.; Chen, B.; Chernoff, Y. O.; Bommarius, A. S., The hofmeister effect on amyloid formation using yeast prion protein, *Protein Science* **2010,** *19,* 47-56.

25. Arakawa, T.; Timasheff, S. N., Preferential interactions of proteins with salts in concentrated solutions, *Biochemistry* **1982,** *21*, 6545-52.

CHAPTER 4

CORRELATING AGGREGATION KINETICS AND STATIONARY DIFFUSION IN PROTEIN - SODIUM SALT SYSTEMS OBSERVED WITH DYNAMIC LIGHT SCATTERING

The following chapter was adapted from our publication in the *Journal of Physical Chemistry B* **2010**, *114* (12) 4383-4387. Adriana San Miguel, Andreas Bommarius, and Sven Behrens contributed to this work.

4.1 Abstract

This chapter compares two manifestations of electrolyte-mediated interaction between globular proteins. Salt-induced protein aggregation is studied with dynamic light scattering (DLS) in solutions of lysozyme and bovine serum albumin (BSA) containing different types of sodium salts. The same types of ions are used in a second series of measurement assessing the effect of more dilute electrolytes on protein diffusivity in non-aggregating protein dispersions. Both aggregation and stable diffusion exhibit strong ion-specificity along the lines of the Hofmeister series: chaotropic counterions act as the strongest coagulants and, in stable protein solutions, lead to the lowest "protein interaction parameter", evaluated as the slope of protein diffusivity versus protein concentration. Within this common qualitative trend, lysozyme and BSA solutions show marked differences, including the sign of the interaction parameter for most of the tested solution compositions. Despite the different nature of lysozyme and BSA, a strong correlation is found in both cases between the ion-specific interaction parameter and the

proteins' aggregation tendency as indicated by the salt concentration required for fast aggregation. The interaction parameter, available via quick and easy DLS measurements on stable protein solutions, may thus serve as a predictor of ion-specific aggregation trends.

4.2 Introduction

Protein stability against aggregation is critically important for both disease markers and therapeutic agents. Protein aggregates are associated with neurodegenerative diseases such as Alzheimer's, Huntington's and Parkinson's disease among many others.[1, 2] In biotechnology, irreversible protein aggregation is a frequently encountered problem in the production, formulation, shipping, and storage of therapeutic proteins. Many therapeutic proteins are on the market and hundreds more are in clinical and preclinical trials.[3-5] Proteins that are currently on the market are prescribed to treat conditions such as diabetes, hemophilia, melanoma, transplant rejection, and myocardial infarction. Aggregation of these proteins is undesirable because it reduces protein efficacy, may incite an immune response,[6, 7] and violates FDA regulations requiring pharmaceutical proteins to be stable both physically and chemically for 18-24 months to be salable (special dispensations to this rule are made).[8, 9]

Protein aggregation is strongly dependent on environmental factors such as temperature, pH, cosolutes, salt type and concentration.[3] Protein unfolding, amyloid formation,[10] and even enzyme deactivation[11-14] have begun to be understood as a function of effects manifested through the Hofmeister series. However, the effects of salt type on protein aggregation are not understood, despite recent success at capturing and modeling

their kinetics.[15, 16] Often therapeutic proteins are solubilized, sterilized, and purified under harshly denaturing conditions (6 M GdnHCl, 8 M Urea). Aggregation may be initiated under these conditions and can propagate through non-covalent interactions and inter-protein disulfide bonding,[17] ultimately limiting biological yield. Understanding protein interaction at the onset of aggregation can help determine optimal processing and storage conditions so that aggregation losses can be minimized.[18]

While the analysis of later aggregation stages represents considerable challenges,[19] the rate constant k_{11} of doublet formation is more easily accessible. This rate constant is defined by:[20, 21]

$$\lim_{t\to 0}\frac{dN_1}{dt} = -k_{11}N_0^2 \qquad \text{(Eqn. 4.1)}$$

where N_1 is the number concentration of singlets and N_0 the initial number concentration of monomers before coagulation takes place. Both thermodynamic and hydrodynamic interactions between the proteins influence the coagulation rate constant $k_{11.}$ In the approximation of irreversible aggregation between isotropically interacting, spherical proteins, k_{11} can be calculated as: [22]

$$k_{11} = \left[\int_{2a}^{\infty}\frac{\exp(u(r)/k_BT)}{4\pi r^2 D\cdot h(r)}dr\right]^{-1} \qquad \text{(Eqn. 4.2)}$$

Here a is the protein radius, k_BT the thermal energy unit, $u(r)$ is the pair interaction energy, and $D(r)$ the separation dependent pair diffusion constant, which takes into

account the hydrodynamic drag and rises monotonically[23] from a zero at contact to the limiting value:

$$\lim_{t\to\infty} D(r) = 2D_0 \qquad \text{(Eqn. 4.3)}$$

where D_0 is the familiar single particle diffusion constant described by the Stokes-Einstein relation (η is the solution viscosity):

$$D_0 = \frac{k_B T}{6\pi\eta a} \qquad \text{(Eqn. 4.4)}$$

From Eq. 4.2 it is clear that repulsive particle interactions and hydrodynamic drag both contribute to stabilize dispersions against aggregation, but the complex interaction between real proteins in solution is not captured nearly well enough by the existing models to permit quantitative predictions. Experimentally, k_{11} can be obtained with relative ease using dynamic light scattering (DLS). The initial increase of the protein's hydrodynamic radius at the onset of aggregation satisfies Eq. 4.5:[24]

$$\frac{1}{r_h(0)}\left(\frac{dr_h(t)}{dt}\right)_{t\to 0} = \frac{I_2(q)}{2I_1(q)}\left(1-\frac{r_{h,1}}{r_{h,2}}\right)k_{11}N_1 \qquad \text{(Eqn. 4.5)}$$

where r_h is defined in analogy to Eq. 4.4 as $r_h(t) = k_BT/ 6\pi\eta D_0(t)$, $r_h(0)$ is the initial value before aggregation sets in, $r_{h,1}$ and $r_{h,2}$ are the hydrodynamic radii of a single protein and a doublet respectively, and their scattering intensities I_1, I_2. The scattering intensities in

principle depend on the scattering angle through the wave vector ***q***. However, the small proteins considered in this study act as point scatterers for the 633 nm laser wavelength used (qr_h << l); therefore, we may safely approximate $I_2/2I_1$ as unity. Using the geometric relation $r_{h,2}/r_{h,1}$ = 1.38 for spheres,[24] and the measured initial change in size, we can solve for the coagulation rate constant k_{11}. After considering these assumptions and approximations, Equation 4.5 simplifies to:

$$k_{11} = \frac{0.275}{R_h(0)N_1}\left(\frac{dR_h(0)}{dt}\right)_{t\to 0} \qquad \text{(Eqn. 4.6)}$$

Interestingly, the mark of protein-protein interactions can be found not only in the time dependence of protein diffusivity in aggregating systems, but also in the concentration dependence of protein diffusivity in non-aggregating systems. In stable protein solutions, protein-protein interaction leads to a concentration dependence of the mutual diffusion coefficient:

$$D(c) = D_0[1 + k_D c + O(c^2)] \qquad \text{(Eqn. 4.7)}$$

This diffusion coefficient and, by extension, the coefficient k_D in the virial expansion (Eqn. 4.7) are readily accessible to dynamic light scattering.[25] The coefficient k_D, known as the protein – protein interaction parameter,[18] sums up first-order effects of both thermodynamic and hydrodynamic particle-particle interactions in dispersions, with hydrodynamic coupling and repulsive thermodynamic interactions both leading to an increase in *D(c)* for the case of spherical particles.[26, 27] For protein systems, the precise

interplay of thermodynamic and hydrodynamic contributions cannot currently be predicted, and attempts to disentangle these two contributions experimentally are fraught with difficulty.[18] In this study, we take a pragmatic, semi-empirical approach to correlate the net interaction parameter k_D of stable protein solutions with aggregation kinetics in unstable solutions of similar ion composition but higher ionic strength, retaining in either case, both thermodynamic and hydrodynamic contributions.

Two model proteins, lysozyme and bovine serum albumin (BSA), were chosen to investigate the relative stabilization or destabilization of protein dispersions that arise in different electrolyte solutions due to Hofmeister effects[28] (for a review on the state of Hofmeister effects, see Kunz[29]). Lysozyme and BSA were chosen because they have been studied extensively and have been established as models for protein-solution and protein-protein interactions. Both proteins are readily available at high purity and assume a roughly spherical conformation in stable solutions.[18, 30]

The present study examines ion-specificity of salt-induced protein aggregation. Using DLS, diffusion coefficients and aggregation rate constants for both proteins are established. The two physical parameters are then related, and we find a strong correlation between protein diffusivity in non-aggregating systems (mutual diffusion coefficients) and aggregating systems (aggregation rate constants). This paper presents a convenient way of inferring information about medium-specific aggregation tendencies from stable protein samples.

4.3 Materials and Methods

4.3.1 Protein Purification and Preparation

Deionized water was used to prepare all solutions. Lysozyme was obtained from Sigma-Aldrich (St. Louis, MO; >90% purity) and was dissolved in an aqueous sodium acetate (Sigma-Aldrich, >99% purity) and acetic acid (Riedel-de-Haen, 96% purity) buffer of pH 4.25. The solution was then filtered using a Whatman Anotop 10, 0.02 µm pore size filter. Filtration removed larger proteins and any other relevant contaminant detectable by electrophoresis or DLS. The true concentration of protein was then determined using a Beckman Coulter DU 800 spectrophotometer at 280 nm using an extinction coefficient of 26.3 $mmol^{-1}$ cm^{-1}.[31]

Bovine serum albumin, Fraction V was obtained from EMD (Gibbstown, NJ, >98% purity) and dissolved in an acetate buffer. The dissolved BSA was then filtered using a Pall Acrodisc syringe filter, 0.2um Supor Membrane. The filtered solution was subsequently loaded onto a GE Healthcare HiPrep 16/60 Sephacryl High Resolution size exclusion chromatography column using an Amersham Pharmacia Biotech AKTA explorer FPLC. The proper elution fractions were collected and concentrated using a 30 kDa MW cut-off Pall JumboSep centrifugal membrane filter. The concentrated solution was then filtered with a Whatman Anotop 10, 0.02 µm pore size filter. Purity was confirmed via SDS-PAGE gel electrophoresis.

4.3.2 Electrolyte Buffer Preparation

All salts used were of > 99% purity, ACS regent grade. Salt solutions were made in acetate solutions as described above containing one of the follow: sodium sulfate anhydrous (Sigma-Aldrich), sodium formate (Aldrich), sodium phosphate monobasic (Sigma-Aldrich), sodium fluoride (BDH), sodium chloride (BDH), sodium bromide (Sigma-Aldrich), sodium nitrate (Sigma-Aldrich) or sodium iodide (EMD). The pH was then adjusted using either sodium hydroxide or the appropriate acid (e.g. sulfuric acid for a sulfate solution). The salt solution was filtered using a Pall Acrodisc syringe filter, 0.2 µm Supor Membrane.

4.3.3 Mutual Diffusion Coefficient Experiments

Diffusivity measurements were carried out at 25 °C, pH 4.25[32] and total ionic strength 0.1 M, 50 mM arising from the acetate buffer and 50 mM of the salt in question. These conditions ensured that the protein was in a globular conformation since the melting point of both proteins in similar solutions is significantly higher (~75°C for lysozyme[33] and ~60°C for BSA[34]).

Salt solutions were mixed with protein solutions of varying protein concentration in a low volume Sarstedt UV-transparent disposable cuvette. The sample was stirred very gently to avoid shear-induced aggregation and to homogenize the solution. The protein - salt solution was then inserted into a Malvern Zetasizer Nano ZS90 for measurement. Twelve runs of 30 seconds each were taken and averaged.

4.3.4 Aggregation Rate Experiments

All aggregation rate experiments were performed at 25 °C and with a 100 mM acetate background buffer. Lysozyme experiments were performed at pH 4.25.[32] BSA experiments were run at pH 4. The lower pH for BSA was chosen to distance the aggregation experiments from BSA's isoelectric point, 4.7.[35]

Samples were prepared similarly to the mutual diffusion coefficient experiments; however, in these experiments a wide range of salt molarities were investigated. Protein - salt solutions were prepared in cuvettes, and then *quickly* inserted into the Zetasizer. The change in particle hydrodynamic radius was monitored for at least 60 minutes.

4.4 Results and Discussion

4.4.1 Interaction Parameters

Figures 4.1A and B show the relative diffusivity of lysozyme and BSA, respectively, in stable sodium salt solutions of increasing protein concentrations. The slope of each curve represents the interaction parameter k_D specific for the given ion and ionic strength. Larger k_D values are indicative of stronger stabilizing (more repulsive) protein-protein interaction. The inferred k_D values for chaotropic counterions (dashed lines, open icons) vary substantially and generally correlate with the Hofmeister series, with k_D decreasing with increasingly chaotropic counterions (Table 4.1). For kosmotropes (solid lines, filled icons), k_D values are larger by comparison and are uniform for lysozyme; whereas, for BSA, they are larger, but are not uniform. For BSA and lysozyme, the results generally correlate with the Hofmeister series as evidenced by the progression of increasing k_D

values as we go from chaotropic to kosmotropic counterions. Sulfate is a notable outlier if used at the same molarity as the other ions (not shown). If used at a molarity lower by a factor of 2^6, however, the results for sulfate fit squarely into the small range observed for the other kosmotropes for lysozyme, as shown (this relation was also used for BSA). A scaling with the inverse sixth power of the counterion valency is familiar from the classical Schulze-Hardy rule for the critical coagulation concentration (CCC) of charged colloidal particles

The values of k_D for lysozyme are positive, whereas most of the values for BSA are negative, implying that at the examined pHs, the protein – protein interactions for BSA are attractive, whereas the lysozyme interactions are repulsive[36] (confirmed by comparing Figure 4.3a and b). Despite the difference in sign, the same Hofmeister trend is apparent in both cases and it is important to note that propensity to aggregate is dictated by *relative* differences in k_D for a given protein. In both cases sulfate had a large positive k_D, suggesting that it will strongly stabilize either protein at the given conditions. This is likely due to sulfate being by far the most kosmotropic counterion used, which would be expected to stabilize strongly.

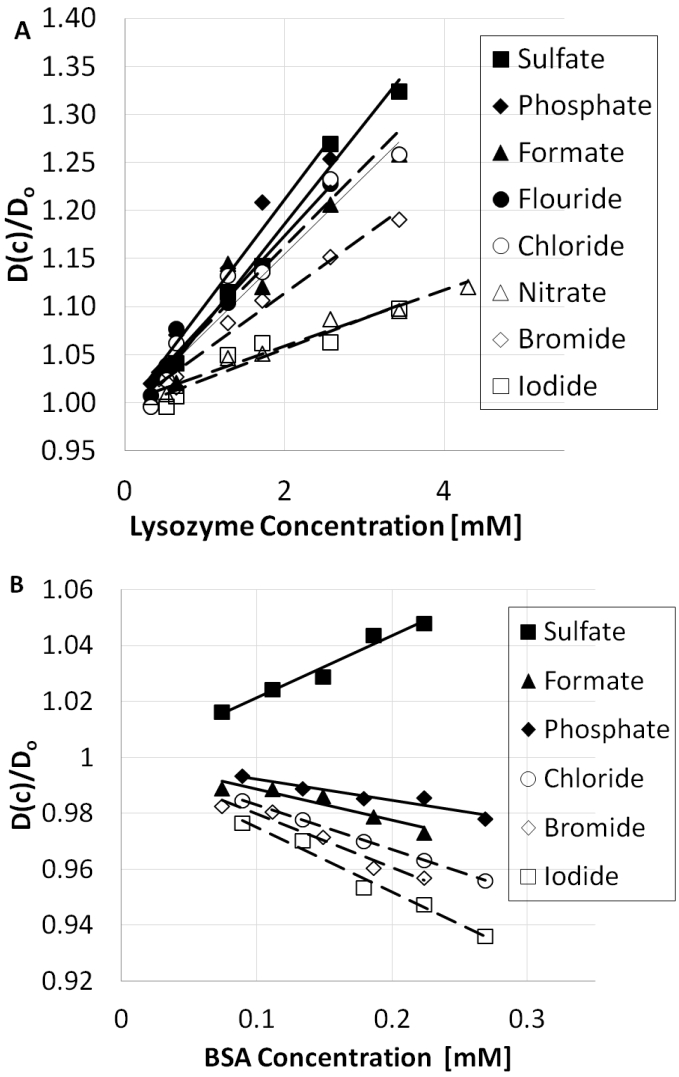

Figure 4.1: Plots of normalized relative mutual diffusion coefficient as a function of protein concentration. Experiments were run at pH 4.25, T = 25 °C, and I = 0.1 M arising to 50% from acetate buffer and 50% from the indicated sodium salt, with the exception of sodium sulfate, which was diluted by a factor of 2^6 compared to the monovalent ions, as explained in the text. (a) The top plot is for lysozyme, $D_0 = (7.57 \pm 0.4) \times 10^{-11}$ m^2/s; (b) the lower plot is for BSA, $D_0 = (3.27 \pm 0.1) \times 10^{-11}$ m^2/s.

Classically, kosmotropes are said to promote water structure, whereas chaotropes are expected to 'break water structure' and interact preferentially with the protein (a more precise and current account of salt interactions is presented in Chapter 1).[26] As a result, chaotropes will tend to accumulate *at* the protein surface while kosmotropes will be

concentrated in the water bulk *away from* the protein. The observed variations between different chaotropes may thus be caused by ion-protein interaction of varying strength. By the same token, the relative similarity of the kosmotropes for lysozyme may stem from their common tendency of being depleted from a zone, the *excluded volume*, around the protein.

For a given counterion, the protein-protein interaction depends on the ionic strength of the solution, and so does the absolute value of k_D. At ionic strengths sufficiently high to induce protein aggregation, k_D becomes inaccessible to DLS because the single protein diffusivity is masked by an ever changing distribution of aggregates. It seems plausible, however, that of several stable protein solutions with different salt types but similar (valency-adjusted) concentration, the ones with the strongest stabilizing interaction should require the largest increase in ionic strength in order to induce aggregation. We therefore hypothesize that the *relative* values of the measured k_D are a robust (and quick!) predictor for the counterion-specific protein aggregation tendency.

4.4.2 Aggregating Protein Concentration Independence

Before beginning aggregation experiments, we confirmed that the coagulation rate constant k_{11} was independent of the initial concentration of either protein, N_1, for both chaotropes and kosmotropes. While this independence would clearly be expected for colloidal particles, it is not obvious for proteins which can undergo rapid conformational changes upon partial unfolding or denaturing.[37] Figure 4.2 shows that the k_{11} for lysozyme - chloride systems is the same despite changing the lysozyme concentration, confirming that our rate constant is in fact a rate *constant*.

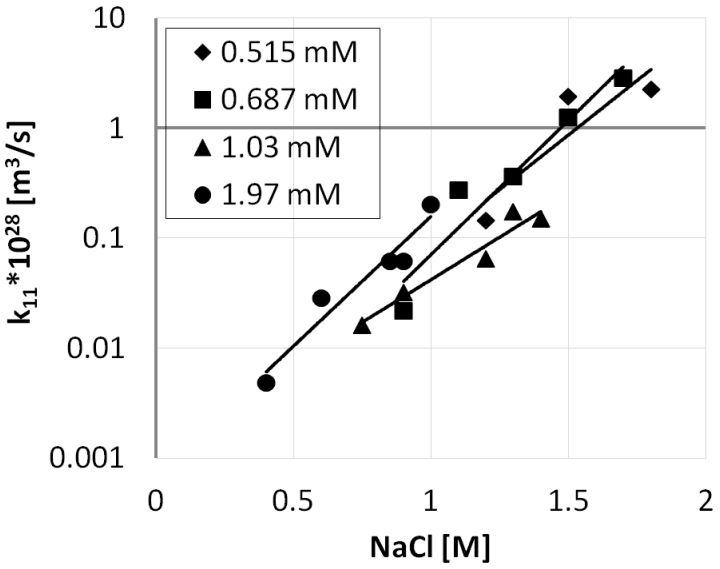

Figure 4.2: Coagulation rate constants for lysozyme−NaCl systems using different lysozyme concentrations. Icons represent different lysozyme molarities. Within experimental uncertainty, the four protein molarities yield essentially the same rate constant for a given salt molarity.

4.4.3 Protein Aggregation Kinetics

Like the diffusivities (Figs. 1), our results for the aggregation rate constant k_{11} (Fig. 4.3a, b) again show marked differences between the chaotropes and relative uniformity between the kosmotropes for lysozyme and a general Hofmeister trend for BSA. The results follow a clear Hofmeister trend for both proteins, with the most chaotropic ions inducing aggregation at the lowest ion strength. The ionic strength required for kosmotropes to induce fast aggregation was very similar for lysozyme, ~1.5 M. At lower ionic strength, in the slow aggregation regime, even these more kosmotropic solutions for lysozyme show a Hofmeister trend for both proteins as BSA does.

Table 4.1 summarizes the important findings from the two sets of experiments. To compare the effect salts had on aggregation, we needed to establish k_{11} value that could

be related across both proteins and all salts that would signify "fast" aggregation. k_{11} = 10^{-28} m^3/s satisfied our condition. We therefore use the ionic strength of salt required to achieve "fast" aggregation I_s as our measure of long-term stability

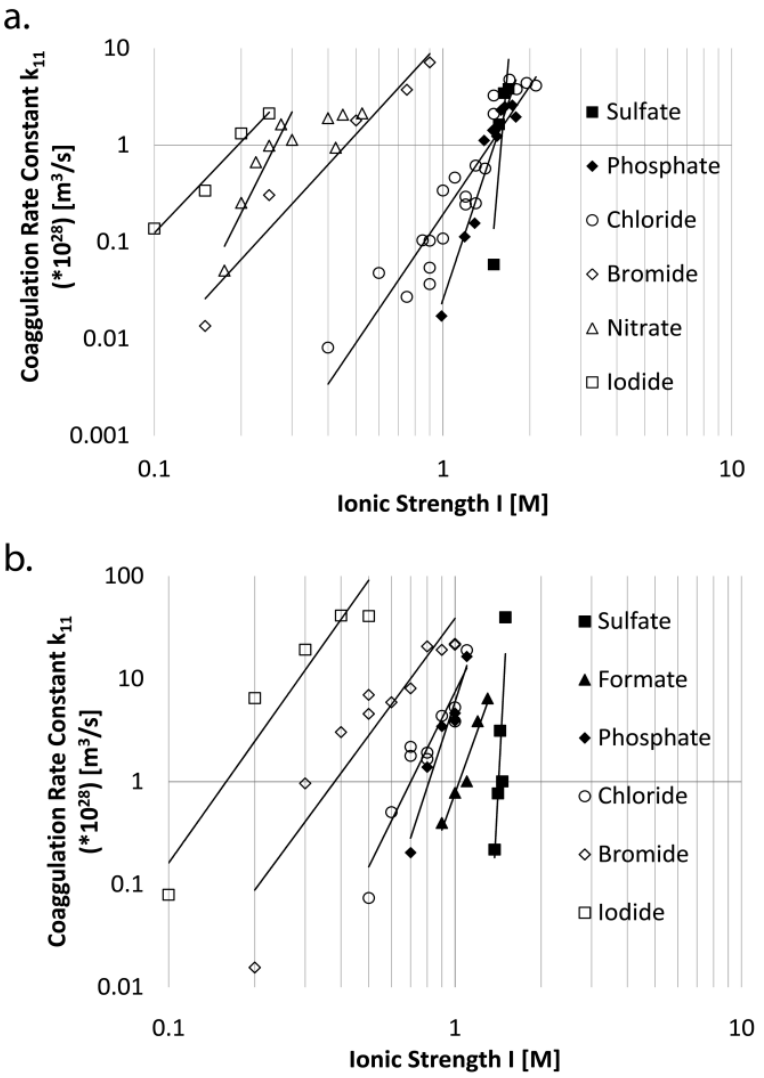

Figure 4.3: Coagulation rate constant, k_{11}, as a function of ionic strength. (a) Lysozyme experiments were run at pH 4.25 and T = 25 °C in a 0.1M sodium acetate buffer (top). (b) BSA experiments were run at pH 4.0 and T = 25 °C in a 0.1 M sodium acetate buffer (bottom).

The CCC value for certain ions was determined. This value is the salt concentration at which additional salt no longer accelerates aggregation. This phenomenon can be clearly observed as a plateau in k_{11} versus salt concentration (Figures 4.3 a and b). These values are presented in Table 4.1 below.

Table 4.1 Ionic strength I_s of solution at $k_{11} = 10^{-28}$ m^3/s, critical coagulation constants (CCC) for selected ions, the interaction parameter k_D, experimental Jones-Dole B viscosity coefficients[38]

Ion	Lysozyme			BSA			Jones-Dole B[38]
	I_s [M]	*CCC* [M]	k_D [M^{-1}]	I_s [M]	*CCC* [M]	k_D [M^{-1}]	
I^-	0.23	-	32 ± 5	0.08	0.4	-232 ± 19	-0.068
NO_3^-	0.28	0.3	29 ± 2	-	-	-	-0.046
Br^-	0.55	-	60 ± 4	0.2	0.8	-193 ± 24	-0.032
Cl^-	1.51	1.5	84 ± 8	0.45	1.1	-161 ± 2	-0.007
HCO_2^-	-	-	81 ± 9	0.61	-	-111 ± 22	0.052
$H_2PO_4^-$	1.55	1.5	111 ± 9	0.76	-	-76 ± 13	0.340
F^-	-	-	89 ± 6	-	-	-	0.1
SO_4^{-2}	1.63	-	105 ± 8	1.36	-	223 ± 22	0.208

4.4.4 Correlating k_D and I_s

Figure 4.4a and b show a strong correlation between k_D and I_s, which is quantified by a linear correlation coefficient of $R^2 = 0.93$ for lysozyme and $R^2 = 0.92$ for BSA. The Hofmeister trend is expressed in the fact that both k_D and I_s increase gradually from the highly chaotropic (iodide) to very kosmotropic (sulfate) solutions.

These plots confirm our hypothesis that protein aggregation can be predicted using the interaction parameter of stable solutions at low ionic strength. This correlation is very useful because characterizing aggregation kinetics, as in Figure 4.3, can take days

or even weeks depending on protein and aggregation conditions, as opposed to finding the interaction parameter which can be done in less than 30 minutes and can be adapted to a high-throughput micro-titer assay.[39]

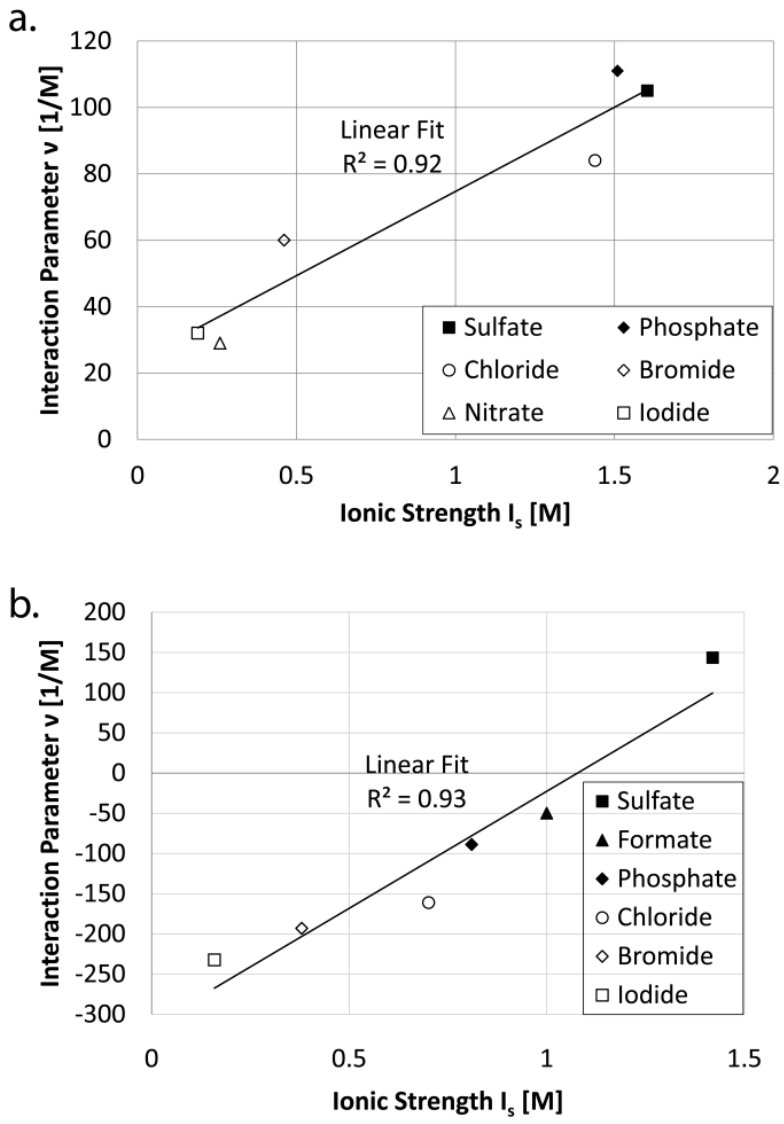

Figure 4.4 Relating k_D and ionic strength at $k_{11} = 10^{-28}$ m^3/s. (a) Correlation for lysozyme; (b) correlation for BSA.

The two proteins studied have different functions and size (lysozyme MW= 14.4 kDa; BSA MW= 67 kDa), and markedly different values for k_D, with sulfate solutions representing an outlier only in the case of BSA, but not for lysozyme (Fig. 4.1). Despite all of these inherent differences, there is, for both proteins, a strong correlation between the ion-specific interaction parameter k_D and the ionic strength I_s required to induce fast aggregation with the given type of ion. This insensitivity of the correlation seen in Fig. 4.4 to differences in protein properties instills confidence in the robustness of predictions for aggregation tendencies from DLS data on stable solutions.

4.5 Conclusion

In this work, we studied the mutual diffusion coefficients and coagulation rate constants for lysozyme and BSA in sodium salt systems using dynamic light scattering. For both proteins and both experiments, we found stabilizing trends against aggregation akin to the Hofmeister series. Chaotropes induced aggregation at lower ionic strengths, had lower interaction parameters k_D, and exhibited variance between each other; whereas kosmotropes required much higher ionic strengths to aggregate, and had larger k_D values. This work suggests that k_D for stable protein systems can be used for *quick* and easy predictions of ion-specific aggregation trends. The observations for sulfate in the BSA system unparalleled in the lysozyme system and we do not have a satisfying explanation at this point. Nonetheless the correlation works beautifully for two very different proteins and is thus shown to be remarkably robust!

4.6 References

1. Eisenberg, D.; Jucker, M., The amyloid state of proteins in human diseases, *Cell* **2012,** *148*, 1188-203.

2. Prusiner, S. B., Prions, *Proceedings of the National Academy of Science of the United States of America* **1998,** *95*, 13363-83.

3. Chi, E. Y.; Krishnan, S.; Randolph, T. W.; Carpenter, J. F., Physical stability of proteins in aqueous solution: Mechanism and driving forces in nonnative protein aggregation, *Pharmaceutical Research* **2003,** *20*, 1325-36.

4. Reichert, J. M., Which are the antibodies to watch in 2012?, *Mabs* **2012,** *4*, 1-3.

5. Mullard, A., Can next-generation antibodies offset biosimilar competition?, *Nature Reviews Drug Discovery* **2012,** *11*, 426-28.

6. Rosenberg, A. S., Effects of protein aggregates: An immunologic perspective, *Aaps Journal* **2006,** *8*, E501-E07.

7. Wang, W.; Singh, S. K.; Li, N.; Toler, M. R.; King, K. R.; Nema, S., Immunogenicity of protein aggregates-concerns and realities, *International Journal of Pharmaceutics* **2012,** *431*, 1-11.

8. Cleland, J. L.; Powell, M. F.; Shire, S. J., The development of stable protein formulations - a close look at protein aggregation, deamidation, and oxidation, *Critical Reviews in Therapeutic Drug Carrier Systems* **1993,** *10*, 307-77.

9. Ganan-Jimenez, A.; Brake, B., Q5c -stability testing of biotechnological / biological products. ICH, Ed. 1995.

10. Yeh, V.; Broering, J. M.; Romanyuk, A.; Chen, B. X.; Chernoff, Y. O.; Bommarius, A. S., The hofmeister effect on amyloid formation using yeast prion protein, *Protein Science* **2010,** *19*, 47-56.

11. Bommarius, A. S.; Karau, A., Deactivation of formate dehydrogenase (fdh) in solution and at gas-liquid interfaces, *Biotechnology Progress* **2005,** *21*, 1663-72.

12. Broering, J. M.; Bommarius, A. S., Evaluation of hofmeister effects on the kinetic stability of proteins, *Journal of Physical Chemistry B* **2005,** *109*, 20612-9.

13. Broering, J. M.; Bommarius, A. S., Cation and strong co-solute effects on protein kinetic stability, *Biochemical Society Transactions* **2007,** *35*, 1602-5.

14. Broering, J. M.; Bommarius, A. S., Kinetic model for salt-induced protein deactivation, *Journal of Physical Chemistry B* **2008,** *112*, 12768-75.

15. Roberts, C. J., Non-native protein aggregation kinetics, *Biotechnology and Bioenginering* **2007,** *98*, 927-38.

16. Andrews, J. M.; Roberts, C. J., Non-native aggregation of alpha-chymotrypsinogen occurs through nucleation and growth with competing nucleus sizes and negative activation energies, *Biochemistry* **2007,** *46*, 7558-71.

17. Militello, V.; Casarino, C.; Emanuele, A.; Giostra, A.; Pullara, F.; Leone, M., Aggregation kinetics of bovine serum albumin studied by ftir spectroscopy and light scattering, *Biophysical Chemistry* **2004,** *107*, 175-87.

18. Liu, W.; Cellmer, T.; Keerl, D.; Prausnitz, J. M.; Blanch, H. W., Interactions of lysozyme in guanidinium chloride solutions from static and dynamic light-scattering measurements, *Biotechnology and Bioenginering* **2005,** *90*, 482-90.

19. Lattuada, M.; Wu, H.; Sandkuhler, P.; Sefcik, J.; Morbidelli, M., Modelling of aggregation kinetics of colloidal systems and its validation by light scattering measurements, *Chemical Engineering Science* **2004,** *59*, 1783.

20. Barany, S.; Stuart, M. A. C.; Fleer, G. J., Coagulation rate of silica dispersions investigated by single-particle optical sizing, *Colloids and Surfaces a-Physicochemical and Engineering Aspects* **1996,** *106*, 213-21.

21. Holthoff, H.; Egelhaaf, S. U.; Borkovec, M.; Schurtenberger, P.; Sticher, H., Coagulation rate measurements of colloidal particles by simultaneous static and dynamic light scattering, *Langmuir* **1996,** *12*, 5541-49.

22. Behrens, S. H.; Borkovec, M., Influence of the secondary interaction energy minimum on the early stages of colloidal aggregation, *Journal of Colloid and Interface Science* **2000,** *225*, 460-65.

23. Honig, E. P.; Roeberse.Gj; Wiersema, P. H., Effect of hydrodynamic interaction on coagulation rate of hydrophobic colloids, *Journal of Colloid and Interface Science* **1971,** *36*, 97-&.

24. Holthoff, H.; Schmitt, A.; FernandezBarbero, A.; Borkovec, M.; CabrerizoVilchez, M. A.; Schurtenberger, P.; HidalgoAlvarez, R., Measurement of absolute coagulation rate constants for colloidal particles: Comparison of single and multiparticle light scattering techniques, *Journal of Colloid and Interface Science* **1997,** *192*, 463-70.

25. Berne, B. J.; Pecora, R., *Dynamic light scattering*. John Wiley & Sons: New York, NY, 1976.

26. Dickinson, E., Chapter 2. Dispersions of interacting colloidal particles, *Annual Reports on the Progress of Chemistry, Section C: Physical Chemistry* **1983,** *80*.

27. Russel, W. B.; Saville, D. A.; Schowalter, W. R., *Colloidal dispersions*. Cambridge University Press: Cambridge, UK, 1983.

28. Zhang, Y. J.; Cremer, P. S., Interactions between macromolecules and ions: The hofmeister series, *Current Opinions in Chemical Biology* **2006,** *10*, 658-63.

29. Kunz, W.; Lo Nostro, P.; Ninham, B. W., The present state of affairs with hofffieister effects, *Current Opinion in Colloid & Interface Science* **2004,** *9*, 1-18.

30. Tu, R. S.; Breedveld, V., Microrheological detection of protein unfolding, *Physical Review E* **2005,** *72*.

31. Steiner, R. F., Structural transitions of lysozyme, *Biochimica Et Biophysica Acta* **1964,** *79*, 51-&.

32. Georgalis, Y.; Umbach, P.; Raptis, J.; Saenger, W., Lysozyme aggregation studied by light scattering .1. Influence of concentration and nature of electrolytes, *Acta Crystallographica Section D-Biological Crystallography* **1997,** *53*, 691-702.

33. Jacob, J.; Krafft, C.; Welfle, K.; Welfle, H.; Saenger, W., Melting points of lysozyme and ribonuclease a crystals correlated with protein unfolding: A raman spectroscopic study, *Acta Crystallographica Section D-Biological Crystallography* **1998,** *54*, 74-80.

34. Arakawa, T.; Kita, Y., Stabilizing effects of caprylate and acetyltryptophanate on heat-induced aggregation of bovine serum albumin, *Biochimica Et Biophysica Acta-Protein Structure and Molecular Enzymology* **2000,** *1479*, 32-36.

35. Ku, J. R.; Stroeve, P., Protein diffusion in charged nanotubes: "On-off" behavior of molecular transport, *Langmuir* **2004,** *20*, 2030-32.

36. James, S.; McManus, J. J., Thermal and solution stability of lysozyme in the presence of sucrose, glucose, and trehalose, *Journal of Physical Chemistry B* **2012**.

37. Smith, L. J.; Fiebig, K. M.; Schwalbe, H.; Dobson, C. M., The concept of a random coil - residual structure in peptides and denatured proteins, *Folding & Design* **1996,** *1*, R95-R106.

38. Collins, K. D., Charge density-dependent strength of hydration and biological structure, *Biophysical Journal* **1997,** *72*, 65-76.

39. Rubin, J.; Linden, L.; Coco, W. M.; Bommarius, A. S.; Behrens, S. H., Salt-induced aggregation of a monoclonal human immunoglobulin g1, *Journal of Pharmaceutical Sciences* **2013,** *102*, 377-86.

CHAPTER 5

SALT-INDUCED AGGREGATION OF A MONOCLONAL HUMAN IMMUNOGOBULIN G1 ANTIBODY

This chapter builds on the work done in chapter 4 and was adapted from our work published in the *Journal of Pharmaceutical Sciences* **2013,** *102* (2):377-386. Lars Linden, Wayne Coco, Andreas Bommarius, and Sven Behrens also contributed to this work.

5.1 Abstract

Physical stability is critical for any therapeutic protein's efficacy and economic viability. No reliable theory exists to predict stability *de novo,* and modeling aggregation is challenging as this phenomenon can involve orientation effects, unfolding, and the rearrangement of non-covalent bonds inter- and intra-molecularly in a complex sequence of poorly understood events. Despite this complexity, the simple observation of protein concentration-dependent diffusivity in *stable,* low ionic-strength solutions can provide valuable information about a protein's propensity to aggregate at higher salt concentrations and over longer times. We recently verified this notion using two model proteins, and others have shown that this strategy may be applicable to antibodies as well. Here we expand our previous study to a monoclonal hIgG1 antibody and discuss both merits and limitations of stability assessments based on the diffusional virial coefficient k_D. We find this parameter to be a good predictor of relative protein stability in solutions of different chaotropic salts, and a telling heuristic for the effect of kosmotropes. Both temperature and glycosylation are seen to have a strong influence on k_D, and we examine

how these factors affect stability assessments. Protein unfolding is monitored with a fluorescence assay to assist in interpreting the observed aggregation rates.

5.2 Introduction

Antibodies represent the fastest growing class of human therapeutics.[1,2] They treat a wide range of conditions, including transplant rejection, Non-Hodgkin's lymphoma, multiple sclerosis and a variety of cancers.[1] As of March 2012, 34 monoclonal antibodies (mAbs) were approved for sale in the US and EU, 28 of which are actively marketed and nine of the 28 have achieved blockbuster status.[3,4]

Irreversible protein aggregation is a common and undesirable occurrence in many stages of biopharmaceutical manufacturing including during fermentation, purification, formulation, and storage. Aggregates are detrimental because they reduce the efficacy of the treatment,[5] and may elicit an immune response.[6] Due to these concerns, the ICH has regulated that a biological pharmaceutical must have a shelf-life greater than six months (>12 months is recommended) under its prescribed storage conditions to be salable (Q5C ICH § 4.3 (1995)).[7]

The physical stability of antibodies, like that of all proteins, is strongly influenced by their solvent conditions (pH, co-solutes, temperature, ionic strength, etc.).[8,9] Salts play a critical role in protein stability as they are used in buffers, stabilizers, acidifiers and as tonicity agents in pharmaceutical formulations.[8] Salts exert both ion-specific (Hofmeister) and non-specific effects on proteins; consequently, both the salt concentration and salt *type* are crucial factors to understanding protein stability/aggregation.[10]

Often during clinical trials, accelerated tests of protein stability are employed using exaggerated conditions (temperature, shaking, ionic strength, light, relative humidity, etc.). Even these accelerated studies or "stress" tests often take 3 – 6 months to conduct.[8] In order to restrict the number of conditions to be tested, researchers often look to *in silico* screening techniques[11] and to physical or thermodynamic properties indicative of stability.

A commonly used indicator of protein physical stability is the osmotic second virial coefficient B_{22}. This thermodynamic parameter measures protein inter-particle interactions and is most often used to determine crystallization conditions.[12,13] Methods commonly used to determine B_{22}, such as static light scattering,[14,15] analytical ultracentrifugation, or self-interaction chromatography[16] are comparatively time consuming and thus not well suited for high-throughput analysis.[17-19]

We previously proposed a fast and convenient technique for evaluating protein stability, and successfully applied it to two model proteins.[20] Our method for predicting trends of salt-induced aggregation analyzes the protein diffusivity in stable solutions at lower salt concentrations than would be required to actually trigger any appreciable aggregation. In these stable samples, we measure the dependence of protein diffusivity on the protein concentration and evaluate the protein-protein interaction parameter k_D given by the linear coefficient in the virial expansion

$$D(c) = D_0[1 + k_D c + O(c^2)] \qquad \text{(Eqn. 5.1)}$$

where *D(c)* is the concentration dependent mutual diffusion coefficient conveniently accessible by dynamic light scattering in a matter of minutes, D_0 is the diffusion coefficient at infinite dilution, and *c* is the molar protein concentration. The interaction parameter k_D is related to the osmotic virial coefficient

$$B_{22} = \frac{N_A}{2}\int_{2a}^{\infty}\left(1-\exp\left[u(r)/k_BT\right]\right)4\pi r^2 dr \qquad \text{(Eqn. 5.2)}$$

via[21]

$$k_D = 2B_{22} - (\zeta_1 + 2\nu) \qquad \text{(Eqn. 5.3)}$$

Here N_A is Avogadro's number, a the protein radius, $u(r)$ the pair interaction energy as a function of the center-to-center separation between two proteins, k_BT the thermal energy unit, ζ_1 the linear coefficient from the virial expansion of the friction coefficient, and ν the protein's molar volume. As Equation 5.3 shows, k_D accounts for both the thermodynamic protein interaction, reflected in B_{22}, and the hydrodynamic interaction, reflected in ζ_1. Similarly, both thermodynamic and hydrodynamic interactions generally affect aggregation kinetics: the rate constant k_{11} of aggregation in the initial stages, for example, can be expressed as

$$k_{11} = \left[\int_{2a}^{\infty}\frac{\exp(u(r)/k_BT)}{4\pi r^2 D\cdot h(r)}dr\right]^{-1} \qquad \text{(Eqn. 5.4)}$$

Here *h(r)* is a separation dependent hydrodynamic correction to the bulk diffusion coefficient *D*, and the pair potential *u(r)* again represents the thermodynamic interaction. Equation 5.4 strictly applies to irreversible aggregation between isotropically interacting rigid spheres,[22] whereas proteins are generally non-spherical, non-rigid because of their folding/unfolding degrees of freedom, and interact anisotropically because of non-uniform surface charge distributions. One might nonetheless expect the actual rate of protein aggregation to be governed by a similar interplay of thermodynamic and hydrodynamic interaction, the same forces that also determine the interaction parameter k_D (Eqns. 5.2 and 5.3). Experimentally, we have indeed found a very strong correlation between k_D for stable protein solutions of different salt compositions and the stability against aggregation upon further addition of the same salts.[20]

The interaction parameter k_D can thus indicate relative protein stability in a fast assay that does not consume or degrade the protein. Our previous investigation was limited, however, to the model proteins lysozyme and BSA.[20] A recent study by Saluja *et al.*[17] suggests that the concept may be extended to predict the aggregation behavior of monoclonal antibodies and even shows k_D to be a more sensitive indicator of aggregation propensity than B_{22} for the investigated systems.

In this chapter we take a closer look at the limitations of stability assessments based on the interaction parameter k_D when applied to a pharmaceutically relevant monoclonal human immunoglobulin G1 (IgG1) antibody and its aglycosylated counterpart. While the relative stability of these antibodies in different chaotropic solutions is accurately reflected in measured values of k_D, the influence of different

kosmotropic media on protein stability cannot be resolved in the same way. We further show that caution is warranted when interpreting variations in the interaction parameter caused by (de)glycosylation or temperature changes. Lastly, we study the antibodies' folding state during salt-induced aggregation using the hydrophobic residue binding dye 8-anilino-1-naphthalenesulfonic acid (ANS) and relate the findings to the observed aggregate growth.

5.3 Materials and Methods

5.3.1 Antibodies

A pair of human IgG1 monoclonal antibodies (M_W = 145 kDa) was used as the basis for this study. The two proteins were a glycosylated and an aglycosylated version of a protein with the same amino acid sequence and a pI of 8.23. The aglycosylated version was generated by introducing the mutation N297A into the heavy chain as described previously.[23] The purified proteins were provided by Bayer Pharma AG (Germany) in 25 mM acetate buffer (pH 5.5) and 150 mM sodium chloride. The formulation was purified via buffer exchange cross-flow and size-exclusion chromatography, then sterile filtered and frozen in liquid nitrogen. The glycosylated IgG1 was present at 362 μM (52.3 mg/mL) and the aglycosylated antibody was provided at 80 μM (11.49 mg/mL). The concentration of the antibodies was determined prior to experimentation using a molar extinction coefficient of 235,480 $(M*cm)^{-1}$.

5.3.2 Salt Buffer Preparation

All salts used were of > 99% purity, ACS reagent grade. Salt solutions were prepared in the isotonic acetate buffer described above. Solutions contained one of the following: sodium citrate (J.T. Baker)/ citric acid (Sigma-Aldrich), sodium sulfate anhydrous (Sigma-Aldrich), sodium acetate (Sigma-Aldrich)/ acetic acid (Riedel-de Haen, purity 96%), sodium formate (Aldrich), sodium fluoride (BDH), sodium chloride (BDH), sodium bromide (Sigma-Aldrich), sodium nitrate (Sigma-Aldrich), sodium iodide (EMD), sodium thiocyanate (Sigma-Aldrich). After dissolving salt in the buffer described above, the pH was readjusted, if necessary, to 5.5 ± 0.05 using either sodium hydroxide or the appropriate acid (i.e., sulfuric acid for a sulfate solution). The salt solution was then filtered through a hydrophilic polyethersulfone membrane with 0.2 μm pores (Pall Acrodisc® syringe filter with Supor® membrane).

5.3.3 Interaction Parameter Determination

Diffusivity measurements were carried out at 25, 35 and 45 °C, pH 5.5, and ionic strength 0.225 M (175 mM arising from the ubiquitous background buffer described above and 50 mM from the salt being tested). In these conditions the protein remains stable in its native conformation (T_ms shown in Table 5.2 and Appendix C).

Prepared salt solutions and protein solutions were mixed in a Corning black-walled 96-well plate with final protein concentrations between 12 and 180 μM (1.4 and 26 mg/mL). The samples were stirred very gently to provide adequate mixing while avoiding shear-induced aggregation. They were then capped by a layer of silicon oil to prevent solvent evaporation and investigated by dynamic light scattering (DLS) using a

Wyatt DynaPro plate reader, which operates in a backscattering geometry (158^0). A set of experiments (for reasons described in section 5.4.1) using paraffin or white mineral oil instead of silicon to cap wells was also performed. Silicon and paraffin oil had no effect on the readings as they are insoluble in water. Every well was read 10 consecutive times for 20 second each. Diffusivity readings obtained from DLS measurements at the same protein concentration were averaged (e.g. Fig. 5.1).

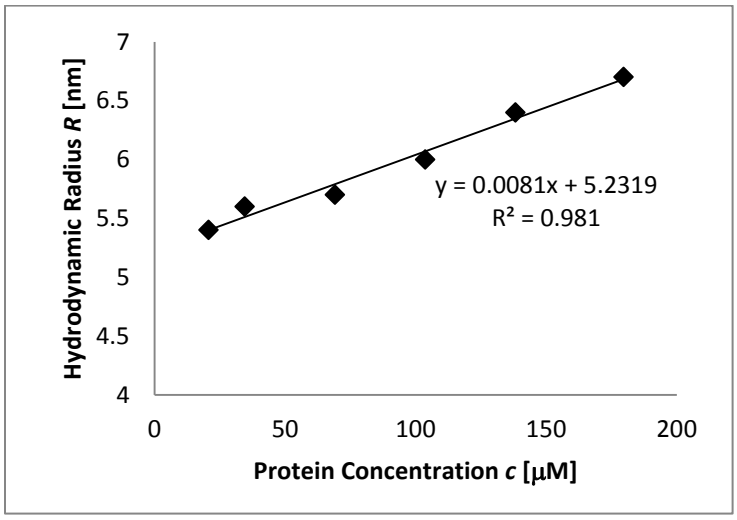

Figure 5.1: Apparent hydrodynamic radius *R(c)* versus protein concentration as measured by dynamic light scattering (DLS) in NaBr at 25^0C. Extrapolation to zero protein concentration yields the actual hydrodynamic protein radius R_0.

The Stokes-Einstein equation (Eqn. 5.5) relates the apparent radius to the mutual diffusion coefficient

$$D = \frac{k_B T}{6\pi\eta R} \qquad \text{(Eqn. 5.5)}$$

where $k_B T$ is the thermal unit and η is the medium viscosity. We can therefore plot

$$\frac{R_0}{R}(c) = \frac{D(c)}{D_0} = 1 + k_D c + O(c^2) \qquad \text{(Eqn. 5.6)}$$

as shown in Figure 5.2 (D_0 is the diffusion coefficient at infinite dilution, found from the infinite dilution radius in Fig. 5.1). The interaction parameter k_D is obtained as the initial slope of this curve (shown in Fig. 5.2 with units of μM^{-1}).

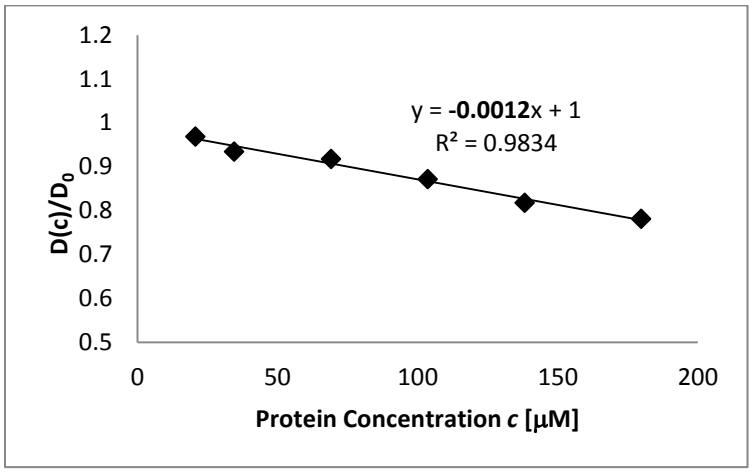

Figure 5.2: Normalized diffusion coefficient versus protein concentration. The slope of the regression line is the interaction parameter.

5.3.4 Aggregation Rate Experiments

Aggregation rate experiments were performed at 35 and 45 °C. Samples were prepared in 96-well plates similarly to the diffusivity experiments; however, in these experiments, a wide range of salt molarities were investigated. The hydrodynamic radius of each sample was tracked over a minimum of 12 hours (Fig. 5.3). The change in particle hydrodynamic radius over time was monitored and used to calculate the initial aggregation rate k_{11}.[20]

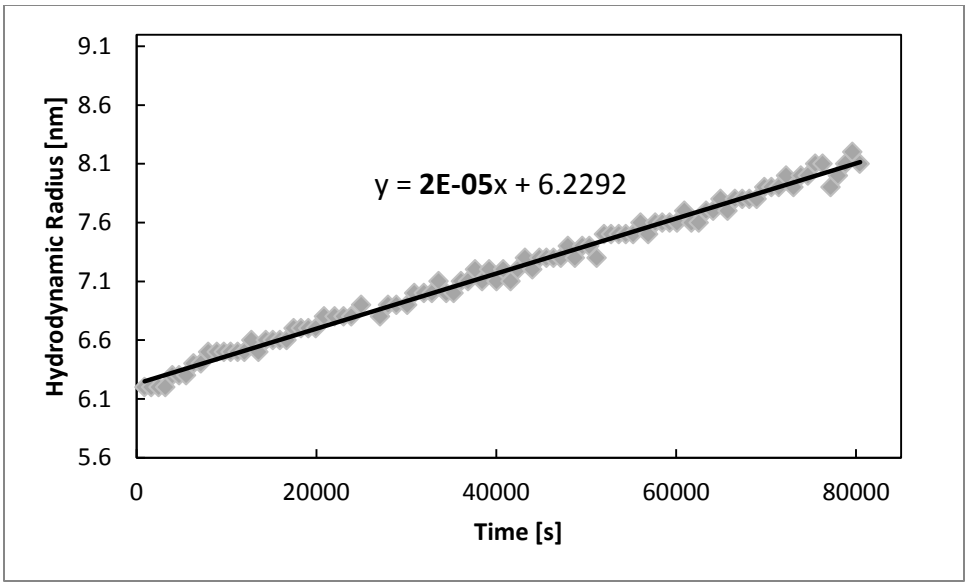

Figure 5.3: Aggregation of the glycosylated antibody in 0.75 M SCN^-. The linear regression line and equation give the initial radius in nm (y-intercept) and change in radius over time in nm/s (slope).

The initial increase of the protein's hydrodynamic radius R_h at the onset of aggregation satisfies (also described in Chapter 4):[24]

$$\frac{1}{R_h(0)}\left(\frac{dR_h(0)}{dt}\right)_{t\to 0} = \frac{I_2(q)}{2I_1(q)}\left(1-\frac{R_{h,1}}{R_{h,2}}\right)k_{11}N_1 \qquad \text{(Eqn. 5.7)}$$

where $R_h(0)$ is the initial value before aggregation sets in, $R_{h,1}$ and $R_{h,2}$ are the hydrodynamic radii of a single protein and a doublet, respectively, and I_1 and I_2 are their respective scattering intensities. N_1 is the number concentration of singlets in solution. The scattering intensities in principle depend on the scattering angle through the wave vector **q**. However, the small proteins considered in this study act as point scatterers for the 830 nm laser wavelength used ($q\,R_h << 1$); therefore, we may safely approximate

$I_2/2I_1$ as unity. Using the geometric relation $R_{h,2}/ R_{h,1} = 1.38$ for spheres,[24] and the measured initial change in size, Eqn. 5.7 simplifies and can be rearranged as follows:

$$k_{11} = \frac{0.275}{R_h(0)N_1}\left(\frac{dR_h(0)}{dt}\right)_{t\to 0} \qquad \text{(Eqn. 5.8)}$$

From Eqn. 5.8 we can solve for the coagulation rate constant k_{11} graphically given that we know N_1 (the number of monomers we begin the experiment with) by measuring $dR_h(0)/dt$ via DLS, as in Fig. 5.3.From Figure 5.3 we can obtain $R_h(0)$ [nm] (y-intercept) and $dR_h(0)/dt$ [nm/s] (slope).

5.3.5 ANS Binding

A solution of 8-anilino-1-naphthalenesulfonic acid (ANS, Sigma-Aldrich) was prepared daily in the acetate buffer described above. Samples were prepared in duplicates in a black-walled 96-well plate. All experiments were conducted at 35 ^{0}C, the protein concentration was 3.5 μM (0.4 mg/mL, for both proteins), and 60 μM ANS was present in each well in addition to the salt in question. For every salt, a pair of wells without protein, but containing the same concentration of salt and ANS, were run as controls. The fully loaded well plate was inserted into a preheated BioTek Instruments Synergy H4 Hybrid Multi-Mode Microplate Reader. Using an excitation wavelength of 360 nm and an emission wavelength of 475 nm, the fluorescence signal in each well was read every ten minutes for 12 hours. The background fluorescence obtained from the protein-free controls was subtracted from each sample's fluorescence. The initial slope in the

logarithm of the fluorescence signal versus time was interpreted as an apparent initial rate of unfolding.

5.3.6 Melting Temperatures

The antibodies' melting temperatures were determined using a Jasco J-810 circular dichroism (CD) spectrophotometer (Easton, MD) equip with a Peltier temperature controller. Experiments were conducted at a protein of 120 μg/ml and ionic strength of 200 mM of a given salt. A linear 1 ^{0}C/minute temperature ramp was run from 30 – 90 ^{0}C and the change in CD ellipticity at 218 nm (β-sheet) was monitored. The data were then normalized and melting temperatures determined by loss of signal.

5.4 Results

5.4.1 Interaction Parameter

Figure 5.4 shows interaction parameters obtained for the glycosylated and non-glycosylated hIgG1 respectively, for a range of different salts and three temperatures. Salts are organized by their Jones-Dole viscosity B-coefficient (at 25 ^{0}C) on the x-axis; this allows the reader to easily distinguish between chaotropic (B < 0) and kosmotropic (B > 0) anions. Table 5.1 lists the ions used in this study along with their B-values taken from the literature.[25]

Table 5.1: Jones-Dole B-coefficient values for anions investigated.[25]

Anion	SCN^-	I^-	ClO_4^-	Br^-	Cl^-	HCO_2^-	F^-	SO_4^{2-}	$CH_3CHO_2^-$
B-value	-0.103	-0.068	-0.061	-0.032	-0.007	0.052	0.10	0.208	0.25

Although weak intermolecular interactions, such as reversible dimerization are possible at the protein concentrations used and would alter the value of k_D, we do not observe such phenomena as evidenced by the polydispersity index of 0.1 for most of our measurements (the lowest possible reading for our instrument).

The interaction parameters for the glycosylated antibody (Figure 5.4A) follow a clear trend along the lines of the Hofmeister series. This trend gets blurred with increasing temperature. The most chaotropic salt investigated (thiocyanate, B = -0.103) yields the most negative k_D. Less chaotropic salts lead to larger (less negative) values of k_D. Kosmotropes give k_D values similar to each other at all three temperatures and yield the least negative k_D values.

Sulfate (B = 0.208) is the only divalent ion in this series of experiments. If tested at the same molarity or ionic strength as all the other salts, k_D would have been considerably lower (not shown). However, if we scale the molarity by a factor of 2^6 then sulfate behaves more similar to the other kosmotropes (Figure 5.4). Such scaling by the inverse sixth power of the counterion's valency is familiar from the classical Schulze-Hardy rule for the critical coagulation constant (CCC) of charged colloidal particles.[26]

The non-glycosylated antibody's k_D values (Figure 5.4B) are generally more negative than the values for their glycosylated counterpart. As with the glycosylated protein, the clearest trend is observed for the non-glycosylated protein at 25 ^{0}C. The most chaotropic counterions lead to the lowest k_D and most kosmotropic counterions to the highest. At elevated temperatures (35 and 45 ^{0}C), k_D does not vary significantly between salts, and substantial scatter makes it difficult to discern any systematic trend.

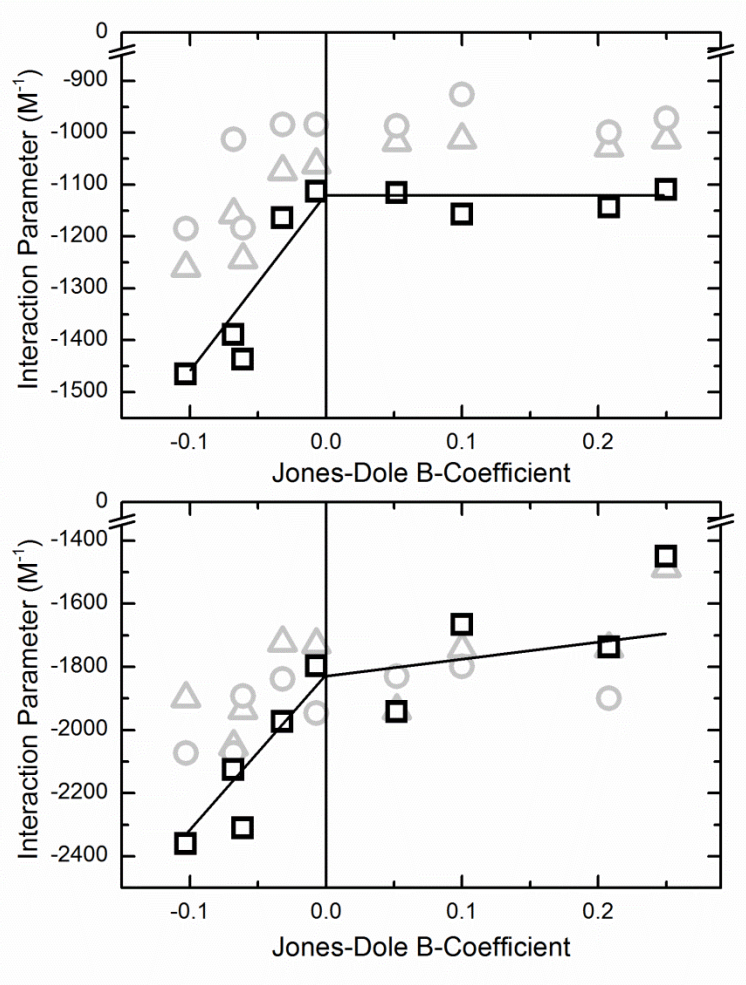

Figure 5.4: Interaction parameters for glycosylated (A) and non-glycosylated (B) IgG1 at 25°C (□), 35° (Δ), and 45°C (○). Error for k_D at 25 ^{0}C is presented in Table 5.2.

To ensure that the silicon oil was not affecting our k_D measurements, we performed k_D experiments with the non-glycosylated protein using paraffin oil (Fig. 5.5) or white mineral oil (not shown) as the capping oil. The use of paraffin or silicon oil to cap wells produced generally similar results with respect to the Hofmeister trend observed at 25 ^{0}C and lack thereof at higher temperatures; either oil is suitable for this application. The results from experiments with white mineral oil are not shown because of significant scatter; we do not recommend using white mineral oil for this application.

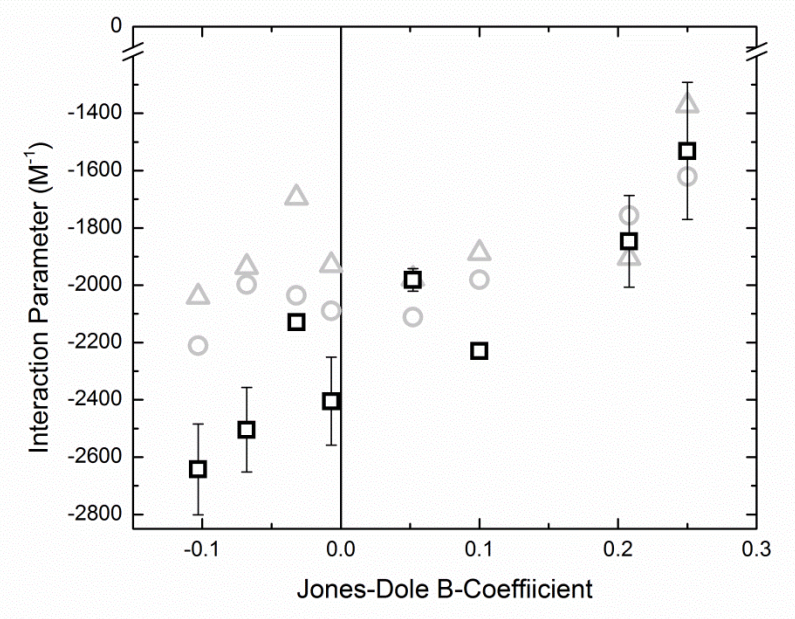

Figure 5.5: Interaction parameters for the aglycosylated protein at 25 ^{0}C (□), 35 ^{0}C (Δ), and 45 ^{0}C (o) using paraffin oil to prevent solvent evaporation.

While plots of the *normalized* diffusion coefficient *D(c)/D0* as in Fig. 5.4 are useful because they directly yield k_D, this representation does not allow to judge the absolute magnitude of the diffusion coefficient. In Fig. 5.6 we have therefore also plotted the absolute diffusion coefficient D_0 used for the normalization and obtained by extrapolating the measured diffusivities to zero antibody concentration. In this limit, the diffusivity should not be affected by specific, ion-mediated protein-protein interaction, and Fig. 5.6 confirms that D_0 does not depend on the type of salt ion present but only on temperature, as one should expect. The values for both the glycosylated and aglycosylated antibody are approximately the same, as one would expect since the two proteins are macroscopically the same [only differing in their glycosylation patterns].

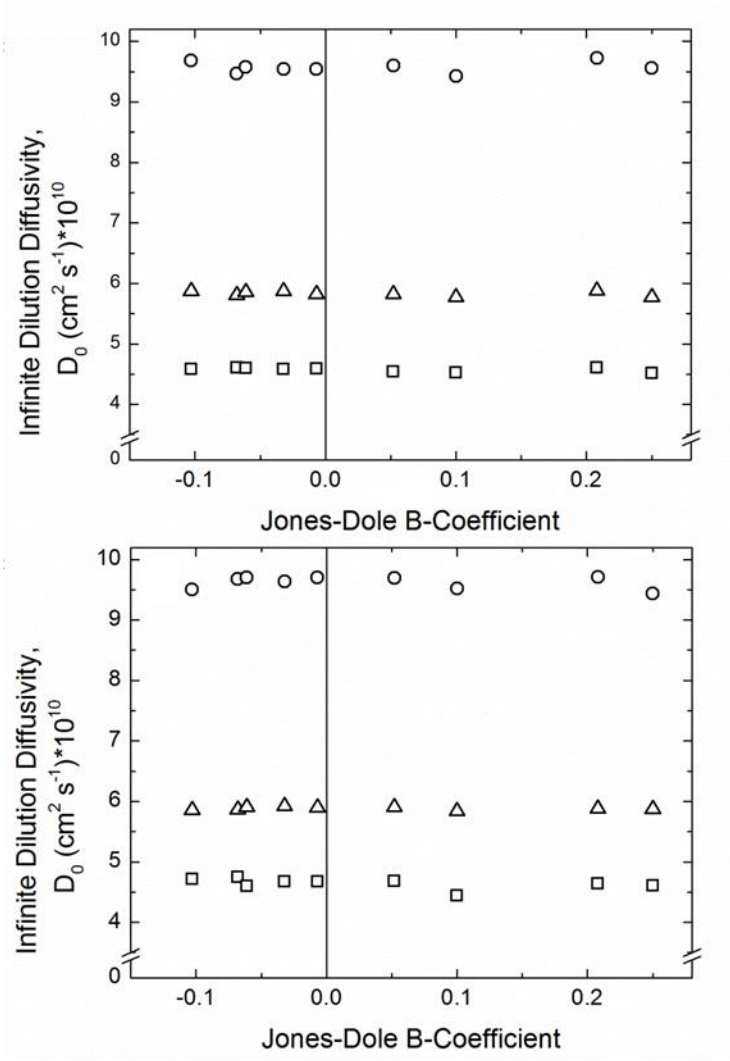

Figure 5.6: Infinite dilution diffusivities for the glycosylated (top) and aglycosylated (bottom) IgG1 at 25 ^{0}C (□), 35 ^{0}C (Δ), and 45 ^{0}C (o).

5.4.2 Aggregation Kinetics

Elevated salt concentrations were employed to induce aggregation of our IgG1 antibodies, and the salt-dependent aggregation rates were measured using DLS. Little to no aggregation was observed for most salts at 25^{0}C over 24 hours (not shown). However, aggregation could be detected more easily and in a shorter time frame (12 hours) at 35^{0}C; these data are presented in Figure 5.7. Accelerating aggregation by means of increasing

temperature is a common method for fast assessments of long-term stability.[8,27] Aggregation experiments at 45^{0}C were also conducted (Fig. 5.8).

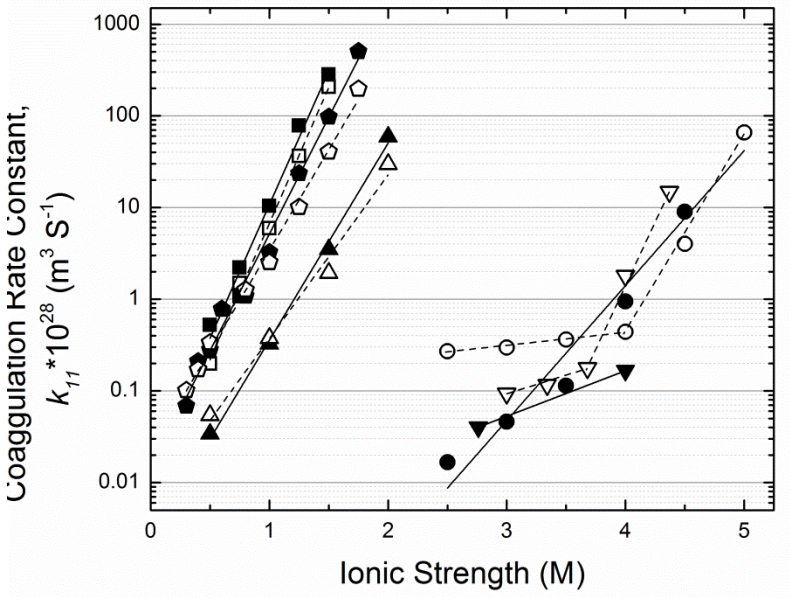

Figure 5.7: Coagulation rate constants as function of ionic strength at 35°C for thiocyanate (■), iodide (▲), perchlorate (pentagon), bromide (●), and chloride (▼). Closed icons are for the glycosylated antibody and open icons are for aglycosylated. Fitting error bars (not shown) generated by Excel Linest were on the order of or smaller than the data point icons.

In the 25 mM acetate background buffer at 35^{0}C, the glycosylated protein did not aggregate over 12 hours; however, the aglycosylated antibody aggregated over 12 hours at a rate of k_{11} = 0.081*10^{-28} m^3/s. At 45^{0}C, the rate constants of aggregation for the glycosylated and aglycosylated mAbs were k_{11} = 0.2*10^{-28} and 0.55*10^{-28} m^3/s, respectively.

Figure 5.7 shows the aggregation rate constant k_{11} of both antibodies in solutions of different chaotropes. As with the interaction parameter, we see a Hofmeister trend where k_{11} at constant ionic strength generally increased with increasing chaotropicity. Thiocyanate caused aggregation at the lowest ionic strength (~1 M), and weaker

chaotropes, such as bromide and chloride, required much higher salt concentrations (~4 M) to destabilize the protein. Surprisingly, glycosylation did not systematically affect the aggregation rates (Fig. 5.7): in the presence of very strong chaotropes (thiocyanate, iodide, and perchlorate) no significant differences between the aggregation rates of glycosylated and aglycosylated antibodies are observed at all, whereas for the weak chaotrope bromide glycosylation does appear to provide some stabilization. This effect, however, is significant only at ionic strengths (below 4 M NaBr) where aggregation is already slow (< 10^{-28} m^3/s).

Complementing the reported aggregation data at 35^{0}C, Figure 5.8 shows aggregation rate constants measured at 45^{0}C. Aggregation rates were roughly an order of magnitude faster at 45 ^{0}C versus 35^{0}C, but still showed the same Hofmeister trend.

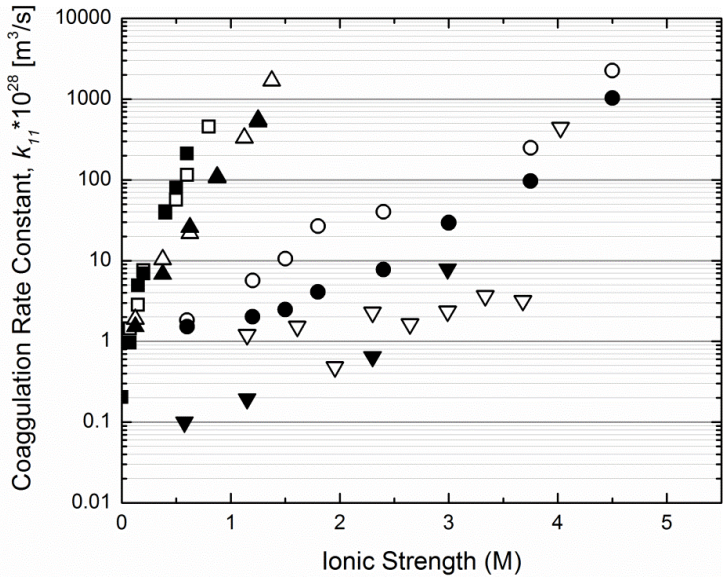

Figure 5.8: Coagulation rate constants as function of ionic strength at 45°C for the chaotropic anions thiocyanate (■), iodide (▲), bromide (●), and chloride (▼). Solid markers are for the glycosylated antibody and open markers are for the aglycosylated one.

Aggregation experiments with kosmotropes are summarized in Figure 5.9. Unlike experiments with chaotropes, they did not show a simple increase in k_{11} with increasing kosmotropicity. Instead, three regimes were apparent: (1) no observable aggregation, (2) slow aggregation, and (3) rapid aggregation with almost instantaneous precipitation. Coagulation rate constants in regime (2) (not shown) were all below 10^{-28} m^3/s and showed no systematic trend. Regime (3) aggregated too fast to measure. Interestingly, for acetate and formate, moderate salt concentrations did not induce any aggregation (regime (1)). With acetate, precipitation or gelation of either antibody (i.e. regime (3)) could not be achieved in the entire ionic strength range (up to 3.75 M).

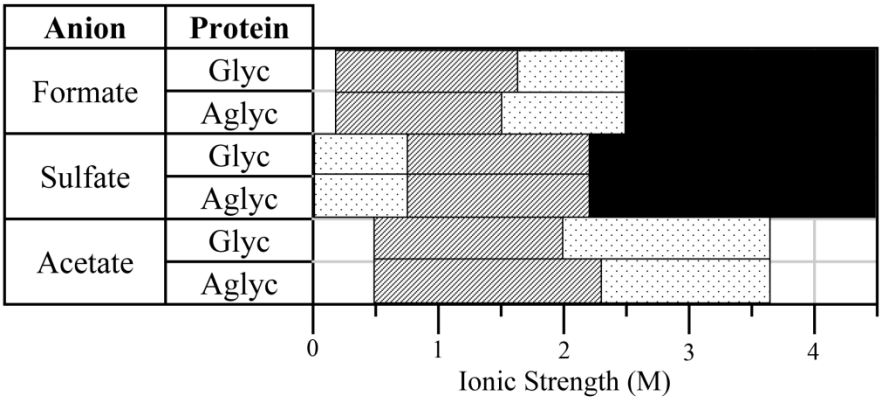

Figure 5.9: Molarities of a given kosmotropes to induce no aggregation (dotted), slow aggregation (shaded grey, $k_{11} < 1*10^{-28}$ m^3 s^{-1}) or instantaneous aggregation (black) for glycosylated ("Glyc") and aglycosylated ("Aglyc") antibodies.

To aid stability comparisons in the chaotropic solutions, we adopt as a metric for the stability against salt-induced aggregation the ionic strength I_s required to trigger aggregation at an initial rate of $k_{11} = 10^{-28}$ m^3 s^{-1}. This same reference value of k_{11} was previously used in our study of lysozyme and BSA in Chapter 4.[28] The results for I_s, along with the values of the interaction parameter k_D, are reported in Table 5.2.

Table 5.2: Summary of interaction parameters at 25^{0}C, ionic strength I_s at k_s (k_{11} = 1*10^{-28} m^3/s), and CD determined melting temperatures (± 1 ^{0}C). Two T_ms are reported because IgGs exhibit two-stage melting behavior corresponding to the melting of the Fc and Fab domains. CD melts are presented in Appendix C. The error reported for k_D is the fitting error as determined by the Excel Linest function.

Ion	Glycosylated			Non-glycosylated		
	I_s (M)	k_D (M^{-1})	T_{m1}/T_{m2} (^{o}C)	I_s (M)	k_D (M^{-1})	T_{m1}/T_{m2} (^{o}C)
SCN^-	0.65	-1465 ± 75	-	0.71	-2233 ± 192	-
I^-	1.21	-1387 ± 54	-	1.19	-2125 ± 245	-
ClO_4^-	0.72	-1436 ± 143	66/77	0.76	-2310 ± 155	66/78
Br^-	3.99	-1164 ± 76	-	4.18	-1973 ± 171	-
Cl^-	N/A	-1113 ± 31	69/79	3.96	-1796 ± 154	68/76
HCO_2^-	N/A	-1115 ± 81	-	N/A	-1941 ± 134	-
F^-	-	-1157 ± 21	-	-	-1665 ± 153	-
SO_4^{2-}	N/A	-1143 ± 44	73/80	N/A	-1737 ± 332	70/78
$CH_3CHO_2^-$	N/A	-1109 ± 30	-	N/A	-1450 ± 248	-

5.4.3 Correlating k_D and I_s

Figure 5.10 presents the correlation between the ionic strength I_s inducing aggregation at a rate of $k_{11} = 10^{-28}$ m^3 s^{-1} and the protein – protein interaction parameter k_D. Only data for the chaotropic counterions are plotted, for reasons discussed earlier.

A strong correlation is found for the glycosylated protein (R^2 = 0.99) and a fair correlation for the aglycosylated protein (R^2 = 0.82). The lower R^2 for the aglycosylated protein is likely derived from the greater uncertainty in k_D (see Table 5.2).

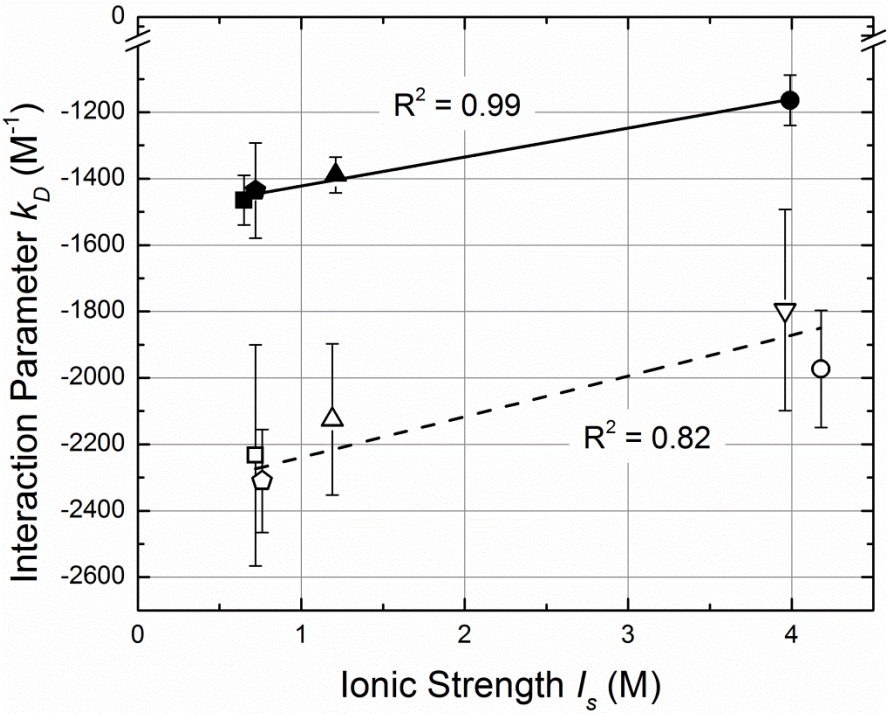

Figure 5.10: Correlating the ionic strength at k_{11} = 1*10^{-28} m^3/s for thiocyanate (■), iodide (▲), perchlorate (pentagon), bromide (●), and chloride (▼) to their respective interaction parameters with fitting error bars shown. Closed icons are for the glycosylated antibody and open icons are for the aglycosylated form.

5.4.4 Unfolding and Aggregation

In chaotropic solutions, increasing salt concentrations always led to faster aggregation (Fig. 5.7); in kosmotropic solutions (Fig. 5.9), however, the same was not always true. In acetate and formate, both antibodies aggregated slowly at low salt concentrations, but at moderate concentrations no aggregation was observed. We suspected that the antibodies' folding state had a strong bearing on this behavior and conducted ANS binding experiments to examine the role of unfolding in the aggregation process.

ANS is a dye which becomes strongly fluorescent upon binding to exposed hydrophobic residues. The more unfolded a protein is, the more ANS binds to it and enhances the fluorescence intensity.[29] By monitoring the fluorescence signal we

determined the extent of unfolding at the beginning of data acquisition (t = 0) and the *rate* of unfolding at this time in aggregating samples.

Figures 5.11A and B show the rate of protein unfolding (ANS binding) and initial extent of unfolded states in chaotropes, respectively. Chaotropes cause a rapid rate of unfolding/ denaturation (Fig. 5.11A) and significant immediate unfolding upon addition of salt (Fig. 5.11B). The ionic strength at which the unfolding rate in a solution of a given salt becomes non-zero roughly matches our DLS results for the ionic strength at which we could first detect aggregation (Figure 5.7). Further, as one can see in the k_{11} curves (Figure 5.7), a 'kink' was found for chloride and bromide; these kinks are also present in our ANS experiments (Figure 5.11A) at the same ionic strengths (for chloride and bromide between 3.2 – 3.7 M and 3.6 – 4.2 M, respectively).

Figure 5.11B demonstrates that some salt concentrations induced significant immediate unfolding, such as thiocyanate above 1.5 M. For the thiocyanate concentrations above 1.5 M, for example, aggregates were visible to the eye within seconds, indicating that a high degree of unfolding leads to almost instantaneous aggregation. Bromide and chloride above 2.5 M also begin to show some degree of unfolding at time zero, signifying incipient instability.

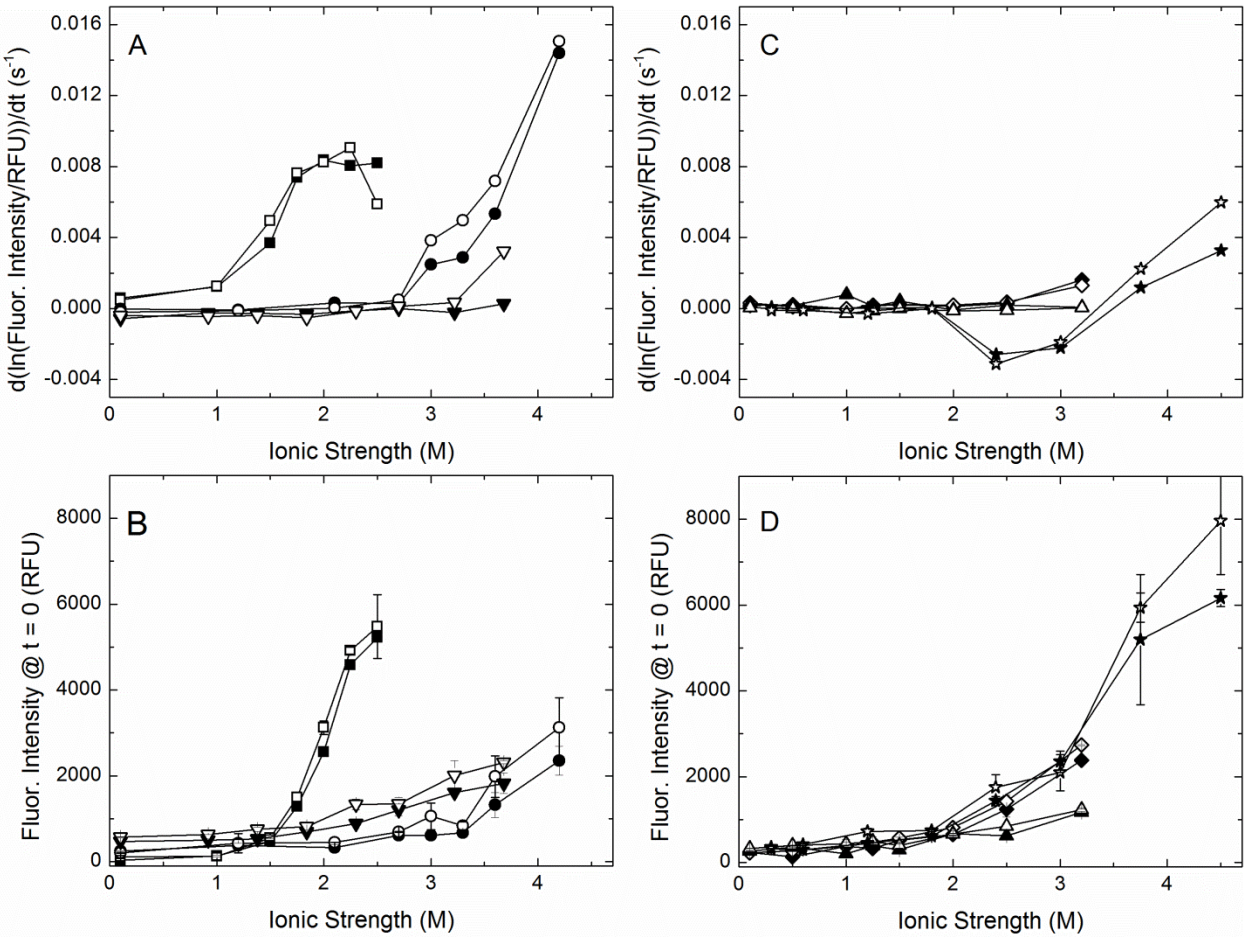

Figures 5.11: ANS binding rates for chaotropes (A) and kosmotropes (C); fitting error bars generated by Excel Linest were on the order of or smaller than the data point icons. Initial ANS binding is displayed for chaotropes (B) and kosmotropes (D); error shown is ± SD. Chaotropes (A, B) include thiocyanate (■), bromide (●), and chloride (▼). Kosmotropes (C, D) include formate (♦), acetate (▲) and sulfate (hexagon). Closed icons are for the glycosylated and open icons are for aglycosylated antibody.

Figures 5.11C and D describe the rate of ANS binding and initial ANS binding (t= 0), respectively, for both antibodies in the presence of kosmotropes. Sulfate stabilizes the folded structure below an ionic strength of 1.5 M, beyond which we see the initial unfolding rate become non-zero; at I = 2 - 3 M the rate of binding decreased over time, and beyond 3 M instantaneous precipitation occurred. The decrease in ANS binding at

I=2-3 M is likely an effect of the protein equilibrating with the sulfate solution and refolding over time; thus reducing ANS binding.

In the presence of acetate or formate, the rate of unfolding for both proteins is zero (Fig. 5.11C) and both proteins are in their native conformation (Fig. 5.11D) up to 1.5 M salt. At 2 M salt, both antibodies show some degree of unfolding (Fig. 5.11D), yet the rate of unfolding is zero (Fig. 5.11C). It is likely that the rate of the slight unfolding in this instance is too rapid to measure. This result indicates that despite modest unfolding, the antibodies are still stable. This stable, slightly unfolded conformation helps explain why at moderate concentrations of acetate and formate no aggregation is observed (Figure 5.9).

Glycosylation is seen to have a small stabilizing effect on the folding structure in chloride, bromide and sulfate solutions. Acetate and formate solutions were generally stable, therefore, no significant difference in stability was observed due to glycosylation.

From these experiments we find that substantial aggregation and substantial unfolding always go hand in hand. In the case of formate and acetate, however, slow aggregation is found without significant unfolding (below 1.5M) and slight unfolding without aggregation (at 2.0 - 2.5 M formate or above 2.5 M acetate).

5.5 Discussion

5.5.1 Manifestation of Hofmeister Effects

In all three sets of experiments (interaction parameter, salt-induced aggregation, and unfolding state experiments), a common trend along the lines of the Hofmeister series

was observed. Chaotropes introduced instability, the extent of which depended on the chaotropicity of the anion. Kosmotropes stabilized the antibodies; however, the effect of different kosmotropes did not vary greatly. This Hofmeister trend, where chaotropes vary significantly, but kosmotropes do not, has been observed previously in the case of lysozyme's propensity to aggregate[20] and the kinetic destabilization of horse liver alcohol dehydrogenase, α-chymotrypsin, and mRFP activity.[30]

This phenomenon can be rationalized by chaotropes' natural tendency to accumulate *at* the protein surface while kosmotropes act *around* the protein. Weakly hydrated chaotropes adsorb onto hydrophobic surfaces or interfaces (such as air-water interfaces or hydrocarbons on proteins).[31,32] The more chaotropic the ion, the stronger this effect and more tightly the ion will bind to a protein[33] and in turn the greater the observed effect.

The lack of difference between the effects of kosmotropes can be attributed to their *indirect* effect on protein. Kosmotropes are strongly hydrated ions, meaning they interact preferentially with water and not with the proteins' surface.

Aggregation in presence of sulfate and formate showed a three-stage behavior; precipitation did not occur in acetate (see Table 5.1). At moderate salt concentrations for acetate and formate (regime 1), both antibodies were well stabilized. Although the DLS data showed no aggregation, ANS experiments revealed that some degree of unfolding occurred (Fig 5.11D). The slightly unfolded state was stable, as the rate of unfolding was zero (Fig 5.11C). This type of behavior is reminiscent of salting-in behavior. Although kosmotropes are classically known as salting-out agents, the phenomena of kosmotropic anions at low concentrations salting-in at a pH below the isoelectric point is well known

as the "reverse" Hofmeister series (in this case pH = 5.5, pI = 8.23).[34,35] The origin of this behavior is not well established, but it has been argued that that the strongly hydrated kosmotropic counterions can stabilize dispersions by inducing repulsive structural forces.[36]

In all, we found acetate, the strongest kosmotrope tested, to be the most stabilizing anion. Additionally, it provides the benefit of excellent buffering properties.

5.5.2 Temperature Effects

Temperature was varied in both the aggregation rate and interaction parameter experiments. As one might expect, increasing temperature accelerated aggregation; aggregation rates at 45 ^{0}C were greater for all salts than those at 35 ^{0}C. As the temperature was raised from 25 ^{0}C to 45 ^{0}C the difference between k_D values of different anions decreased significantly, rendering k_D a less sensitive indicator of ion-specific interactions.

The k_D values also became less negative with increasing temperature. From our studies on lysozyme and BSA, we observed that larger k_D values were strongly correlated with increased stability when comparing solution of identical ionic strength and temperature, but different ionic composition.[20] From our current study, we see that stability variations with changing temperature at a fixed solution composition cannot be inferred in the same way from the interaction parameter. A temperature increase and the ensuing viscosity decrease significantly raise the overall magnitude of the diffusion coefficient, rendering relative variations due to protein interactions less significant and

thus reducing the magnitude of k_D and its sensitivity to the medium composition. We therefore recommend determining the interaction parameter at 25 ^{0}C.

5.5.3 Glycosylation

Although glycosylation is well known for its stabilizing effect[37], this study only revealed few instances in which the behavior of the glycosylated and aglycosylated antibody differed systematically, and usually these differences were not very pronounced. The observable most sensitive to glycosylation was the interaction parameter k_D, as can be appreciated by comparing the scales of Figures 5.4A and B. Aggregation rates (Figure 5.7), by contrast, were not affected nearly as much (and not at all in the presence of strong chaotropes).

We may rationalize why k_D appears generally more sensitive to glycosylation than k_{11} by considering their dependence on the interaction energy profile *u(r)* illustrated in Figure 5.12. While the aggregation rate k_{11}, according to Eq. 5.4, is governed by the maximum (barrier height) in *u(r)*, the interaction parameter k_D (Eqs. 5.2 and 5.3) is most sensitive to the depth of the primary energy minimum reached upon contact. Modulations of the protein-protein interaction that affect both energy extrema should alter both k_D and k_{11}, but the very short-ranged steric interaction due to oligosaccharides, may change the depth of the energy at contact without extending far enough to strongly affect the energy barrier.

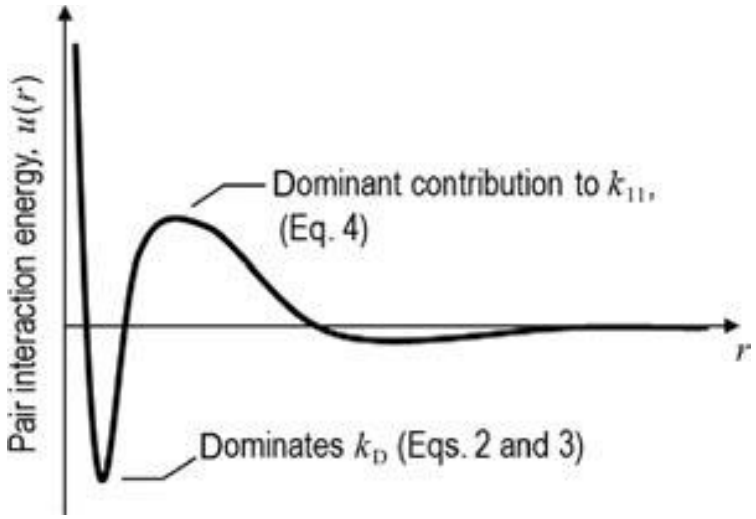

Figure 5.12: Pair interaction potential profile

We nonetheless note that glycosylation does lower the rate of aggregation in the presence of bromide in a regime below 4 M (Figure 5.7) where glycosylation also appears to reduce the rate and extent of unfolding according to the ANS experiments (Figure 5.11). Finally, in the presence of chloride, the aglycosylated antibody showed a nonzero unfolding rate at high ionic strength (Figure 5.11A) and achieved aggregation rates of $k_{11} > 1*10^{-28}$ m^3/s, whereas the glycosylated antibody did neither.

5.6 Conclusion

Previously, the "protein interaction parameter" k_D accessible by DLS was shown to be a fast and reliable predictor for the ion-specific destabilization of globular model proteins by different sodium salts.[20] This work extends the study to the ion-induced destabilization of a monoclonal human IgG1 antibody, with regard to both the aggregation and folding state of the antibody, and additionally examines the influence of temperature and glycosylation. In agreement with our previous work, this work shows that a significantly lower k_D for one electrolyte composition over another at the same ionic strength is

suggestive of lower relative stability. The interaction parameter k_D was best determined at room temperature (25 ^{0}C) as higher temperatures obscured Hofmeister effects. This interaction parameter was found to be a good predictor of ion specific aggregation trends in the chaotropic regime and a telling heuristic in kosmotropic solutions. We found k_D to be very sensitive to glycosylation. Despite the strong influence of both temperature and glycosylation on k_D, these effects do not correlate with stability.

Accelerated tests of protein stability are a critical part of bringing a drug to market quickly. We have shown that, when interpreted with caution, the interaction parameter for stable protein solutions can offer valuable clues about the relative stability in much more saline, aggregating conditions. The required diffusivity data are accessible fast and without sample degradation by a non-invasive, high-throughput technique, making the analysis of interaction parameters a highly promising tool for faster and more directed screening of therapeutic proteins.

5.7 References

1. Carter, P. J., Potent antibody therapeutics by design, *Nature Reviews Immunology* **2006,** *6*, 343-57.

2. Daugherty, A. L.; Mrsny, R. J., Formulation and delivery issues for monoclonal antibody therapeutics, *Advanced Drug Delivery Reviews* **2006,** *58*, 686-706.

3. Elvin, J. G.; Couston, R. G.; van der Walle, C. F., Therapeutic antibodies: Market considerations, disease targets and bioprocessing, *International Journal of Pharmaceutics* **2011**.

4. Reichert, J. M., Marketed therapeutic antibodies compendium, *Mabs* **2012,** *4*, 413-15.

5. Schellekens, H., Immunogenicity of therapeutic proteins: Clinical implications and future prospects, *Clinical Therapeutics* **2002,** *24*, 1720-40.

6. Rosenberg, A. S., Effects of protein aggregates: An immunologic perspective, *Aaps Journal* **2006,** *8*, E501-E07.

7. Ganan-Jimenez, A.; Brake, B., Q5c -stability testing of biotechnological / biological products. ICH, Ed. 1995.

8. Allen, L. V.; Popovich, N. G.; Ansel, H. C., *Ansel's pharmaceutical dosage forms and drug delivery systems*. 9th ed.; Lippincott Williams & Wilkins: Philadelphia, 2010.

9. Chi, E. Y.; Krishnan, S.; Randolph, T. W.; Carpenter, J. F., Physical stability of proteins in aqueous solution: Mechanism and driving forces in nonnative protein aggregation, *Pharmaceutical Research* **2003,** *20*, 1325-36.

10. Baldwin, R. L., How hofmeister ion interactions affect protein stability, *Biophysical Journal* **1996,** *71*, 2056-63.

11. Lauer, T. M.; Agrawal, N. J.; Chennamsetty, N.; Egodage, K.; Helk, B.; Trout, B. L., Developability index: A rapid in silico tool for the screening of antibody aggregation propensity, *Journal of Pharmaceutical Sciences* **2012,** *101*, 102-15.

12. Liu, W.; Cellmer, T.; Keerl, D.; Prausnitz, J. M.; Blanch, H. W., Interactions of lysozyme in guanidinium chloride solutions from static and dynamic light-scattering measurements, *Biotechnology and Bioengineering* **2005,** *90*, 482-90.

13. Chi, E. Y.; Krishnan, S.; Kendrick, B. S.; Chang, B. S.; Carpenter, J. F.; Randolph, T. W., Roles of conformational stability and colloidal stability in the aggregation of recombinant human granulocyte colony-stimulating factor, *Protein Science* **2003,** *12*, 903-13.

14. Alford, J. R.; Kendrick, B. S.; Carpenter, J. F.; Randolph, T. W., Measurement of the second osmotic virial coefficient for protein solutions exhibiting monomer-dimer equilibrium, *Analytical Biochemistry* **2008,** *377*, 128-33.

15. Attri, A. K.; Minton, A. P., New methods for measuring macromolecular interactions in solution via static light scattering: Basic methodolog, and application to nonassociating and self-associating proteins, *Analytical Biochemistry* **2005,** *337*, 103-10.

16. Tessier, P. M.; Lenhoff, A. M.; Sandler, S. I., Rapid measurement of protein osmotic second virial coefficients by self-interaction chromatography, *Biophysical Journal* **2002,** *82*, 1620-31.

17. Saluja, A.; Fesinmeyer, R. M.; Hogan, S.; Brems, D. N.; Gokarn, Y. R., Diffusion and sedimentation interaction parameters for measuring the second virial coefficient and their utility as predictors of protein aggregation, *Biophysical Journal* **2010,** *99*, 2657-65.

18. Lehermayr, C.; Mahler, H. C.; Mader, K.; Fischer, S., Assessment of net charge and protein-protein interactions of different monoclonal antibodies, *Journal of Pharmaceutical Sciences* **2011,** *100*, 2551-62.

19. Bommarius, A. S.; Broering, J. M.; Chaparro-Riggers, J. F.; Polizzi, K. M., High-throughput screening for enhanced protein stability, *Current Opinion in Biotechnology* **2006,** *17*, 606-10.

20. Rubin, J.; San Miguel, A.; Bommarius, A. S.; Behrens, S. H., Correlating aggregation kinetics and stationary diffusion in protein-sodium salt systems observed with dynamic light scattering, *Journal of Physical Chemistry B* **2010,** *114*, 4383-87.

21. Saito, S.; Hasegawa, J.; Kobayashi, N.; Kishi, N.; Uchiyama, S.; Fukui, K., Behavior of monoclonal antibodies: Relation between the second virial coefficient (b(2)) at low concentrations and aggregation propensity and viscosity at high concentrations, *Pharmaceutical Research* **2012,** *29*, 397-410.

22. Behrens, S. H.; Borkovec, M., Influence of the secondary interaction energy minimum on the early stages of colloidal aggregation, *Journal of Colloid and Interface Science* **2000,** *225*, 460-65.

23. Hristodorov, D.; Fischer, R.; Joerissen, H.; Muller-Tiemann, B.; Apeler, H.; Linden, L., Generation and comparative characterization of glycosylated and aglycosylated human igg1 antibodies, *Molecular Biotechnology* **2012**.

24. Holthoff, H.; Schmitt, A.; FernandezBarbero, A.; Borkovec, M.; CabrerizoVilchez, M. A.; Schurtenberger, P.; HidalgoAlvarez, R., Measurement of absolute coagulation rate constants for colloidal particles: Comparison of single and multiparticle light scattering techniques, *Journal of Colloid and Interface Science* **1997,** *192*, 463-70.

25. Collins, K. D., Ions from the hofmeister series and osmolytes: Effects on proteins in solution and in the crystallization process, *Methods* **2004,** *34*, 300-11.

26. Hiemenz, P.; Rajagopalan, R., *Principles of colloid and surface chemistry*. 3rd ed.; Marcel Dekker: New York, 1997.

27. Weiss, W. F.; Young, T. M.; Roberts, C. J., Principles, approaches, and challenges for predicting protein aggregation rates and shelf life, *Journal of Pharmaceutical Sciences* **2009,** *98*, 1246-77.

28. Rubin, J.; Miguel, A. S.; Bommarius, A. S.; Behrens, S. H., Correlating aggregation kinetics and stationary diffusion in protein-sodium salt systems observed with dynamic light scattering (vol 114, pg 4383, 2010), *Journal of Physical Chemistry B* **2011,** *115*, 10778-78.

29. Semisotnov, G. V.; Rodionova, N. A.; Razgulyaev, O. I.; Uversky, V. N.; Gripas, A. F.; Gilmanshin, R. I., Study of the molten globule intermediate state in protein folding by a hydrophobic fluorescent-probe, *Biopolymers* **1991,** *31*, 119-28.

30. Broering, J. M.; Bommarius, A. S., Evaluation of hofmeister effects on the kinetic stability of proteins, *Journal of Physical Chemistry B* **2005,** *109*, 20612-9.

31. Collins, K. D., Sticky ions in biological-systems, *Proceedings of the National Academy of Sciences of the United States of America* **1995,** *92*, 5553-57.

32. Pegram, L. M.; Wendorff, T.; Erdmann, R.; Shkel, I.; Bellissimo, D.; Felitsky, D. J.; Record, M. T., Why hofmeister effects of many salts favor protein folding but not DNA helix formation, *Proceedings of the National Academy of Sciences of the United States of America* **2010,** *107*, 7716-21.

33. RiesKautt, M.; Ducruix, A., Inferences drawn from physicochemical studies of crystallogenesis and precrystalline state, *Macromolecular Crystallography, Pt A* **1997,** *276*, 23-59.

34. Bostrom, M.; Tavares, F. W.; Finet, S.; Skouri-Panet, F.; Tardieu, A.; Ninham, B. W., Why forces between proteins follow different hofmeister series for ph above and below pi, *Biophysical Chemistry* **2005,** *117*, 217-24.

35. Zhang, Y. J.; Cremer, P. S., The inverse and direct hofmeister series for lysozyme, *Proceedings of the National Academy of Sciences of the United States of America* **2009,** *106*, 15249-53.

36. Peula-Garcia, J. M.; Ortega-Vinuesa, J. L.; Bastos-Gonzalez, D., Inversion of hofmeister series by changing the surface of colloidal particles from hydrophobic to hydrophilic, *Journal of Physical Chemistry C* **2010,** *114*, 11133-39.

37. Sola, R. J.; Griebenow, K., Effects of glycosylation on the stability of protein pharmaceuticals, *Journal of Pharmaceutical Sciences* **2009,** *98*, 1223-45.

CHAPTER 6

GAUGING COLLOIDAL AND THERMAL STABILITY IN HUMAN IGG1 – SUGAR SOLUTIONS THROUGH DIFFUSIVITY MEASUREMENTS

This work was submitted for publication in February 2013 under the same title. Lars Linden, Andreas Bommarius, and Sven Behrens will be authors on this publication as well.

6.1 Abstract

Monoclonal antibodies are the fastest growing class of biotherapeutics. Ensuring their colloidal stability in liquid dispersions is crucial for maintaining therapeutic efficacy and economic viability. Sugars are often added to increase the colloidal and thermal stability of protein; yet, determining which sugar is the most stabilizing requires time and sample-consuming stability tests. Here we show that the extent of stabilization by different sugars can be gauged by analyzing the proteins' diffusive virial coefficient k_D. This protein interaction parameter is measured conveniently in a non-invasive, high-throughput manner using dynamic light scattering. It is found to correlate closely with experimental dimerization rate constants and melting temperatures for antibodies in different sugar solutions. The proposed analysis thus provides a rapid test of the subtle differences between inherently similar sugar-protein interactions; it should greatly facilitate the formulation of protein therapeutics.

6.2 Introduction

Monoclonal antibodies (mAbs) and antibody-derivatives constitute the fastest growing class of biopharmaceuticals.[1] Antibodies are effective in treating a wide range of cancers, autoimmune diseases, inflammation, and potentially even amyloid diseases, such as Alzheimer's.[1-3] As of March 2012, 28 mAbs were actively marketed in the United States and/or the European Union.[4] The combined sale of the top ten grossing antibodies in 2011 was 52.2 billion USD and the commercial market for mAbs is expected to continue to grow rapidly.[5] Six of the top ten selling drugs in 2013 are predicted to be mAbs and nearly 350 antibody-derived therapeutics are currently in development.[5, 6]

Although great advances in antibody engineering have brought many successes to market,[7] the field of biologics still struggles with pervasive physical protein instability (for review see Ref.[2, 8]). Irreversible protein aggregation is a familiar and adverse occurrence during the fermentation, purification, formulation, and storage of biopharmaceuticals, such as antibodies. Aggregates are detrimental because they reduce the therapy's efficacy, are aesthetically undesirable, and, most importantly, may incite an immunogenic response within the patient.[9-11] To avoid these issues, the International Conference on Harmonization and FDA have regulated that a biopharmaceutical must have a shelf-life greater than six months (>12 months is recommended) under manufacturer prescribed storage conditions to be salable [Q5C ICH § 4.3 (1995)].

To comply with governmental regulations, researchers work to optimize the storage solution environment of mAbs by toggling solution parameters such as the pH,

temperature, viscosity, and excipients (salts, sugars, surfactants), to name a few.[12] Sugars are common protein structure stabilizers added to liquid formulations and used to stabilize proteins during lyophilization.[2, 8, 13-15]

According to the preferential interaction model proposed by Arakawa and Timasheff (1982)[13, 16-18] the stabilization of protein solutions by sugar is caused by the preferential hydration of proteins and exclusion of sugar from the protein – water interface. Sugars, having many hydrogen bonding sites, preferentially interact with each other and with the bulk water, rather than with more hydrophobic molecules (*i.e.* proteins). The sugars' preference for staying in the bulk solution creates an *excluded volume* of pure water around protein, and elevates interfacial tension. Following the Le Chatelier's principle, such a system will minimize the water–protein interfacial area to curtail the thermodynamically unfavorable solvent–protein interactions. As a consequence, protein is forced into its most compact conformation: the native state.[17]

Sugars are also employed during lyophilization to prevent cold denaturation of protein.[19] As temperature decreases rapidly, sugars become vitrified and create a rigid, glassy matrix. Proteins are evenly dispersed throughout the sugar matrix and their conformational mobility is severely restricted, thus preventing aggregation.[20-22] An extensive network of hydrogen bonds between the vitrified sugar and dispersed proteins is thought to maintain the native state.[23]

To expedite the formulation process, accelerated stability tests are often conducted at elevated temperatures (30 ^{0}C +); however, these "stress" tests take days to months to conduct and are resource intensive.[2, 24] To minimize *a priori* the number of formulations to be tested, researchers look to *in silico* behavior[25, 26] or thermodynamic

properties, such as T_g or the second osmotic virial coefficient B_{22}, to gauge stability before embarking on lengthy stress tests.[8, 12, 15, 27] Although these measures are useful, none of them are broadly applicable, robust, convenient, and/or fast enough to be effective high-throughput screens of stability.[28-30]

We previously proposed a convenient, high-throughput technique for determining within minutes the relative differences in the long-term stability of protein solutions with different salt compostition.[29, 31] This technique uses rapid dynamic light scattering (DLS) measurements to evaluate the protein – protein interaction parameter k_D in stable dispersions. This interaction parameter is the linear coefficient in the virial expansion of the proteins' mutual diffusion coefficient,

$$D(c) = D_0[1 + k_D c + O(c^2)], \qquad \text{(Eqn. 6.1)}$$

where D_0 is the diffusion coefficient at infinite dilution, and c is the molar protein concentration. k_D is related to the familiar osmotic second virial coefficient B_{22} via[32]

$$k_D = 2B_{22} - (\zeta_1 + 2\upsilon), \qquad \text{(Eqn. 6.2)}$$

where ζ_1 is the linear coefficient from the virial expansion of the friction coefficient, and υ is the protein's molar volume. The thermodynamic (B_{22}) and hydrodynamic (ζ_1) protein-protein interaction that affect protein diffusivity also govern protein aggregation. In the initial stages, aggregation kinetics is characterized the rate constant k_{11} of dimer formation, which can be expressed, in the idealized case of isotropic interaction between rigid spherical proteins, as[33]

$$k_{11} = \left\{ \int_{2a}^{\infty} \frac{\exp[u(r)/k_B T]}{4\pi^2 D \cdot h(r)} dr \right\}^{-1}. \qquad \text{(Eqn. 6.3)}$$

Here, k_BT is a thermal energy unit, the pair interaction energy $u(r)$ reflects the thermodynamic interaction, and $h(r)$ is a separation-dependent hydrodynamic correction to the bulk diffusion coefficient D. We have demonstrated a close connection between experimental values of the aggregation rate constant and the interaction parameter for model proteins[29] and a pair of human IgG1 antibodies in a variety of salt solutions, and pointed out both merits and some limitations[31] of using k_D to infer protein stability. Other research groups have also found k_D to be an apropos and telling indicator of stability for both mAbs and model proteins in saline solutions.[30, 34, 35]

The utility of k_D is not limited to estimating protein stability in salt solutions. The Kalonia and Gokarn groups have shown that k_D, determined in low protein concentrations, is a good predictor of mAb stability in highly concentrated, viscous formulations;[36-38] Mirarefi and Zukoski used k_D to find crystallization conditions for lysozyme;[39] and James and McManus have shown that k_D is a good measure of thermal and colloidal stability for lysozyme – sugar solutions at different pH.[40]

In the present work, we investigate the stabilizing effect of sugars on an aglycosylated human IgG1 antibody using k_D. Although glycosylated mAbs are more commonplace, aglycosylated mAbs are easier, cheaper, and faster to produce; as a result, they are gaining more attention (for review on aglycosylated mAbs see[41]). Aglycosylated mAbs are, in some respects, less stable than their glycosylated counterparts, therefore greater attention much be paid to ensure their colloidal and thermal stability as they enter later clinical trials.[31, 41-44] To quantify colloidal and thermal stability we use the (inverse of the) dimerization rate constant k_{11} and the apparent melting temperature $T_{m,app}$ found though circular dichroism (CD), respectively. All of the sugars investigated improve the

colloidal and thermal stability of our antibody. We find good correlations between k_D and both of our stability measures across the collection of sugars tested.

6.3 Materials and Methods

6.3.1 Antibody Characteristics and Purification

An aglycosylated human immunoglobulin G1 (hIgG1) antibody with a molecular weight of 145 kDa and isoelectric point of 8.23 was used as the basis of this study. The antibody contained a N297A mutation in the heavy chain to eliminate glycosylation on that asparagine residue, as described previously.[45] Bayer Pharma AG (Berlin, Germany) provided the purified protein at 11.49 mg/mL (80μM) in a pH 5.5 buffer containing 25 mM acetate and 150 mM sodium chloride. Purification was performed via size-exclusion and buffer exchange cross-flow chromatography. The protein was then sterile filtrated and frozen in liquid nitrogen. Prior to experimentation, the protein concentration was determined using a molar extinction coefficient of 234,480 M^{-1} cm^{-1}.

6.3.2 Sugar Solution Preparation

All saccharides used were ≥98% purity, unless otherwise stated. Stock sugar solutions were prepared in the isotonic acetate buffer described above. Solutions contained one of the following excipients: D-(-)-fructose, D-(+)-glucose, D-mannitol, D-maltose monohydrate (90%, impurities are glucose and maltotriose), D-(+)-trehalose (Sigma-Aldrich, St. Louis, MS), sucrose (MP Biomedical Inc., Santa Ana, CA), D-sorbitol, or xylitol (Alfa Aesar, Ward Hill, MA). None of the sugars caused the pH to deviate more than 0.05 pH units from 5.5, so no additional pH adjustment was necessary. The sugar

solutions were sterile filtered through a 0.2 μm PallAcrodisc syringe filter with Supor membrane (Pall Corporation, Port Washington, NY).

6.3.3 Interaction Parameter Evaluation

Concentration dependent diffusivity measurements were conducted at 25 ^{0}C in the aforementioned buffer (25 mM acetate, 150 mM sodium chloride, pH 5.5). Samples contained a final concentration of 100 mM of a given sugar. Under these conditions the antibody remains stable in its native conformation for over 24 hours (*i.e.* no change in hydrodynamic radius). Prepared sugar solutions were mixed in Corning black-walled 96-well plates with a final protein concentrations ranging from 1.49 to 10.34 mg/mL (9.24 to 71.31 μM). Samples were gently mixed, then capped by a layer of silicon oil to prevent solvent evaporation. Silicon oil has been shown to have no effect on interaction parameter measurements or aggregation in quiescent systems.[31, 46] Samples were investigated by DLS using a Wyatt DynaPro plate reader instrument (Santa Barbara, CA) to measure protein diffusivity/size. The instrument operates in backscatter geometry (158^0) using the 830 nm wavelength illumination from a GaAs laser. Each sample well was read 10 consecutive times for 30 seconds each. The diffusivity readings were averaged then normalized by the diffusivity at infinite dilution. The interaction parameter k_D was determined as the slope of normalized diffusivity versus protein concentration. An illustrative example of how to calculate k_D is provided in the Chapter 5.

6.3.4 Dimerization Rate Experiments

Aggregation experiments were performed at 5.1 mg/mL antibody at 45 ^{0}C. Each sample contained 500 mM of a given sugar. The refractive index and viscosity of each sugar solution was determined as described and tabulated in the Supporting Information. The antibodies were monomeric and natively folded at the beginning of each experiment, as evidenced by a low initial polydispersity index [coefficients of variation below 0.1 obtained *via* cumulant fit of the intensity autocorrelation function in DLS], uniform initial radii in all sugar solutions, and melting temperatures well above 45 ^{0}C. Samples were prepared in 96-well plates similar to the diffusion experiments. The hydrodynamic radius of each sample was tracked continuously over at least 65 hours. The change in protein hydrodynamic radius over time was monitored and used to calculate the initial aggregation rate constant k_{11}. A sample calculation is presented in the Chapter 5.

6.3.5 Circular Dichroism Melts

The antibody's melting temperature was determined using a Jasco J-810 circular dichroism spectrophotometer (Easton, Maryland) equipped with a Peltier temperature controller. Experiments were conducted at a protein concentration of 120 μg/mL. The same sugar concentration (500 mM) was used for this set as in the aggregation rate measurements. A linear 1 ^{0}C/min temperature ramp was run from 35 ^{0}C to 95 ^{0}C and the ellipiticity of absorbed light was monitored at a wavelength of 218 nm (sensitive to β-sheets). The data were then normalized and the apparent melting temperatures inferred from the loss of 50% of the maximum signal.

The enthalpy change upon melting was calculated by assuming a two-state melting model,

$$N \underset{k_{fold}}{\overset{k_{unfold}}{\rightleftharpoons}} U \quad , \qquad \text{(Eqn. 6.4)}$$

where k_{unfold} and k_{fold} are the rates of unfolding and folding, respectively. An equilibrium constant for this reaction may be written as $K = k_{unfold}/k_{fold}$. We can write the concentration of native [N] and unfolded [U] protein in terms of the total protein concentration C_o and the folded fraction F as $[N] = C_oF$ and $[U] = C_o(1\text{-}F)$ and insert these relationships into the equilibrium constant:

$$K = \frac{k_{unfold}}{k_{fold}} = \frac{[U]}{[N]} = \frac{1-F}{F} \quad . \qquad \text{(Eqn. 6.5)}$$

The Gibb's free energy for the melting experiments may be determined using

$$\Delta G = -RT \ln K = \Delta H^0 - T\Delta S^0 \quad . \qquad \text{(Eqn. 6.6)}$$

If the heat capacities of the folded and unfolded antibodies are the same, then ΔH^o and ΔS^o are constant over the temperature range studied.[47] T_m is taken as the temperature at which half of the protein is folded (F = 0.5):

$$\Delta G(T_m) = -RT_m \ln\left(\frac{1-0.5}{0.5}\right) = \Delta H^0 - T_m\Delta S^0 \quad , \qquad \text{(Eqn. 6.7)}$$

and hence

$$\Delta S^0 = \frac{\Delta H^0}{T_m} \quad . \qquad \text{(Eqn. 6.8)}$$

Combining equations 5, 6, and 8 we obtain the van't Hoff equation, which is used to determine ΔH^o graphically:[47]

$$-RT\ln\left(\frac{1-F}{F}\right)=\Delta H^{0}\left(1-\frac{T}{T_{m}}\right) \qquad \text{(Eqn. 6.9)}$$

6.4 Results and Discussion

6.4.1 Protein Concentration-Dependent Diffusion

The interaction parameter for the hIgG1 was determined in a variety of saccharide solutions (Figure 1). The sign and magnitude of k_D indicate whether the protein interactions are repulsive (positive k_D) or attractive (negative k_D) and how [relatively] strong those interactions are.[40] All of the sugars increased k_D compared to the control, suggesting that they all stabilized the protein to varying degrees. The k_D values for the mono-saccharides (glucose, mannitol, sorbitol, and xylitol) were all similar despite differences in their molecular weight, oxidation state, and number of hydroxyl groups. The di-saccharides (maltose, sucrose, and trehalose) also yielded k_D values comparable to each other (and greater than those obtained from the mono-saccharide solutions). A summary is presented in Table 6.1below.

Table 6.1: Summary of results. Molecular weight M_W, interaction parameters k_D ± fitting error, coagulation rate constants k_{11} ± standard deviation, and melting data are presented.

Sugar type	M_W **[Da]**	k_D **[M^{-1}]**	$k_{11}*10^{30}$ **[$m^3\ s^{-1}$]**	$R_{h,\ t=0}$ **[nm]**	$T_{m,app}$ **[^{0}C]**	$\Delta T_{m,app}$ **[^{0}C]**	ΔH_m **[kcal mol^{-1}]**
Buffer	-	-3279 ± 166	96.6 ± 11	5.6	72.3	-	77.6 ± 3.3
Glucose	180.2	-2571 ± 146	42.2 ± 4	5.5	76.8	4.5	85.7 ± 3.9
Maltose	342.3	-1947 ±315	-	5.6	79.6	7.3	96.4 ± 4.8
Mannitol	182.2	-2564 ± 199	55.9 ± 9	5.2	77.2	4.9	87.9 ± 3.4
Sorbitol	182.2	-2532 ± 94	42.1 ± 3	5.5	77.2	4.9	95.2 ± 1.7
Sucrose	342.3	-1684 ± 117	17.4 ± 3	5.5	80.8	8.5	86.4 ± 3.7
Trehalose	378.3	-2023 ± 194	27.2 ± 13	5.4	78.4	6.1	133 ± 6.5
Xylitol	152.2	-2460 ± 32	-	5.4	75.7	3.4	111.5 ± 5.3

Our calculation of k_D assumes that concentration-dependent changes in diffusivity and apparent protein size are a result of protein – protein interactions and not changes in the *actual* size of the protein. While the actual size of some proteins may change with concentration through reversible self-association, unfolding upon dilution, or aggregation, we do not believe this is the case here.[37, 38] Self-association, should be reflected in the polydispersity. For all of our experiments we consistently observed a polydispersity index of 0.1 (the lowest possible reading for the instrument), so we conclude that our k_D measurements detect the monomeric antibody and are truly measures of protein – protein interactions.

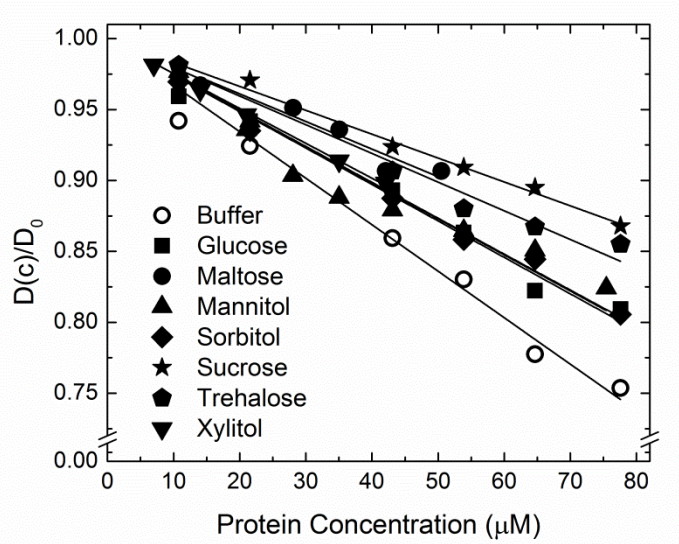

Figure 6.1: Normalized mutual diffusivity versus protein concentration. k_D from the slope of the curves above (Eqn. 6.1).

6.4.2 Thermally-Induced Dimerization

Aggregation was induced thermally at 45 ^{0}C to evaluate how much stabilization the sugars afforded our hIgG1. Little or no aggregation was detected at 35 ^{0}C and aggregation proceeded too rapidly to accurately capture the initial stages at 55 ^{0}C (data

not shown). Figure 6.2 shows the evolution of the protein radius as seen by DLS in a representative aggregation experiment from which k_{11} can be calculated. The k_{11} values for all the sugars tested are presented in Table 6.1.

At 500 mM all of the sugars tested slowed the rate of aggregation compared to the buffered control. Aggregation in di-saccharide solutions was notably slower than aggregation in the presences of the mono-saccharides. Di-saccharides slowed aggregation compared to the control by a factor of about four, whereas mono-saccharides slowed aggregation by a factor of approximately two (Table 1). The greater stabilization in di- versus mono-saccharides may be a result of greater viscosity or to greater exclusion of the sugar from the protein surface.[16, 17] Regardless of the mechanism, these stress tests clearly indicate that sugars like sucrose and trehalose significantly enhance our aglycosylated antibody's stability against aggregation.

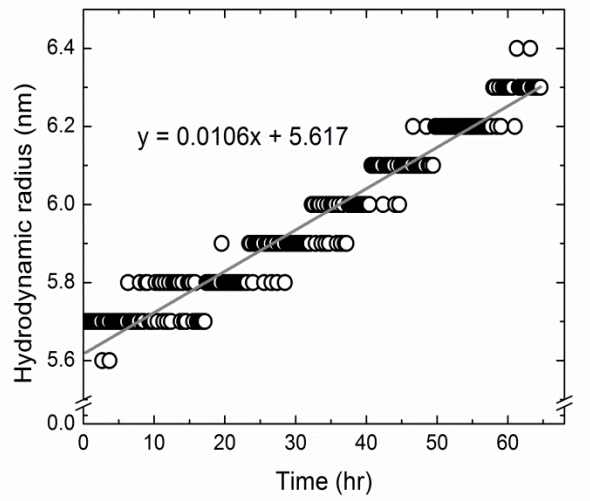

Figure 6.2: hIgG1 aggregation in buffer at 45 ^{0}C over 65 hours. The y-intercept is the initial radius (R_o) and slope (dR/dt) is rate of aggregation. See Chapter 5 for a detailed example of how to calculate k_{11} from this data.

6.4.3 Apparent Melting Temperature and Melting Intermediate

The antibody's apparent melting temperature $T_{m,app}$ was determined in various sugar solutions via CD. These T_m values are "apparent" because the unfolding is partially kinetically controlled, and an absolute T_m measurement would require an infinitely (impractically) slow ramp rate. The reported $T_{m,app}$ are nonetheless a consistent, reproducible approximation of T_m, and useful for comparing different formulations.

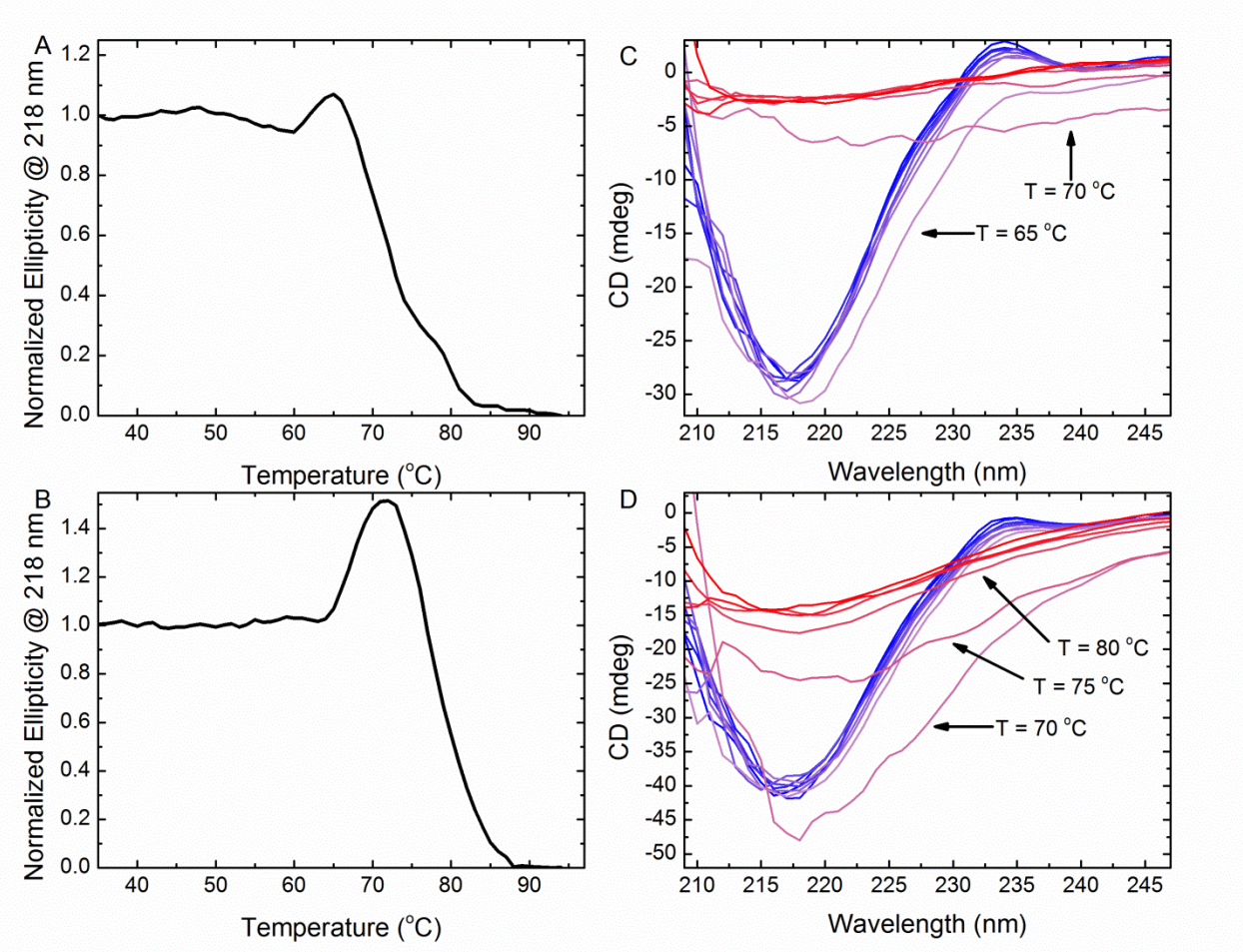

Figure 6.3: CD melts of aglycosylated hIgG1 in (A) buffer and (B) trehalose read at 218 nm. Full spectra scans every 5 ^{0}C are shown for (C) buffer and (D) trehalose. The blue to red color gradient corresponds to traces from 30 to 95 ^{0}C, respectively. A melting intermediate can be inferred from the labeled curves in C and D and the humps in A and B.

Figure 6.3A shows the melt of the hIgG1 in the buffer. While it is possible to distinguish two melting transitions at ~71 ^{0}C and ~79 ^{0}C corresponding to the denaturation of the Fab and then Fc domains[48] in Figure 6.3A, such a distinction was not possible for CD melts with sugars, as in Figure 6.3B; consequently, a single $T_{m,app}$ is reported for all melts. The $T_{m,app}$ reported is the temperature at which the CD signal is half its maximum (i.e. 50% of the signal from the top of the hump). Melting temperatures determined at 50% decay of the initial baseline correlate well to $T_{m,app}$ determined from the top of the hump (R^2 = 0.996, Fig. 6.4). A collection of all the $T_{m,app}$s is presented in Table 6.1 along with $\Delta T_{m,app}$ ($\Delta T_{m,app} = T_{m,app}^{Sugar} - T_{m,app}^{Buffer}$).

All the sugars are seen to improve thermal stability, and again the effect is more pronounced for the di-saccharides than for the mono-saccharides. The added stabilization of the sugars ranged from increasing $T_{m,app}$ by 3.4 ^{0}C in xylitol to 8.5 ^{0}C in sucrose. Other researchers have observed that sugars also increase the T_m of model proteins.[15, 18, 23, 40] Kaushik and Bhat suggest the mechanism of this phenomenon is due to sugars (and other polyols) influencing water-mediated effects, such as increasing surface tension and preferentially hydrating proteins,[18] much like kosmotropic anions do.[49] These effects encourage the native state by making the expansion of the protein – solvent interfacial area associated with unfolding energetically unfavorable. Crowding forces are likely also at play here, as larger sugars tend to stabilize more effectively.[50]

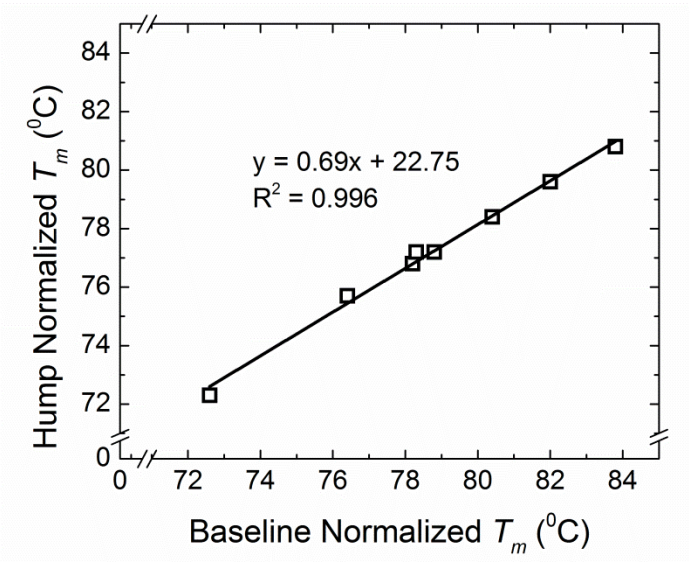

Figure 6.4: Correlation between T_m determined by baseline and hump normalization.

During our melts in sugar solutions, the CD signal notably increased before the protein completely melted, as can be clearly seen in the presence of trehalose (Fig. 6.3B). This hump was reproducibly apparent in all experiments with sugars. The ratio of the top of the hump to the initial, native baseline was unchanged when protein concentration was changed and the hump was found to be reversible (Fig. 6.5). DLS melts (performed as previously published[51]) were unable to capture the hump (or differentiate between solvents), as DLS is insensitive to details of the folding structure (Appendix C). We therefore hypothesize that prior to melting this antibody enters a sugar-stabilized intermediate that gives a stronger CD signal than the native antibody.

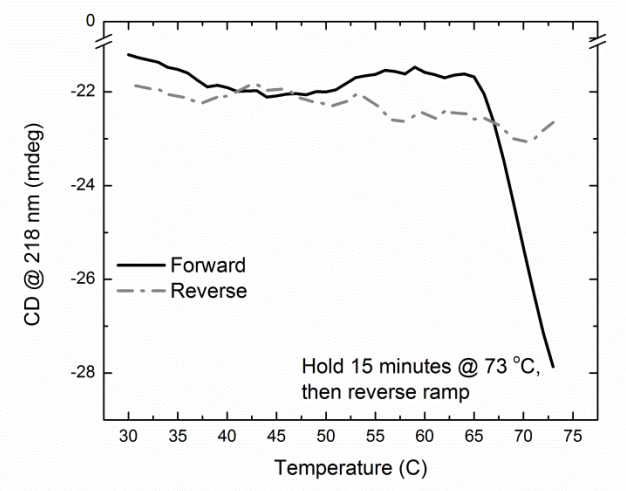

Figure 6.5: Forward then reverse temperature ramp in 500 mM Trehalose. Both ramps were performed at a rate of 1 ^{0}C/min. The temperature was held at 73 ^{0}C (the maximum temperature of this ramp) for 15 minutes to evaluate the kinetic stability of the melting intermediate.

We therefore hypothesize that prior to melting this antibody reversibly forms a sugar-stabilized intermediate that yields a stronger CD signal than the native antibody. In principle, the onset of protein melting can also be detected with DLS,[51] but since DLS is insensitive to details of the folding structure, we did not pursue it here. Instead, we found our hypothesis corroborated by looking at the full wavelength spectra over the course of a melt (Figures 6.3C & D). The native protein and fully denatured protein have distinct CD spectra. If the melt was two-state (N↔U), then - by the principle of superposition - the CD spectra for all temperatures would be some combination of those two spectra. In particular, for any wavelength at which the spectra of the native and the unfolded state coincide, the CD signal should remain constant as one population increases and the other decreases. Thus a two-state system with crossing CD spectra for the two states *necessarily* contains an isosbestic point, and by extension, the absence of an isosbestic point indicates that the system does not simply undergo a transition between two states but evolves through at least one intermediate state.[52, 53] It should be noted that the

presence of an isosbestic point does not preclude the possibility of a three-state system; but its absence eliminates the possibility of a two-state system.

CD spectra from 30 ^{0}C to 95 ^{0}C in buffer and trehalose are presented in Figures 6.3C and D, respectively. Both figures show a peak at 234 nm and a well at 218 nm in the native spectra (blue curves). The spectra for the denatured protein in both figures are significantly flatter and provide weaker signals (bright red curves). As the native spectra decay towards the denatured spectra, we can clearly see that the traces at 65 and 70 ^{0}C in Figure 6.3C and the traces between 70 and 80 ^{0}C in Figure 3D are *not* a mixture of the native and denatured spectra but distinctly different curves. This distinction is observed over a wider temperature range and produces a stronger signal in trehalose solution (Fig. 6.3D) than in buffer only. Neither Figure 6.3C nor D contains an isosbestic point, so we may deduce that the hump observed during our melts is an ephemeral, sugar-stabilized intermediate.

The enthalpies of melting (ΔH_m) were calculated from the top of the intermediate hump to the fully denatured baseline (Table 6.1). The two state model assumed earlier for enthalpy calculation thus corresponds to unfolding of the intermediate $I \leftrightarrow D$, rather than $N \leftrightarrow D$. The inferred melting enthalpies are similar to those previously reported in the literature for other antibodies.[48, 54] All ΔH_m values were larger than for the buffered control. The increased ΔH_m imply that more heat is required to completely unfold the antibody in sugar solutions. These results agree with the notion that unfolding in sugar solution is energetically unfavorable.[50]

6.4.4 Correlating Stability Metrics

To assess the usefulness of the interaction parameter as a predictor of aggregation propensity and thermostability, we studied the correlation of k_D with k_{11} and with $T_{m,app}$ (Figures 6.4A and B, respectively). Both plots revealed strong, roughly linear correlations with a squared correlation coefficient $R^2 \geq 0.91$, suggesting that k_D is indeed a good predictor of antibody stability in saccharide solutions.

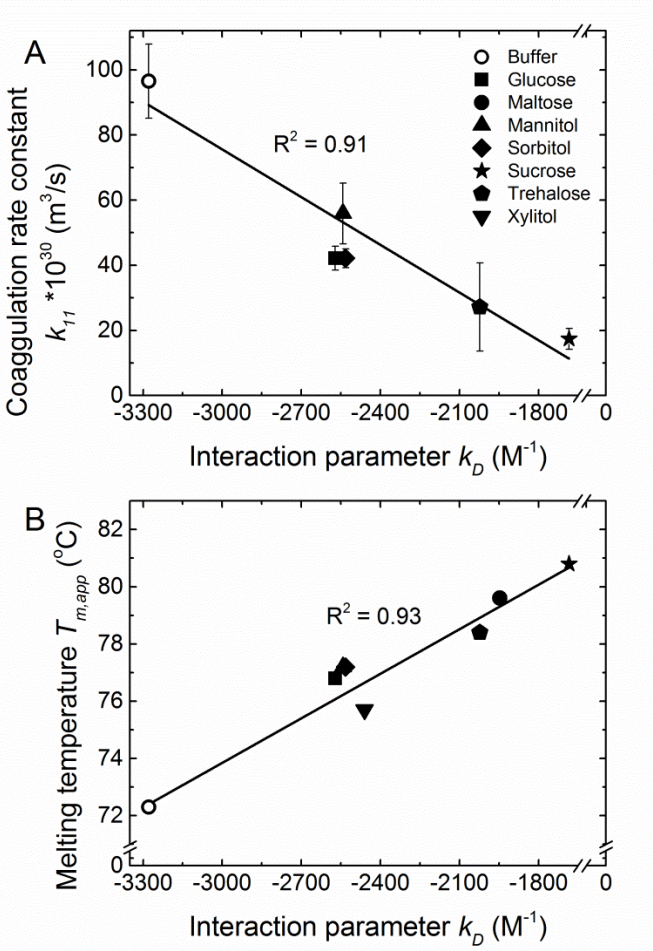

Figure 6.6: Correlations of k_D with (A) k_{11} and (B) $T_{m,app}$. Error for all data sets is presented in Table 6.1.

For media of different salt composition, we previously reported a strong correlation between k_D and protein stability, with both properties showing trends familiar

from the Hofmeister series.[29, 31] Unlike salts, which produce electrostatic and ion-specific effects and can either enhance or reduce protein stability,[55] all sugars tend to have the same qualitative effect proteins. Despite this similarity in saccharide – protein interactions, k_D was seen to resolve subtle quantitative differences in the effect of different sugars and correlate well with aggregation tests and CD melts. In the absence of a ranking system for sugars analogous to the Hofmeister series for salts, the fast stability assessment for protein-sugar solutions afforded by the interaction parameter k_D should prove especially useful for protein formulations.

6.5 Conclusion

We have shown that both the thermostability and the colloidal stability of an aglycosyalted human IgG1 in solution can be improved by sugar excipients. The relative magnitude of these stabilizing effects for different sugars can be gauged by analyzing the diffusive virial coefficient k_D, an interaction parameter accessible fast, without sample loss, and in a high-throughput manner by diffusivity studies using dynamic light scattering. A detailed circular dichroism analysis further suggests that thermally induced unfolding proceeds via a reversibly formed intermediate state that is stabilized by sugars.

6.6 References

1. Demattos, R. B.; Lu, J.; Tang, Y.; Racke, M. M.; Delong, C. A.; Tzaferis, J. A.; Hole, J. T.; Forster, B. M.; McDonnell, P. C.; Liu, F.; Kinley, R. D.; Jordan, W. H.; Hutton, M. L., A plaque-specific antibody clears existing beta-amyloid plaques in alzheimer's disease mice, *Neuron* **2012,** *76*, 908-20.

2. Wang, W.; Singh, S.; Zeng, D. L.; King, K.; Nema, S., Antibody structure, instability, and formulation, *Journal of Pharmaceutical Sciences* **2007,** *96*, 1-26.

3. Carter, P. J., Potent antibody therapeutics by design, *Nature Reviews Immunology* **2006,** *6*, 343-57.

4. Reichert, J. M., Marketed therapeutic antibodies compendium, *Mabs* **2012,** *4*, 413-15.

5. Mullard, A., Can next-generation antibodies offset biosimilar competition?, *Nature Reviews Drug Discovery* **2012,** *11*, 426-28.

6. Reichert, J. M., Which are the antibodies to watch in 2012?, *Mabs* **2012,** *4*, 1-3.

7. Chames, P.; Van Regenmortel, M.; Weiss, E.; Baty, D., Therapeutic antibodies: Successes, limitations and hopes for the future, *British Journal of Pharmacology* **2009,** *157*, 220-33.

8. Daugherty, A. L.; Mrsny, R. J., Formulation and delivery issues for monoclonal antibody therapeutics, *Advanced Drug Delivery Reviews* **2006,** *58*, 686-706.

9. Wang, W.; Singh, S. K.; Li, N.; Toler, M. R.; King, K. R.; Nema, S., Immunogenicity of protein aggregates-concerns and realities, *International Journal of Pharmaceutics* **2012,** *431*, 1-11.

10. Hermeling, S.; Crommelin, D. J. A.; Schellekens, H.; Jiskoot, W., Structure-immunogenicity relationships of therapeutic proteins, *Pharmaceutical Research* **2004,** *21*, 897-903.

11. Rosenberg, A. S., Effects of protein aggregates: An immunologic perspective, *Aaps Journal* **2006,** *8*, E501-E07.

12. Chi, E. Y.; Krishnan, S.; Randolph, T. W.; Carpenter, J. F., Physical stability of proteins in aqueous solution: Mechanism and driving forces in nonnative protein aggregation, *Pharmaceutical Research* **2003,** *20*, 1325-36.

13. Chang, L. Q.; Shepherd, D.; Sun, J.; Ouellette, D.; Grant, K. L.; Tang, X. L.; Pikal, M. J., Mechanism of protein stabilization by sugars during freeze-drying and storage: Native structure preservation, specific interaction, and/or immobilization in a glassy matrix?, *Journal of Pharmaceutical Sciences* **2005,** *94*, 1427-44.

14. Cleland, J. L.; Lam, X.; Kendrick, B.; Yang, J.; Yang, T. H.; Overcashier, D.; Brooks, D.; Hsu, C.; Carpenter, J. F., A specific molar ratio of stabilizer to protein is required for storage stability of a lyophilized monoclonal antibody, *Journal of Pharmaceutical Sciences* **2001,** *90*, 310-21.

15. Lu, J.; Wang, X. J.; Liu, Y. X.; Ching, C. B., Thermal and ftir investigation of freeze-dried protein-excipient mixtures, *Journal of Thermal Analysis and Calorimetry* **2007,** *89*, 913-19.

16. Arakawa, T.; Timasheff, S. N., Stabilization of protein-structure by sugars, *Biochemistry* **1982,** *21*, 6536-44.

17. Arakawa, T.; Timasheff, S. N., The stabilization of proteins by osmolytes, *Biophysical Journal* **1985,** *47*, 411-4.

18. Kaushik, J. K.; Bhat, R., Thermal stability of proteins in aqueous polyol solutions: Role of the surface tension of water in the stabilizing effect of polyols, *Journal of Physical Chemistry B* **1998,** *102*, 7058-66.

19. Wang, W.; Nema, S.; Teagarden, D., Protein aggregation--pathways and influencing factors, *International Journal of Pharmaceutics* **2010,** *390*, 89-99.

20. Allison, S. D.; Chang, B.; Randolph, T. W.; Carpenter, J. F., Hydrogen bonding between sugar and protein is responsible for inhibition of dehydration-induced protein unfolding, *Archives of Biochemistry and Biophysics* **1999,** *365*, 289-98.

21. Franks, F.; Hatley, R. H. M.; Mathias, S. F., Materials science and the production of shelf-stable biologicals, *Biopharm-the Technology & Business of Biopharmaceuticals* **1991,** *4*, 38-&.

22. Wang, B.; Tchessalov, S.; Warne, N. W.; Pikal, M. J., Impact of sucrose level on storage stability of proteins in freeze-dried solids: I. Correlation of protein-sugar interaction with native structure preservation, *Journal of Pharmaceutical Sciences* **2009,** *98*, 3131-44.

23. Kaushik, J. K.; Bhat, R., Why is trehalose an exceptional protein stabilizer? An analysis of the thermal stability of proteins in the presence of the compatible osmolyte trehalose, *Journal of Biological Chemistry* **2003,** *278*, 26458-65.

24. Allen, L. V.; Popovich, N. G.; Ansel, H. C., *Ansel's pharmaceutical dosage forms and drug delivery systems*. 9th ed.; Lippincott, Williams & Wilkins: Philadelphia, Pennsylvania, 2010.

25. Lauer, T. M.; Agrawal, N. J.; Chennamsetty, N.; Egodage, K.; Helk, B.; Trout, B. L., Developability index: A rapid in silico tool for the screening of antibody aggregation propensity, *Journal of Pharmaceutical Sciences* **2012,** *101*, 102-15.

26. Auton, M.; Bolen, D. W., Predicting the energetics of osmolyte-induced protein folding/unfolding, *Proceedings of the National Academy of Science of the United States of America* **2005,** *102*, 15065-8.

27. Duddu, S. P.; DalMonte, P. R., Effect of glass transition temperature on the stability of lyophilized formulations containing a chimeric therapeutic monoclonal antibody, *Pharmaceutical Research* **1997,** *14*, 591-95.

28. Polizzi, K. M.; Parikh, M.; Spencer, C. U.; Matsumura, I.; Lee, J. H.; Realff, M. J.; Bommarius, A. S., Pooling for improved screening of combinatorial libraries for directed evolution, *Biotechnology Progress* **2006,** *22*, 961-67.

29. Rubin, J.; San Miguel, A.; Bommarius, A. S.; Behrens, S. H., Correlating aggregation kinetics and stationary diffusion in protein-sodium salt systems observed with dynamic light scattering, *Journal of Physical Chemistry B* **2010,** *114*, 4383-87.

30. Saluja, A.; Fesinmeyer, R. M.; Hogan, S.; Brems, D. N.; Gokarn, Y. R., Diffusion and sedimentation interaction parameters for measuring the second virial coefficient and their utility as predictors of protein aggregation, *Biophysical Journal* **2010,** *99*, 2657-65.

31. Rubin, J.; Linden, L.; Coco, W. M.; Bommarius, A. S.; Behrens, S. H., Salt-induced aggregation of a monoclonal human immunoglobulin g1, *Journal of Pharmaceutical Sciences* **2012**.

32. Saito, S.; Hasegawa, J.; Kobayashi, N.; Kishi, N.; Uchiyama, S.; Fukui, K., Behavior of monoclonal antibodies: Relation between the second virial coefficient (b-2) at low concentrations and aggregation propensity and viscosity at high concentrations, *Pharmaceutical Research* **2012,** *29*, 397-410.

33. Behrens, S. H.; Borkovec, M., Influence of the secondary interaction energy minimum on the early stages of colloidal aggregation, *Journal of Colloid and Interface Sciences* **2000,** *225*, 460-65.

34. Lehermayr, C.; Mahler, H. C.; Mader, K.; Fischer, S., Assessment of net charge and protein-protein interactions of different monoclonal antibodies, *Journal of Pharmaceutical Sciences* **2011,** *100*, 2551-62.

35. Liu, W.; Cellmer, T.; Keerl, D.; Prausnitz, J. M.; Blanch, H. W., Interactions of lysozyme in guanidinium chloride solutions from static and dynamic light-scattering measurements, *Biotechnology and Bioengineering* **2005,** *90*, 482-90.

36. Chari, R.; Jerath, K.; Badkar, A. V.; Kalonia, D. S., Long- and short-range electrostatic interactions affect the rheology of highly concentrated antibody solutions, *Pharmaceutical Research* **2009,** *26*, 2607-18.

37. Connolly, B. D.; Petry, C.; Yadav, S.; Demeule, B.; Ciaccio, N.; Moore, J. M.; Shire, S. J.; Gokarn, Y. R., Weak interactions govern the viscosity of concentrated antibody solutions: High-throughput analysis using the diffusion interaction parameter, *Biophysical Journal* **2012,** *103*, 69-78.

38. Yadav, S.; Shire, S. J.; Kalonia, D. S., Viscosity behavior of high-concentration monoclonal antibody solutions: Correlation with interaction parameter and electroviscous effects, *Journal of Pharmaceutical Sciences* **2012,** *101*, 998-1011.

39. Mirarefi, A. Y.; Zukoski, C. F., Gradient diffusion and protein solubility:Use of dynamic light scattering to localize crystallization conditions, *Journal of Crystal Growth* **2004,** *265*, 274–83.

40. James, S.; McManus, J. J., Thermal and solution stability of lysozyme in the presence of sucrose, glucose, and trehalose, *Journal of Physical Chemistry B* **2012**.

41. Hristodorov, D.; Fischer, R.; Linden, L., With or without sugar? (a)glycosylation of therapeutic antibodies, *Molecular Biotechnology* **2012**.

42. Gillespie, R.; Nguyen, T.; Macneil, S.; Jones, L.; Crampton, S.; Vunnum, S., Cation exchange surface-mediated denaturation of an aglycosylated immunoglobulin (igg1), *Journal of Chromatography A* **2012,** *1251*, 101-10.

43. Kayser, V.; Chennamsetty, N.; Voynov, V.; Forrer, K.; Helk, B.; Trout, B. L., Glycosylation influences on the aggregation propensity of therapeutic monoclonal antibodies, *Biotechnology Journal* **2011,** *6*, 38-44.

44. Sola, R. J.; Griebenow, K., Effects of glycosylation on the stability of protein pharmaceuticals, *Journal of Pharmaceutical Sciences* **2009,** *98*, 1223-45.

45. Hristodorov, D.; Fischer, R.; Joerissen, H.; Muller-Tiemann, B.; Apeler, H.; Linden, L., Generation and comparative characterization of glycosylated and aglycosylated human igg1 antibodies, *Molecular Biotechnology* **2012**.

46. Thirumangalathu, R.; Krishnan, S.; Ricci, M. S.; Brems, D. N.; Randolph, T. W.; Carpenter, J. F., Silicone oil- and agitation-induced aggregation of a monoclonal antibody in aqueous solution, *Journal of Pharmaceutical Sciences* **2009,** *98*, 3167-81.

47. Persikov, A. V.; Xu, Y. J.; Brodsky, B., Equilibrium thermal transitions of collagen model peptides, *Protein Science* **2004,** *13*, 893-902.

48. Ionescu, R. M.; Vlasak, J.; Price, C.; Kirchmeier, M., Contribution of variable domains to the stability of humanized igg1 monoclonal antibodies, *Journal of Pharmaceutical Sciences* **2008,** *97*, 1414-26.

49. Collins, K. D., Ions from the hofmeister series and osmolytes: Effects on proteins in solution and in the crystallization process, *Methods* **2004,** *34*, 300-11.

50. Politi, R.; Harries, D., Enthalpically driven peptide stabilization by protective osmolytes, *Chemical Communications* **2010,** *46*, 6449-51.

51. Hall, M.; Rubin, J.; Behrens, S. H.; Bommarius, A. S., The cellulose-binding domain of cellobiohydrolase cel7a from trichoderma reesei is also a thermostabilizing domain, *Journal of Biotechnology* **2011,** *155*, 370-76.

52. Hud, N. V.; Smith, F. W.; Anet, F. A. L.; Feigon, J., The selectivity for k+ versus na+ in DNA quadruplexes is dominated by relative free energies of hydration: A thermodynamic analysis by h-1 nmr, *Biochemistry* **1996,** *35*, 15383-90.

53. Lannan, F. M.; Mamajanov, I.; Hud, N. V., Human telomere sequence DNA in water-free and high-viscosity solvents: G-quadruplex folding governed by kramers rate theory, *Journal of the American Chemical Society* **2012,** *134*, 15324-30.

54. Ghirlando, R.; Lund, J.; Goodall, M.; Jefferis, R., Glycosylation of human igg-fc: Influences on structure revealed by differential scanning micro-calorimetry, *Immunology Letters* **1999,** *68*, 47-52.

55. Broering, J. M.; Bommarius, A. S., Evaluation of hofmeister effects on the kinetic stability of proteins, *Journal of Physical Chemistry B* **2005,** *109*, 20612-9.

CHAPTER 7

THE CELLULOSE-BINDING DOMAIN OF CELLOBIOHYDROLASE CEL7A FROM TRICHODERMA RESSEI IS ALSO A THERMOSTABILIZING DOMAIN

This chapter is adapted from our research published in the *Journal of Biotechnology* **2011,** *155* (4): 370-376. Mélanie Hall contributed as much as Jonathan Rubin did to this work. Sven Behrens and Andreas Bommarius also contributed to this work.

7.1 Abstract

The thermostability of cellobiohydrolase I Cel7A from *Trichoderma reesei* was investigated using dynamic light scattering. While the whole enzyme displayed a melting temperature of 59 °C, the catalytic domain obtained via papain-catalyzed proteolysis was shown to denature at 51 °C, and the cellulose-binding domain (with linker attached) melted between 65 – 66 °C. This variation in individual melting temperatures is proposed to account for the full retention of binding capacity of Cel7A at 50 °C, along with a loss of catalytic activity observed for the catalytic domain alone. Thus, the cellulose-binding domain of Cel7A acts as a thermostabilizing domain for the enzyme. The effect of reducing agents on the protein melting behavior was also investigated.

7.2 Introduction

Glycosyl hydrolases catalyze the hydrolysis of a wide variety of polysaccharides, soluble or insoluble, and have been categorized into more than 100 families according to

sequence-based classification (120 as of December 2010, see Carbohydrate Active Enzymes database; URL http://www.cazy.org/).[1] Cellobiohydrolases (E.C. 3.2.1.91) are exoglucanases which cleave off cellobiose, a glucose dimer, from the chain ends of cellulose. Type I cellobiohydrolases are specific for reducing ends whereas type II are for non-reducing ends. These enzymes have been extensively studied at the structural and mechanistic level. Cel7A, a cellobiohydrolase I, is the major cellulolytic enzyme produced by *Trichoderma reesei* (anamorph of *Hypocrea jecorina*) and is currently one of the most investigated cellulases for biofuel applications. Major improvements are required in the enzymatic hydrolysis of cellulosic biomass before cellulosic ethanol can compete economically with corn-derived ethanol or petrol.[2]

Cel7A consists of three domains, (i) a 434 amino acid (aa) catalytic domain (CD) where glycosyl hydrolysis occurs,[3] (ii) a 36 aa cellulose-binding domain (CBD) that anchors the enzyme onto the cellulose surface and allows processive motion along individual cellulose chains,[4] and (iii) a 24 aa heavily O-glycosylated linker that connects these two domains. The linker likely transfers the energy required for processive motion from the CD (generated through the catalytic event) to the CBD and provides necessary spatial separation between the two domains.[5-8]

The hydrolysis of cellulose with cellulases is usually carried out at moderate temperatures (50 °C is frequently encountered), due to the relatively low thermostability of cellulases from mesophilic organisms. Current research trends are directed towards using cellulases from extremophiles and improving their thermostability, a property favorable from an industrial process perspective. Increasing the process temperature lowers the viscosity of the system, leads to higher specific activities,[9] and is significant

for overall improvement of the system (such as optimization of mass transfer rates and reduction of possible microbial contamination[10]). The ability to do so without compromising the stability of the catalyst represents a major challenge.

A variety of techniques including directed evolution, rational design, and use of structure-guided consensus[11-13] have been employed to enhance the thermostability of enzymes; some successful cases have been reported for cellulases specifically. Voutilainen et al. (2007) applied random mutagenesis to *Melanocarpus albomyces* cellobiohydrolase Cel7B and obtained single variants with improved unfolding temperature (T_m) that also showed more effective hydrolytic activity at higher temperature than the wild-type.[14] They also successfully employed structure-guided protein engineering to improve both T_m and activity at elevated temperature of cellobiohydrolase Cel7A from *Talaromyces emersonii*.[15] The use of SCHEMA, a computational approach to identifying blocks of sequence that minimize structural disruption when they are recombined in chimeric proteins, proved successful in creating a family of thermostable cellobiohydrolases II chimeras that displayed greatly enhanced half-lives of thermal inactivation.[16] The same approach was recently applied to cellobiohydrolases I.[17] In all these examples, the mutated residues were located within the catalytic domain and not the cellulose-binding domain. Yet, this binding domain may also play an important role for the overall thermostability of cellulases, as suggested indirectly by recent examples of increased activity at 70 °C of thermophilic single module GH-7 family cellobiohydrolase[18] and endoglucanase catalytic domains[19] upon fusion with mesophilic cellulose-binding domains. So far, the thermostability and

thermostabilizing property of the CBD of cellulases have not been investigated independently.

While investigating the potential use of the cellulose-binding domain of Cel7A from *T. reesei* in a pretreatment step of cellulose for more efficient enzymatic hydrolysis, we discovered that the binding capacity of full-length cellulases was retained after extended incubation time at 50 °C (cellulose-binding domain specific property) while their catalytic activity was dramatically reduced (catalytic domain-specific property).[20] Intrigued by these results, we initiated a study to compare the respective responses of CBD, CD and Cel7A to heat treatment with or without reducing agents present. This study is the first to monitor temperature-induced transitions in Cel7A *and* in its constituent domains (CD and CBD) separately. Light scattering measurements with a combined evaluation of intensity fluctuations and time-averaged scattering intensities were used to detect the onset of unfolding and aggregation for each of the domains and Cel7A as a whole.

7.3 Materials and methods

7.3.1 Materials

Avicel PH-101, cellulases from *T. reesei* (159 FPU mL^{-1}), and β-glucosidase (from almonds, 2.32 U mg^{-1}) were obtained from Sigma (St. Louis, MO, USA). The [micro] BCA protein assay kit and the Coomassie (Bradford) protein assay kit were obtained from Thermo Fischer Scientific (Rockford, IL, USA). Papain was obtained from Fluka as lyophilized powder from *Carica papaya* (9.84 U mg^{-1}). Centrifugal devices with

polyethersulfone membranes ('Jumbosep' and 'Macrosep') were from Pall Life Sciences (Ann Arbor, MI, USA). All experiments and assays were run at least in duplicate.

7.3.2 Cel7A Purification

Cel7A was purified from *T. reesei* cellulase cocktail by means of anion-exchange chromatography as previously published.[21] Purity was confirmed by SDS-PAGE.[20] After purification, Cel7A's buffer was exchanged to sodium acetate buffer (50 mM, pH 5) through multiple dilution/concentration iterations using a polyethersulfone membrane (molecular weight cut-off of 10 kDa) in a Macrosep device.

7.3.3 Cellulase Proteolysis and CBD Isolation

Cellulase cleavage using papain was adapted from published procedures[22,23] using purified Cel7A solution prepared as described above and stored in sodium acetate buffer (50 mM, pH 5). Papain was activated in ammonium acetate buffer (50 mM, pH 6) at 30 °C and 170 rpm for 30 min and added to Cel7A solution (1:5, w/w; 1:5, v/v). The digestion was performed at 30 °C for 2 h (completion checked *via* SDS-PAGE). The mixture was then filtered through 30 kDa membrane. The filtrate (containing the CBD) was diluted and passed through a 30 kDa membrane again to ensure no CD contamination. The diluted CBD solution was subsequently concentrated using a 3 kDa membrane. Both the CD and CBD solutions were analyzed for protein content using the micro BCA assay.

7.3.4 MALDI-TOF Mass Spectrometry

Purified CBD was obtained as described above, except that the buffer was ammonium acetate 50 mM pH 6.0 which was used in place of sodium acetate to drastically improve the signal-to-noise ratio in the mass spectrometer (MS). MALDI-TOF MS was performed on a PerSeptive Biosystems Voyager-DE STR (Framingham, USA). The spectra were acquired in linear mode, and the matrix used was sinapinic acid. A 10 mg mL^{-1} solution of the matrix was made in 50:50 (v:v) water:acetonitrile containing 0.1% formic acid by volume. Equal volumes of the matrix solution and the CBD solution were mixed, and the resulting solution was spotted onto the MALDI plate. A total of 500 laser shots were combined to produce the final spectrum.

7.3.5 Cellulose Enzymatic Hydrolysis

Cellulases and catalytic domains were incubated at 50 °C for 15 h and then added (300 μg mL^{-1} and 125 μg mL^{-1}, respectively) to a cellulose mixture (20 mg mL^{-1} in sodium acetate buffer, 50 mM, pH 5) that had been incubated at 50 °C for 1 h at 900 rpm. The hydrolysis was run at 50 °C and 900 rpm and the conversion was monitored after 6 h and 22 h by performing DNS assay on the supernatant.

7.3.6 Enzyme Adsorption Experiments

Avicel samples (20 mg mL^{-1}) in sodium acetate buffer (50 mM, pH 5) were incubated at 50 °C for 1 h at 900 rpm, and then cooled down to 4 °C. Cellulases (which had been incubated in sodium acetate buffer at 50 °C for 15 h or stored at 4 °C since purchase) were added in various amounts and the mixture was further agitated for 30 min at 4 °C.

After centrifugation, the supernatant was collected and protein content analysis was performed using the BCA protein assay kit.

7.3.7 Dynamic Light Scattering and T_m Determination

Purified samples were passed through a 0.02 μm aluminum oxide Whatman Anotop filter prior to light scattering measurements. DLS measurements were performed at a scattering angle of 90° in a Malvern Zetasizer Nano-ZS90 (Worcestershire, United Kingdom) and for the weakly scattering CBD probes under 150° angle, using a precision goniometer setup (ALV/DLS/SLS-5022F, Langen, Germany). In each case the hydrodynamic radius was obtained from a second order cumulant fit to the intensity autocorrelation function.

For Cel7A and the catalytic domain, T_m was determined on the Malvern Zetasizer using a programmed temperature ramp from 30 °C to 70 °C with 1 °C min^{-1} increments. The sample was equilibrated for 1 min at each temperature set-point before taking a single 30 s measurement. The melting temperature was identified as the lowest temperature inducing a significant increase in hydrodynamic raidus R_h compared to the native state.

For the much smaller CBD, DLS correlograms and intensity recordings were accumulated for 5 min at 150° angle for improved sensitivity using the precision goniometer setup. When no indication of protein melting was observed, the measurement was repeated after exposure of the sample cuvette to a PolyScience Digital Temperature Controller water bath for 5 min at an increasingly elevated temperature. The lowest bath temperature inducing a response in the scattering intensity and DLS size is reported as T_m. Application of this method to the full-size Cel7A confirmed the melting point value

determined independently with the Zetasizer as described above to within 1 °C, thus validating the approach for the CBD.

Melting temperature experiments were also conducted in the presence of reducing agents. Concentrated dithiothreitol (DTT) and β-mercaptoethanol solutions were prepared in 50 mM sodium acetate buffer pH 5.0. The concentrated DTT or β -mercaptoethanol solution was then diluted with Cel7A, CD or CBD. The peptide/reducing agent sample was gently stirred, then equilibrated at room temperature (22 ± 1 °C) for 5 min before measurements were taken. The melting temperatures for each reducing agent/peptide combination were determined as described above.

7.4 Results and discussion

7.4.1 Activity, Binding, and Melting Points

The purity, homogeneity, and kinetic thermostability of Cel7A and the CD were confirmed *via* DLS (Figs. 7.1 and 7.2). The samples were held at elevated temperatures for 2 hours then their size distributions were recorded. Figures 7.1 and 7.2 clearly show that the samples are homogeneous and thermo-tolerant below their T_ms. Sizes of the native state are shown in Table 7.1 (Note: Figures 7.1 and 7.2 report the diameter and Table 7.1 reports the radius).

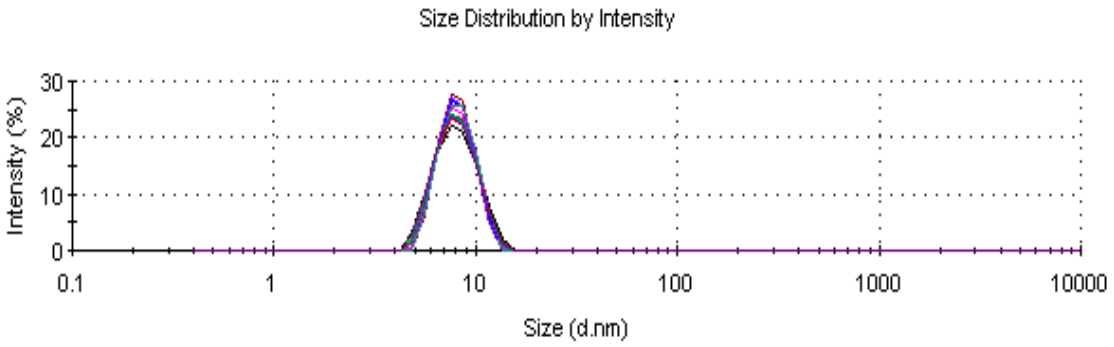

Figure 7.1: DLS size distribution profile for purified Cel7A after 2 hour incubation at 30°C.

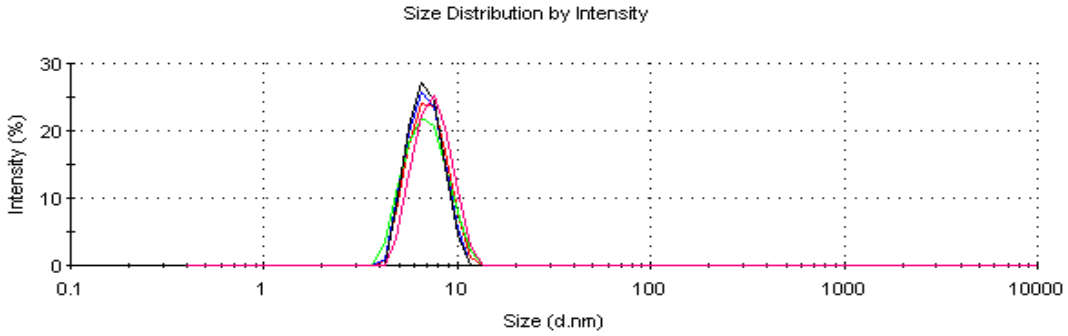

Figure 7.2.:DLS size distribution profile for purified CD_{Cel7A} after 2 hour incubation at 45 °C.

The melting temperatures T_m of Cel7A and CD were determined by analyzing the apparent protein size during a linear temperature ramp (Figs. 7.3 and 7.4); results for T_m are summarized in Table 7.1. The melting point of a protein is defined as the temperature at which the protein denatures. Protein unfolding is accompanied by an increase in size and can lead to protein aggregation and thus to further growth. Dynamic light scattering (DLS) provides a fast and convenient way to monitor the size of proteins, whose diffusivity and hydrodynamic radius R_h are inferred from intensity fluctuations of light scattered by the sample under coherent illumination.[24,25] This method has been already used to assess the stability of various proteins. It was used for instance in the determination of BSA surfactant-induced unfolding and gave results in good agreement

with small-angle neutron scattering (SANS).[26] DLS has also proved useful in thermal denaturation studies: accurate melting point determination was shown for BSA,[27] *T. reesei endo*-1,4-β-xylanase,[28] α-amylase from *Bacillus licheniformis*,[29] and the extracellular hemoglobin of *Glossoscolex paulistus* HbGp[30] and agreed with circular dichroism and fluorescence spectroscopy.[31]

Fig. 7.3 (full markers) illustrates the size change of Cel7A upon thermal denaturation. The observed sharp increase in hydrodynamic radius provides a clear-cut melting point T_m of 59 °C (±1 °C), which agrees well with a previous estimate of 62 °C (±2 °C) obtained from circular dichroism and tryptophan fluorescence.[32] In Chapter 6, we also found that DLS determined melting temperatures were lower than CD T_ms for our IgG1. The reason for the discrepancy in T_ms between the two techniques is likely due to differences in T_m-determination convention.

Table 7.1: Hydrodynamic radii R_h (obtained at room temperature) and melting temperature T_m of Cel7A and its fragments as determined by DLS. The buffer was 50 mM acetate at pH 5.0. Due to the lower concentration of CBD, 1 mM of each reducing agent was used in those melts.

Protein	R_h (nm)	T_m (^{0}C)		
		Buffer	DTT (3mM)	β-mercaptoethanol (3mM)
Cel7A	4.2 ± 0.5	59 ± 1	59 ± 1	59 ± 1
CD_{Cel7A}	3.4 ± 0.5	51 ± 1	61 ± 1	60 ± 1
CBD_{Cel7A} (with linker)	< 1	65.5 ± 0.5	61.5 ± 0.5	63.5 ± 0.5

Figure 7.3 also reports the (time averaged, open markers) scattering intensity. For scattering objects much smaller than the wavelength of light used (633 nm in the present

experiments), the scattering intensity is highest in a condensed, compact conformation;[33] therefore, both protein folding and protein aggregation promote a high scattering intensity. The slight drop in intensity observed along with the initial increase in particle size between 59 and 64 °C (Fig. 7.3B) is thus indicative of protein unfolding, whereas the intensity increase above 65 °C clearly points at aggregation. At the conclusion of the experiment, the initially clear enzyme solution was very turbid and precipitate had formed. A reverse, linear temperature ramp back to room temperature proved that unfolding and aggregations were both irreversible phenomena (data not shown).

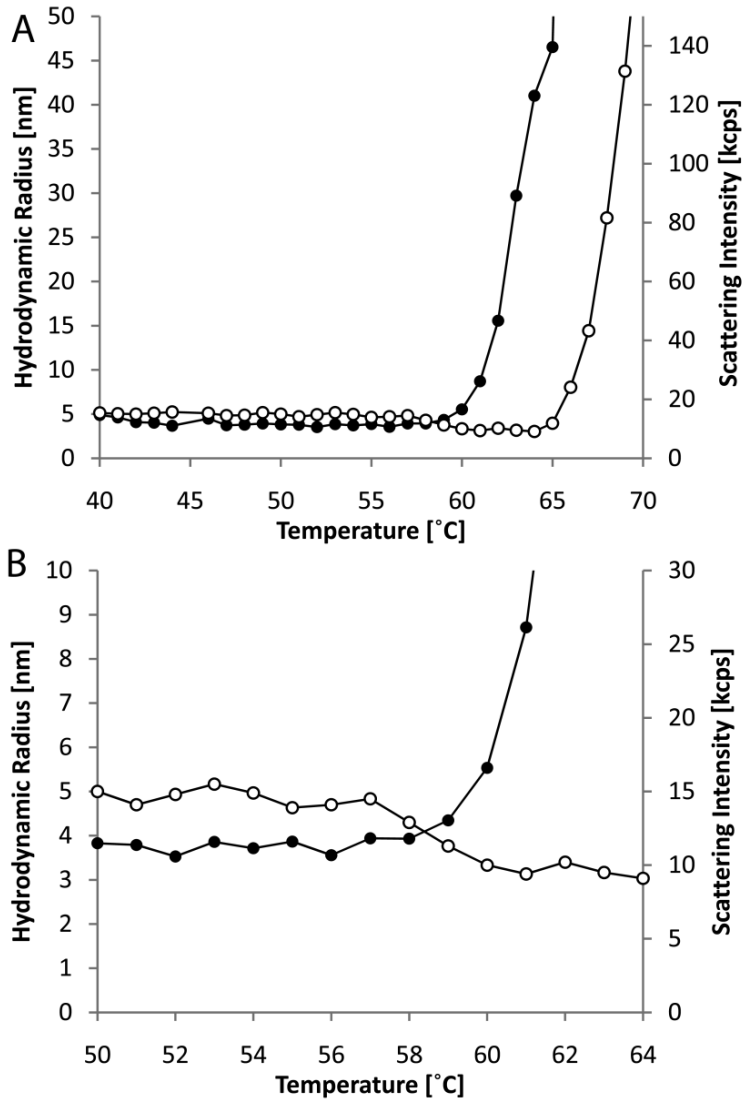

Fig. 7.3. DLS temperature ramp experiments with Cel7A. (●) Hydrodynamic radius (nm) and (o) scattering intensity (kcps) on (A) full scale, and (B) zoomed portion of (A) between 50 and 64 °C to show unfolding behavior.

The catalytic domain exhibits a different melting behavior than the full enzyme (Fig. 7.4). In this case, the increase in R_h already sets in at T_m = 51 °C, and coincides directly with an increase in scattering. This result indicates that aggregates are instantaneously formed upon denaturation of the CD, likely due to hydrophobic patches from different unfolded proteins associating with one another (large aggregates were

visible to the naked eye after completion of the temperature ramp). This difference in thermal stability between the CD and the full enzyme could not be attributed to the CD preparation procedure (2 h at 30 °C during papain cleavage). A control experiment with Cel7A was performed where it was incubation for 2 h at 30 °C prior to DLS temperature ramp. No difference in T_m was observed.

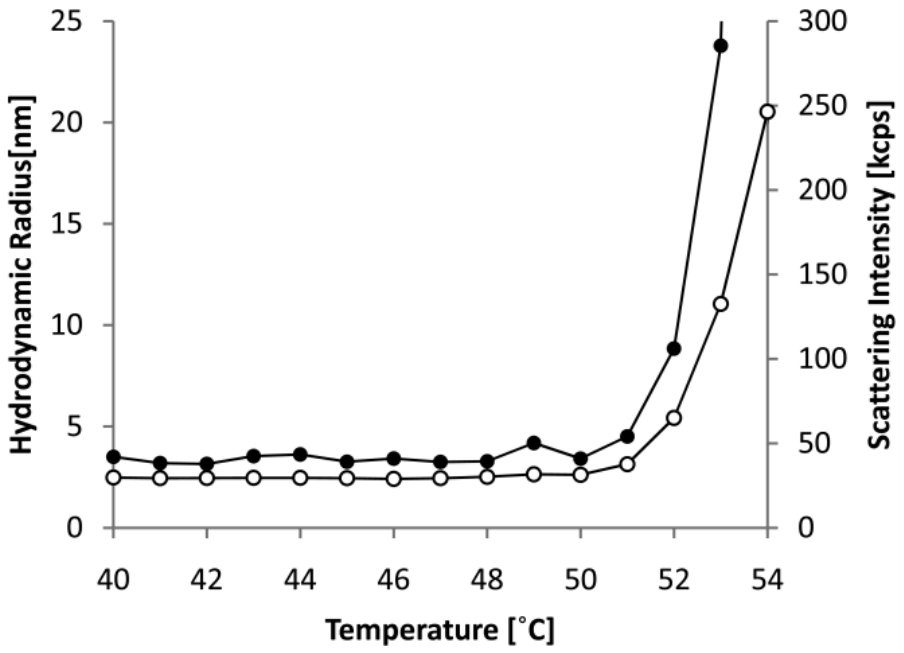

Fig. 7.4. DLS temperature ramp experiments with CD_{Cel7A}. (●) Hydrodynamic radius (nm) and (o) scattering intensity (kcps).

The purity of the CBD sample was of the utmost importance before determining its melting point because even trace amounts of the much larger CD (not visible on SDS-PAGE gel at very low concentration) would significantly skew the size measurements and affect melting behavior. MALDI-TOF mass spectroscopy confirmed the purity of the CBD and also showed the absence of larger molecules (Fig. 7.5A).[20] The different degrees of glycosylation on the linker account for the observed handful of peptides

separated by an average of 162 Da (this mass corresponds to the mass of dehydrohexoses of the O-glycosylated residues).

Characterizing the thermostability of the CBD with DLS proved challenging because of the small domain size (<70 residues, with linker, total size ~8.4-9.4 kDa as measured by MALDI-TOF, Fig. 7.5A) and poor optical contrast, resulting in an extremely weak light scattering signal. Although the exact size of the individual binding domain could not be measured precisely, we can safely assert that the hydrodynamic radius lies well below 1 nm. The CBD melting temperature could be determined more reliably, however, since aggregates formed upon melting are more easily detectable. The technique employed here is akin to the established method for detection of surfactant aggregates by DLS, which allows the estimation of the critical micelle concentration of surfactant molecules that cannot be detected in the non-aggregated state.[34] As indicated in Fig. 7.5B, the CBD size remained below the DLS detection limit (<1 nm) after exposure to temperatures up to 65 °C. After heating to 66 °C, however, an increase in the scattering intensity was observed and a quantitative interpretation of DLS data was possible. It suggests that the signal was dominated by aggregates with a hydrodynamic radius of approximately 1 μm. When heated above 66 °C, the solution became visibly turbid. The CBD thus displays a melting temperature of 65.5 °C (±0.5 °C), higher than the value for the full enzyme by at least 6 °C and much higher than the value for the catalytic domain (by at least 14 °C).

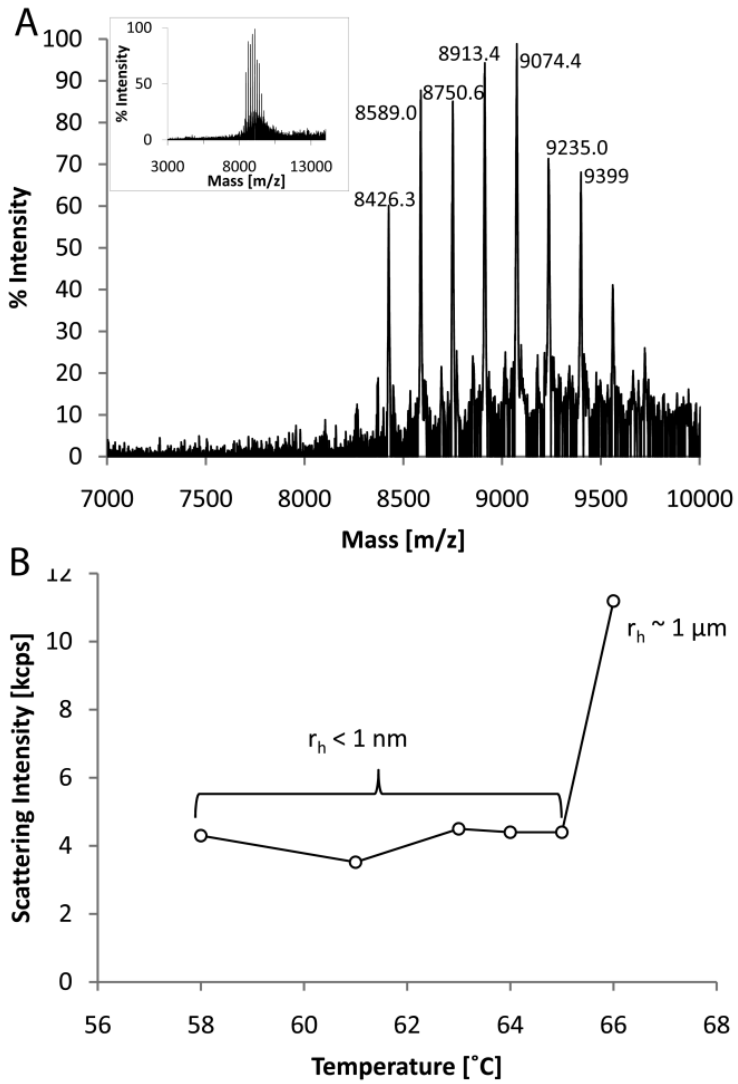

Fig. 7.5. CBD_{Cel7A} purity and melting experiments. (A) MALDI-TOF on CBD in 50 mM ammonium acetate pH 6.0 with inset showing full scale m/z up to 40 kDa; (B) scattering intensity (kcps) as a function of temperature.

Like the CD and unlike the full Cel7A, the CBD was characterized by a single threshold temperature for unfolding and aggregation. The hypothesis that this different behavior of Cel7A is related to a non-cooperative unfolding is tempting. However, if the CBD unfolding within Cel7A indeed occurs at a temperature above the melting point of the whole protein, then its effect on the light scattering signal is masked by the CD-

induced protein aggregation; a sequential unfolding of the different components therefore cannot be established unequivocally. From the present results though, it is obvious that the CBD (with linker attached) confers thermostability to the full-length enzyme and it can thus be described as a thermostabilizing domain (TSD). Such domains have been reported to exist with xylanases, though the whole machinery there is more complex since these enzymes are often composed of catalytic domains linked to one or more noncatalytic domains (including CBDs, TSDs and S-layer-like domains). These xylanase TSDs appear to have other prevailing function than thermostabilization, such as xylan binding (and references within).[35] Such a TSD for instance was added to a xylanase CD and the resulting protein had enhanced thermostability as well as enhanced binding capacity towards xylan and higher activity on insoluble xylan, proving its dual function.[35]

Our data also support the dichotomous behavior observed after incubation of cellulases and their CDs at 50 °C (Table 7.2). Over 100% of binding activity was retained after cellulases were incubated at 50 °C for 15 h (implying that the CBDs were still functional and thus folded) but their catalytic activity (and that of the CDs) was dramatically reduced. While the enzymes could retain 57% of their original activity after incubation at 50 °C for 15 h, the CDs retained only 42%, demonstrating that they are less thermo-tolerant than the full-length enzymes. This phenomenon is understandable with the CDs (given an incubation temperature only 1 °C lower than the T_m, suggesting that the denaturation process has begun and led to a loss of catalytic activity). The reduced activity is more difficult to explain for the full-length enzyme (T_m of 59 °C), except if there is some partial unfolding of the protein at the CD level (but CBD stays intact). Such a partial denaturation (see discussion above) could not be clearly demonstrated by DLS

techniques, however, as no increase in the overall hydrodynamic radius of Cel7A at 50 °C was detected (Fig. 7.3). Thus the loss of catalytic activity of cellulases observed at 50 °C is a kinetic rather than thermodynamic stability issue[36] since the proteins are expected to remain folded at this temperature. It is therefore likely that a gradual denaturation process has started after prolonged incubation at 50 °C (a temperature below their T_m) leading to reduced catalytic activity but no detectable structural changes, i.e. some enzymes are in an inactive state.[37]

Table 7.2: Residual binding capacity and catalytic activity after incubation at 50 °C for 15 h (reference: 100% from cellulases employed after storage at 4 °C). The two binding capacities reported for the native cellulases correspond to different enzyme/cellulose loadings: [a] 90 μg/mg and [b] 150 μg/mg.

	Native Cellulases	CDs
Binding capacity	111%[a] 115%[b]	N/A
Catalytic activity (6 h reaction time)	57%	42%

It is also worth noting that the melting point in this particular case was not correlated with the protein molecular weight (MW) (CBD T_m > Cel7A T_m > CD T_m and CBD MW < CD MW < Cel7A MW, Table 7.1).

7.4.2 Influence of Reducing Agents

The CBD structure resembles a wedge-like fold, where a flat face provides key (aromatic) residues strongly interacting with crystalline cellulose and the whole domain is stabilized by two disulfide bridges.[4,38] Reducing the disulfide bonds likely has an effect on the whole folding of the CBD, and therefore its binding capacity, as a disruption of the

hydrophobic residues arrangement on the flat face would most probably result in a complete loss of interaction with the cellulose surface (it has been reported that reduced Cel7A had lost binding ability on cellulose, i.e. the disulfide-bonded conformation is essential for binding[39]). We initiated experiments to investigate further the role of these bonds on the CBD properties, suspecting that they strongly influenced the thermostability and the denaturation process.

Variations in the T_m of Cel7A were monitored via DLS using various reducing agents (DTT and β-mercaptoethanol). The effect of reducing agents on Cel7A melting point was practically not observable (Table 7.1), even at 20 mM reducing agent concentration (data not shown). The temperature of unfolding was not affected; however, the reducing agents did stabilize the unfolded protein and prevented aggregation. The final solution was clear and the scattering intensity did not increase, demonstrating a lack of aggregation. This behavior is similar what one would expect in strongly chaotropic or surfactant solutions (as discussed in Chapter 1).

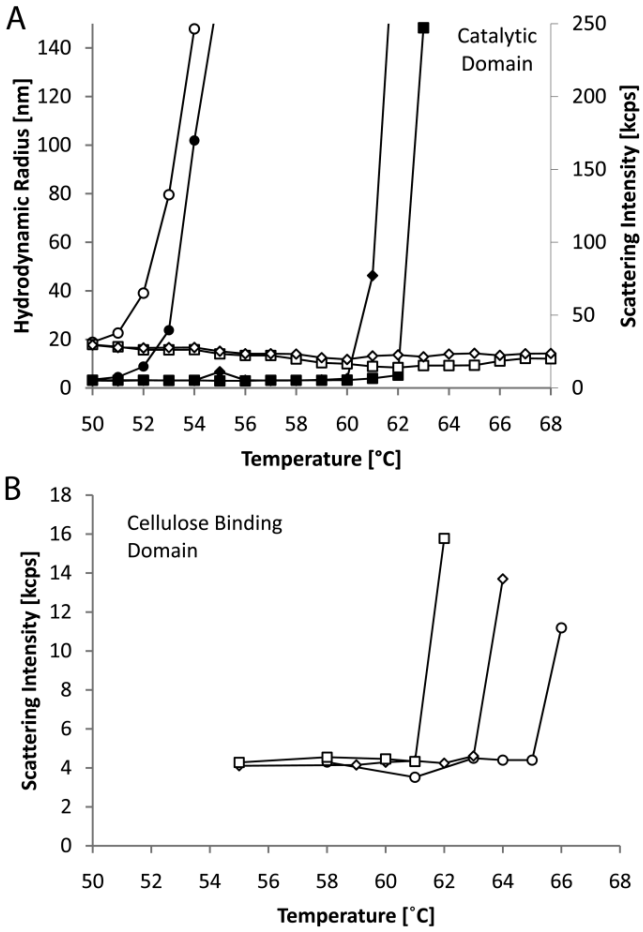

Fig. 7.6. Effect of reducing agents on CD_{Cel7A} and CBD_{Cel7A} T_m. (A) Temperature dependence of hydrodynamic radius R_h (nm) for CD_{Cel7A} containing no reducing agent (●), 3 mM β-mercaptoethanol (■), or 3 mM DTT (♦) and of scattering intensity (kcps, open symbols). (B) Temperature dependence of scattering intensity (kcps) for CBDCel7A solutions containing no reducing agent (○), 1 mM β-mercaptoethanol (□), or 1 mM DTT (◊).

A surprising effect was obtained with CD where both DTT and β-mercaptoethanol stabilized both folded and denatured forms of the protein. Indeed CD T_m increased by 9–10 °C while no jump in scattering intensity was observed at the T_m (Fig. 7.6A), which indicates the absence of aggregates (the solution remained clear), traditionally formed upon CD unfolding. Unfolding, though delayed, did occur, as shown by a substantial increase in the hydrodynamic radius, but the unfolded proteins were

stabilized against aggregation by the reducing agents. Protein aggregation is often due to the formation of intermolecular disulfide bridges between cysteine residues that became accessible after unfolding of the protein[40] and reducing agents such as DTT thus provide a reducing environment that prevents oxidation of cysteine residues and subsequent aggregation.

With the CBD however, the opposite (and more expected) behavior was observed: both reducing agents were found to decrease CBD T_m by 3–4 °C (Table 7.1 and Fig. 7.6B). Since the disulfide bridges were chemically reduced, less energy was required to fully denature the CBD (fewer bonds to break) and thus the melting point appeared to be lower.

7.5 Conclusions

Overall, dynamic light scattering proved to be a powerful non-invasive method to investigate temperature-induced conformational changes in a multi-domain protein and its constituent domains separately. The cellulose-binding domain of Cel7A from *T. reesei* was unambiguously shown to be also thermostabilizing the whole protein: alone, it displayed a melting point 14–15 °C higher than that of the catalytic domain and 6–7 °C higher than that of the whole protein. This conclusion is further supported by kinetic data showing that CD alone losses significantly more catalytic activity than the full enzyme at elevated temperatures.

Reducing agents such as DTT decreased the thermostability of the binding domain, pointing at disruption of otherwise stabilizing disulfide bridges. Efforts to

improve the thermostability of cellulases possessing structurally similar binding domains should concentrate on preserving or amplifying this intrinsic property.

7.6 References

1. Cantarel, B. L.; Coutinho, P. M.; Rancurel, C.; Bernard, T.; Lombard, V.; Henrissat, B., The carbohydrate-active enzymes database (cazy): An expert resource for glycogenomics, *Nucleic Acids Research* **2009,** *37*, D233-D38.

2. Bansal, P.; Hall, M.; Realff, M. J.; Lee, J. H.; Bommarius, A. S., Modeling cellulase kinetics on lignocellulosic substrates, *Biotechnology Advances* **2009,** *27*, 833-48.

3. Divne, C.; Stahlberg, J.; Reinikainen, T.; Ruohonen, L.; Pettersson, G.; Knowles, J. K. C.; Teeri, T. T.; Jones, T. A., The 3-dimensional crystal-structure of the catalytic core of cellobiohydrolase-i from trichoderma-reesei, *Science* **1994,** *265*, 524-28.

4. Kraulis, J.; Clore, G. M.; Nilges, M.; Jones, T. A.; Pettersson, G.; Knowles, J.; Gronenborn, A. M., Determination of the three-dimensional solution structure of the c-terminal domain of cellobiohydrolase i from trichoderma reesei. A study using nuclear magnetic resonance and hybrid distance geometry-dynamical simulated annealing, *Biochemistry* **1989,** *28*, 7241-57.

5. Davies, G.; Henrissat, B., Structures and mechanisms of glycosyl hydrolases, *Structure* **1995,** *3*, 853-59.

6. Gilkes, N. R.; Henrissat, B.; Kilburn, D. G.; Miller, R. C.; Warren, R. A. J., Domains in microbial beta-1,4-glycanases - sequence conservation, function, and enzyme families, *Microbiological Reviews* **1991,** *55*, 303-15.

7. Lynd, L. R.; Weimer, P. J.; van Zyl, W. H.; Pretorius, I. S., Microbial cellulose utilization: Fundamentals and biotechnology, *Microbiology and Molecular Biology Reviews* **2002,** *66*, 506-+.

8. Zhao, X.; Rignall, T. R.; McCabe, C.; Adney, W. S.; Himmel, M. E., Molecular simulation evidence for processive motion of trichoderma reesei cel7a during cellulose depolymerization, *Chemical Physics Letters* **2008,** *460*, 284-88.

9. Viikari, L.; Alapuranen, M.; Puranen, T.; Vehmaanpera, J.; Siika-Aho, M., Thermostable enzymes in lignocellulose hydrolysis, *Biofuels* **2007,** *108*, 121-45.

10. Anbar, M.; Lamed, R.; Bayer, E. A., Thermostability enhancement of clostridium thermocellum cellulosomal endoglucanase cel8a by a single glycine substitution, *Chemcatchem* **2010,** *2*, 997-1003.

11. Bornscheuer, U. T.; Pohl, M., Improved biocatalysts by directed evolution and rational protein design, *Current Opinion in Chemical Biology* **2001,** *5*, 137-43.

12. Lehmann, M.; Wyss, M., Engineering proteins for thermostability: The use of sequence alignments versus rational design and directed evolution, *Current Opinions in Biotechnology* **2001,** *12*, 371-5.

13. Vazquez-Figueroa, E.; Chaparro-Riggers, J.; Bommarius, A. S., Development of a thermostable glucose dehydrogenase by a structure-guided consensus concept, *Chembiochem* **2007,** *8*, 2295-301.

14. Voutilainen, S. P.; Boer, H.; Linder, M. B.; Puranen, T.; Rouvinen, J.; Vehmaanpera, J.; Koivula, A., Heterologous expression of melanocarpus albomyces cellobiohydrolase cel7b, and random mutagenesis to improve its thermostability, *Enzyme and Microbial Technology* **2007,** *41*, 234-43.

15. Voutilainen, S. P.; Murray, P. G.; Tuohy, M. G.; Koivula, A., Expression of talaromyces emersonii cellobiohydrolase cel7a in saccharomyces cerevisiae and rational mutagenesis to improve its thermostability and activity, *Protein Engineering Design & Selection* **2010,** *23*, 69-79.

16. Heinzelman, P.; Snow, C. D.; Wu, I.; Nguyen, C.; Villalobos, A.; Govindarajan, S.; Minshull, J.; Arnold, F. H., A family of thermostable fungal cellulases created by structure-guided recombination, *Proceedings of the National Academy of Sciences of the United States of America* **2009,** *106*, 5610-15.

17. Heinzelman, P.; Komor, R.; Kanaan, A.; Romero, P.; Yu, X. L.; Mohler, S.; Snow, C.; Arnold, F., Efficient screening of fungal cellobiohydrolase class i enzymes for thermostabilizing sequence blocks by schema structure-guided recombination, *Protein Engineering Design & Selection* **2010,** *23*, 871-80.

18. Voutilainen, S. P.; Boer, H.; Alapuranen, M.; Janis, J.; Vehmaanpera, J.; Koivula, A., Improving the thermostability and activity of melanocarpus albomyces cellobiohydrolase cel7b, *Applied Microbiology and Biotechnology* **2009,** *83*, 261-72.

19. Kim, T. W.; Chokhawala, H. A.; Nadler, D. C.; Blanch, H. W.; Clark, D. S., Binding modules alter the activity of chimeric cellulases: Effects of biomass pretreatment and enzyme source, *Biotechnology and Bioengineering* **2010,** *107*, 601-11.

20. Hall, M.; Bansal, P.; Lee, J. H.; Realff, M. J.; Bommarius, A. S., Biological pretreatment of cellulose: Enhancing enzymatic hydrolysis rate using cellulose-binding domains from cellulases, *Bioresource Technology* **2011,** *102*, 2910-15.

21. Hall, M.; Bansal, P.; Lee, J. H.; Realff, M. J.; Bommarius, A. S., Cellulose crystallinity - a key predictor of the enzymatic hydrolysis rate, *Febs Journal* **2010,** *277*, 1571-82.

22. Lemos, M. A.; Teixeira, J. A.; Mota, M.; Gama, F. M., A simple method to separate cellulose-binding domains of fungal cellulases after digestion by a protease, *Biotechnology Letters* **2000,** *22,* 703-07.

23. Vantilbeurgh, H.; Tomme, P.; Claeyssens, M.; Bhikhabhai, R.; Pettersson, G., Limited proteolysis of the cellobiohydrolase i from trichoderma-reesei - separation of functional domains, *Febs Letters* **1986,** *204,* 223-27.

24. Berne, B. J.; Pecora, R., *Dynamic light scattering: With applications to chemistry, biology, and physics*. John Wiley & Sons: New York, 1976.

25. Chu, B., *Laser light scattering: Basic principles and practice*. Academic Press: Boston, 1991.

26. Chodankar, S.; Aswal, V. K.; Kohlbrecher, J.; Vavrin, R.; Wagh, A. G., Surfactant-induced protein unfolding as studied by small-angle neutron scattering and dynamic light scattering, *Journal of Physics-Condensed Matter* **2007,** *19*.

27. Jachimska, B.; Wasilewska, M.; Adamczyk, Z., Characterization of globular protein solutions by dynamic light scattering, electrophoretic mobility, and viscosity measurements, *Langmuir* **2008,** *24,* 6866-72.

28. Janis, J.; Rouvinen, J.; Leisola, M.; Turunen, O.; Vainiotalo, P., Thermostability of endo-1,4-beta-xylanase ii from trichoderma reesei studied by electrospray ionization fourier-transform ion cyclotron resonance ms, hydrogen/deuterium-exchange reactions and dynamic light scattering, *Biochemical Journal* **2001,** *356,* 453-60.

29. Nazmi, A. R.; Reinisch, T.; Hinz, H. J., Calorimetric studies on renaturation by cacl2 addition of metal-free alpha-amylase from bacillus licheniformis (bla), *Journal of Thermal Analysis and Calorimetry* **2008,** *91,* 141-49.

30. Santiago, P. S.; Moura, F.; Moreira, L. M.; Domingues, M. M.; Santos, N. C.; Tabak, M., Dynamic light scattering and optical absorption spectroscopy study of ph and temperature stabilities of the extracellular hemoglobin of glossoscolex paulistus, *Biophysical Journal* **2008,** *94,* 2228-40.

31. Strucksberg, K. H.; Rosenkranz, T.; Fitter, J., Reversible and irreversible unfolding of multi-domain proteins, *Biochimica Et Biophysica Acta-Proteins and Proteomics* **2007,** *1774,* 1591-603.

32. Boer, H.; Koivula, A., The relationship between thermal stability and ph optimum studied with wild-type and mutant trichoderma reesei cellobiohydrolase cel7a, *European Journal of Biochemistry* **2003,** *270,* 841-48.

33. Hulst, H. C. v. d., *Light scattering by small particles*. Dover Publications: New York, 1981.

34. Guo, Q.; Singh, V.; Behrens, S. H., Electric charging in nonpolar liquids because of nonionizable surfactants, *Langmuir* **2010,** *26*, 3203-07.

35. Khan, M. I.; Sajjad, M.; Ali, I.; Ahmad, S.; Akhtar, M. W., Influence of transposition and insertion of additional binding domain on expression and characteristics of xylanase c of clostridium thermocellum, *Journal of Biotechnology* **2010,** *150*, 1-5.

36. Polizzi, K. M.; Bommarius, A. S.; Broering, J. M.; Chaparro-Riggers, J. F., Stability of biocatalysts, *Current Opinion in Chemical Biology* **2007,** *11*, 220-25.

37. Rogers, T. A.; Daniel, R. M.; Bommarius, A. S., Deactivation of tem-1 beta-lactamase investigated by isothermal batch and non-isothermal continuous enzyme membrane reactor methods, *Chemcatchem* **2009,** *1*, 131-37.

38. Linder, M.; Mattinen, M. L.; Kontteli, M.; Lindeberg, G.; Stahlberg, J.; Drakenberg, T.; Reinikainen, T.; Pettersson, G.; Annila, A., Identification of functionally important amino-acids in the cellulose-binding domain of trichoderma-reesei cellobiohydrolase-i, *Protein Science* **1995,** *4*, 1056-64.

39. Johansson, G.; Stahlberg, J.; Lindeberg, G.; Engstrom, A.; Pettersson, G., Isolated fungal cellulase terminal domains and a synthetic minimum analog bind to cellulose, *Febs Letters* **1989,** *243*, 389-93.

40. Kelly, S. T.; Zydney, A. L., Effects of intermolecular thiol-disulfide interchange reactions on bsa fouling during microfiltration, *Biotechnology and Bioengineering* **1994,** *44*, 972-82.

CHAPTER 8

CONCLUSIONS, PERSPECTIVES, AND RECCOMENDATIONS

Proteins are incredibly versatile molecules. They are antibodies, enzymes, prions, chaperones, and hormones. They are an essential component of life, and maintaining their stability is a compulsory aspect of survival. Organisms have developed complex stress response systems and crude cryptobiotic mechanisms to ensure the physical stability of their proteins in the event of environmental change.[1-3] Like an organism, proteins actuate biotechnological processes as well. Proteins catalyze reactions and are the products. The biochemical engineer's cardinal objective is to ensure continual protein stability and operational harmony. The engineer's toolbox is ever expanding with new strategies and more fundamental understanding of biomolecular processes.[4-6]

Researchers can take two main routes to improving and establishing protein physical stability: (i) protein mutations and (ii) solution optimization. Protein mutagenesis is a powerful tool that can dramatically improve stability and catalytic efficiency;[6,7] however, many rounds of mutation and a significant screening effort are required to develop an enhanced protein. These tasks are time-consuming, resources-intensive, and not guaranteed to be productive. But with high risk comes high reward.[8-11] Whether the catalyst or biopharmaceutical is a wild-type or a mutant, determining the most favorable environmental conditions is a fundamental part of process or product development. Solution optimization is a less radical, yet highly-effective approach to protein stabilization. Factors, such as ionic composition, temperature, pH, and co-solutes affect all proteins: prions enzyme, antibodies or otherwise. These variables can protect the native protein from deactivation or, if not considered, can denature protein. Water-mediated effects are the salient determinant of protein physical stability and understanding them is the crux of this dissertation.

Ion – water affinity dictate ion-specific protein interactions. For prion proteins in Chapters 2 and 3, chaotropes slowed aggregation because they kept Sup35NM monomeric and unfolded; while kosmotropes encouraged folding and, in turn, rapid aggregation. The differences in aggregation kinetics produced different prion variants that had varied morphologies and infectivity. Results from Chapter 3 combined with findings by Chen *et al*.[12] bolstered our argument that salts induce different prion strains. While Chapter 2 provides a satisfying explanation of how and why prion strains form in different salts, the question remains as to whether strain formation is unique to salts or is it a kinetic phenomenon. If amyloid was formed quickly in sucrose, or close to the isoelectric point (this would probably form amorphous aggregates), or at high temperature would we then form strong [*PSI*$^{+}$]? Is the converse true? That is, would forming amyloid in SDS, or far from the isoelectric point, or in low temperatures cause weak [*PSI*$^{+}$]?

Part of this question has already been answered by Jonathan Weissman, who has shown that at low temperatures we form strong [*PSI*$^{+}$] and at high temperatures we form weak [*PSI*$^{+}$].[13] However, the literature is inconsistent when reporting the kinetics of temperature induced aggregation.[14,15] Some report that amyloid formation at 4 °C is slower than at 37 °C, others report the opposite. Future work should conclusively elucidate the effect of temperature on Sup35NM aggregation kinetics.

The major question or hypothesis relating to this work that I'd like to forward for future work to examine is:

Fast aggregation kinetics form imperfect amyloids, which in vivo are strong prions; conversely, slow forming amyloids are physically more stable and are weak prions.

In essence, this hypothesis postulates that aggregation kinetics dictate strains. This can be tested, first by looking at the well-characterized temperature system, then finding

another dichotomous environmental condition (e.g. high/low temperature, chaotrope/kosmotrope). I recommend looking at the effect of surface tension on amyloid formation. As mentioned in Chapters 1-3, on a molecular level Hofmeister effect are caused by differences in interfacial tension and water affinity. Whether or not the solute molecule is an ion may not matter. I posit that surfactants would act like chaotropes: reducing surface tension, slowing amyloid formation, inducing weak [PSI^{+}]. Osmolytes, such as trehalose or sucrose, would act like kosmotropes: increasing surface tension, encouraging aggregation, and predominately producing strong [PSI^{+}]. Other systems could certainly be tested, for example working at pH below Sup35NM's pI (5.3). Would our findings be reversed at pH 4? Literature states that the Hofmeister series is inverted below a proteins pI,[16] so potentially yes. Going forward, future work should be aimed at testing the hypothesis above and perhaps testing the same rational against other prion proteins to show if this hypothesis is universal or Sup35p specific.

Ion-specificity also plays a major role in pharmaceutical formulation. Chapters 4 and 5 detail a rapid technique to predict the favorability of ion – protein interactions. In this case, chaotropes caused aggregation and kosmotropes were more stabilizing. Ostensibly, this behavior is the opposite of that seen in Chapter 2 and 3. The ions' action in both cases is in fact, the same. The prions in Chapters 2 and 3 began unfolded and aggregate upon folding, whereas in Chapters 4 and 5 the protein began folded and upon unfolding they aggregated. Chapter 6 examined how well the protein – protein interaction parameter, developed in Chapter 4, gauged colloidal and thermal stability in saccharide solutions. Since Chapter 6 worked exclusively with sugars, which increase surface tension and all sugars stabilized, as kosmotropes did in Chapters 4 and 5. I believe that ionic interactions are not nearly as important as solute – water affinity in how a solute affects protein stability. This idea is very similar to the above discussion on prion kinetics and surface tension.

Future work regarding the interaction parameter could look at applicability to other stabilizers, such as amino acids, or other solution conditions, such as pH. Although these experiments would be simple and quick to perform as our lab has competency in determining the interaction parameter in any solution, this research would be horizontal.

For more novel research on the interaction parameter, I propose a case study. The study would take a protein, such as the one in Chapter 6, and through solution alterations, maximize its k_D. Sugars, salts, pH would be changed and the interaction would, in turn, be examine to see the positive [or negative] effects of the change. The product of the study should be a complete formulation, with a strongly positive k_D. The formulation should then be corroborated by a long-term stability tests and characterizations to prove stability more conventionally. This study would show that k_D can be used for more than just an initial screen and give a concrete application of how to formulate using our technique.

All in all, this dissertation has two major findings: (i) chaotropes and kosmotropes form different strains of [PSI^+] and (ii) the interaction parameter can be used to rapidly predict protein stability in electrolyte or saccharide solutions. The common thread of protein stability and solvent conditions runs through-out this work. Hopefully the reader has a renewed appreciation and a deeper understanding of water-mediated effects on protein stability.

8.1 References

1. Davis-Searles, P. R.; Saunders, A. J.; Erie, D. A.; Winzor, D. J.; Pielak, G. J., Interpreting the effects of small uncharged solutes on protein-folding equilibria, *Annual Review of Biophysics and Biomolecular Structure* **2001,** *30*, 271-306.

2. Jaenicke, R., Protein stability and molecular adaptation to extreme conditions, *European Journal of Biochemistry* **1991,** *202*, 715-28.

3. Kregel, K. C., Heat shock proteins: Modifying factors in physiological stress responses and acquired thermotolerance, *Journal of Applied Physiology* **2002,** *92*, 2177-86.

4. Bommarius, A. S.; Broering, J. M., Established and novel tools to investigate biocatalyst stability, *Biocatalysis and Biotransformation* **2005,** *23*, 125-39.

5. Polizzi, K. M.; Bommarius, A. S.; Broering, J. M.; Chaparro-Riggers, J. F., Stability of biocatalysts, *Current Opinion in Chemical Biology* **2007,** *11*, 220-25.

6. Bommarius, A. S.; Blum, J. K.; Abrahamson, M. J., Status of protein engineering for biocatalysts: How to design an industrially useful biocatalyst, *Current Opinion in Chemical Biology* **2011,** *15*, 194-200.

7. Bommarius, A. S.; Riebel-Bommarius, B. R., *Biocatalysis: Fundementals and Applications*. Wiley Vch: New York, 2004.

8. Abrahamson, M. J.; Vazquez-Figueroa, E.; Woodall, N. B.; Moore, J. C.; Bommarius, A. S., Development of an amine dehydrogenase for synthesis of chiral amines, *Angewandte Chemie International Edition* **2012,** *51*, 3969-72.

9. Park, J. T.; Hirano, J.-I.; Thangavel, V.; Riebel, B. R.; Bommarius, A. S., Nad(p)h oxidase v from lactobacillus plantarum (noxv) displays enhanced operational stability even in absence of reducing agents, *Journal of Molecular Catalysis B: Enzymatic* **2011,** *71*, 159-65.

10. Yanto, Y.; Hall, M.; Bommarius, A. S., Nitroreductase from salmonella typhimurium: Characterization and catalytic activity, *Organic & Biomolecular Chemistry* **2010,** *8*, 1826-32.

11. Savile, C. K.; Janey, J. M.; Mundorff, E. C.; Moore, J. C.; Tam, S.; Jarvis, W. R.; Colbeck, J. C.; Krebber, A.; Fleitz, F. J.; Brands, J.; Devine, P. N.; Huisman, G. W.; Hughes, G. J., Biocatalytic asymmetric synthesis of chiral amines from ketones applied to sitagliptin manufacture, *Science* **2010,** *329*, 305-9.

12. Chen, B.; Bruce, K. L.; Newnam, G. P.; Gyoneva, S.; Romanyuk, A. V.; Chernoff, Y. O., Genetic and epigenetic control of the efficiency and fidelity of cross-species prion transmission, *Molecular Microbiology* **2010,** *76*, 1483-99.

13. Chien, P.; Weissman, J. S.; DePace, A. H., Emerging principles of conformation-based prion inheritance, *Annual Review of Biochemistry* **2004,** *73*, 617-56.

14. Scheibel, T.; Bloom, J.; Lindquist, S. L., The elongation of yeast prion fibers involves separable steps of association and conversion, *Proceedings of the National Academy of Sciences of the United States of America* **2004,** *101*, 2287-92.

15. Tanaka, M.; Collins, S. R.; Toyama, B. H.; Weissman, J. S., The physical basis of how prion conformations determine strain phenotypes, *Nature* **2006,** *442*, 585-89.

16. Peula-Garcia, J. M.; Ortega-Vinuesa, J. L.; Bastos-Gonzalez, D., Inversion of hofmeister series by changing the surface of colloidal particles from hydrophobic to hydrophilic, *Journal of Physical Chemistry C* **2010,** *114*, 11133-39.

APPENDIX A

MATLAB CODE FOR AMYLOID AGGREGATION KINETICS

```
clear
close all
clc

% This program takes kinetic data and fits it to a sigmoidal curve. The
%outputs are the lag time (tlag), time till 50% maximum signal (thalf), and
%slope @ thalf also known as the elongation rate constant k

%Input time points for x
x = […];

 % Input fluorescent data for y. This data may or may not be normalized.
% Depending on if the data is normalized, then initial guesses for
% the fitting parameters below will need to be adjusted.

y = […];

options = statset('MaxIter',1000,'TolFun',10^-10,'TolX',10^-10);

%These are the fitting parameters. A is the amplitude of the curve. If
%normalized A will generally be unity, if not normalized A shoudl be set at
%about the highest fluorescence value. K is the elongation rate constant. B
%is the lag time guess. K and B do not depend on normalization. In the
%event of very long lag times, increase the initial guess of B.
A = 16000;
K = 0.01;
B = 200;


% The kinetic data may not begin percisely at zero, so the model allows for
% some offset. The following iterative loop attempts to find the most
% appropriate offset with the range given

range = [xxx:x:xxx];
  for i= 1:length(range)
    global offset
    offset = range(i);

%     The nlinfit is the non-linear curve fit to the above data. The data
%     are passed to the curvelag funtion (another file)
```

```
    [k,R,J,COVB,MSE] = nlinfit(x,y,@curvelag, [A K B], options);

    % R^2 error calculation used to determine accuracy of iteration

    error(i) = sum(R.^2);
    parameters(i,:)=k;

    % calculation of thalf

    thalf(i) = k(3)+2/k(2);
end

%Reassigning variables
index = find(error==min(error));
k = parameters(index,:);
A = k(1);
K = k(2);
tlag = k(3);
B = tlag;
offset = range(index);
thalf = thalf(index)

%calculation of error
yfit = k(1)./(1+exp(-k(2)*(x-(k(3)+2/k(2))))) + offset;

SSE = sum((yfit - y).^2);
SST = sum((y-mean(y)).^2);
R2 = 1-SSE/SST;
resid = yfit-y;

%non-linear confidence interval calculation based on fitting error
ci = nlparci([A K B], resid, 'jacobian', J);

% Variable assignment of high and low confidence intervals (ci) for both k
% and thalf (t12)
kcilow = ci(2);
kcihigh = ci(5);
t12cilow = ci(3);
t12cihigh = ci(6);
tlagerr = tlag - t12cilow
kerr = K - kcilow

%output of k and tlag along with confidence intervals

KCI = [kcilow, K, kcihigh]
```

```
tlagCI = [t12cilow, tlag, t12cihigh]


 %The following is a separate .m file named "curvelag.m"

 function [y] = curve(k,x,y)
%This function takes the inputs given from the curvefitlag file and fits
%them to the sigmoidal curve equation below

global offset


y = k(1)./(1+exp(-k(2)*(x-(k(3)+2/k(2))))) + offset;
% residual = sum((ypred-y).^2);
end
```

APPENDIX B

TABULATED SPECIES BARRIER LAG TIMES

Table B1: Data from Figures 3.3. Non-seeded lag times for *S. cerevisiae, S. bayanus,* and *S. paradoxus*. That background buffer for all experiments is PBS. Error reported is fitting error from the nonlinear MATLAB fit.

Ion and concentration	*S. cerevisiae* lag time (hr)	*S. bayanus* lag time (hr)	*S. paradoxus* lag time (hr)
0.2 M sulfate	1.19 ± 0.23	1.86 ± 0.19	3.89 ± 0.24
0.4 M sulfate	0.64 ± 0.37	1.41 ± 0.18	3.46 ± 0.53
PBS	2.80 ± 0.13	2.52 ± 0.38	6.33 ± 0.15
0.2 M chloride	4.29 ± 0.19	3.77 ± 0.38	7.65 ± 0.14
0.4 M chloride	5.69 ± 0.06	4.92 ± 0.21	8.83 ± 0.07
0.2 M perchlorate	7.32 ± 0.13	5.23 ± 0.41	12.5 ± 0.25
0.4 M perchlorate	9.41 ± 0.12	8.16 ± 0.14	13.23 ± 0.25

Table B2: Data from Figure 3.4. Seeded lag times for *S. cerevisiae*, *S. bayanus*, and *S. paradoxus*. That background buffer for all experiments is PBS. The seed donor is the species of the seed; the recipient is the species of the monomer. Error reported is fitting error from the nonlinear MATLAB fit.

Monomer Recipient	Salt Seed Formed In	Species of Seed Donor	Lag time (hr)
S. cerevisiae	Sulfate	*S. cerevisiae*	0.30 ± 0.55
		S. bayanus	5.36 ±0.11
		S. paradoxus	0 ± 0.15
	Chloride	*S. cerevisiae*	0 ± 0.18
		S. bayanus	4.51 ± 0.21
		S. paradoxus	2.68 ± 0.31
	Perchlorate	*S. cerevisiae*	2.54 ± 0.12
		S. bayanus	4.88 ± 0.28
		S. paradoxus	4.37 ± 0.38
	-	No Seed	2.80 ± 0.13
S. bayanus	Sulfate	*S. cerevisiae*	5.67 ± 0.47
		S. bayanus	0
		S. paradoxus	4.81 ± 0.28
	Chloride	*S. cerevisiae*	5.11 ± 0.12
		S. bayanus	0
		S. paradoxus	4.56 ± 0.36
	Perchlorate	*S. cerevisiae*	5.00 ± 0.24
		S. bayanus	3.84 ± 0.24
		S. paradoxus	4.48 ± 0.28
	-	No Seed	5.19 ± 0.38
S. paradoxus	Sulfate	*S. cerevisiae*	2.97 ± 0.34
		S. bayanus	11.08 ± 0.20
		S. paradoxus	2.05 ± 0.39
	Chloride	*S. cerevisiae*	7.01 ± 0.47
		S. bayanus	12.16 ± 0.49
		S. paradoxus	0
	Perchlorate	*S. cerevisiae*	7.44 ± 1.54
		S. bayanus	12.3 ± 0.21
		S. paradoxus	0.84 ± 1.03
	-	No Seed	6.33 ± 0.15

Table B3: Data from Figure 3.5. *S. bayanus* and *S. paradoxus* monomer were seeded with *S. cerevisiae* seeds formed in different salt buffers. 0.4 M of additional salt was added to the PBS background buffer during heterologous seeding. Error reported is fitting error from the nonlinear MATLAB fit.

Monomer Recipient	Salt in Aggregation Solution	Salt Seed Formed In	Lag time (hr)
S. bayanus	Sulfate	Sulfate	2.28 ± 0.44
		Chloride	1.65 ±0.53
		Perchlorate	1.63 ± 0.40
	Chloride	Sulfate	5.38 ± 0.72
		Chloride	5.13 ± 0.30
		Perchlorate	6.64 ± 0.87
	Perchlorate	Sulfate	6.95 ± 0.50
		Chloride	>15
		Perchlorate	>15
	None	Sulfate	5.67 ± 0.47
		Chloride	5.11 ± 0.12
		Perchlorate	5.00 ± 0.24
S. paradoxus	Sulfate	Sulfate	1.92 ± 0.32
		Chloride	2.94 ± 0.16
		Perchlorate	0
	Chloride	Sulfate	9.17 ± 0.71
		Chloride	12.98
		Perchlorate	>15
	Perchlorate	Sulfate	>15
		Chloride	>15
		Perchlorate	>15
	None	Sulfate	2.97 ± 0.34
		Chloride	7.01 ± 0.47
		Perchlorate	7.44 ± 1.54

APPENDIX C

ANTIBODY MELTS

Pertaining to data from chapter 5:

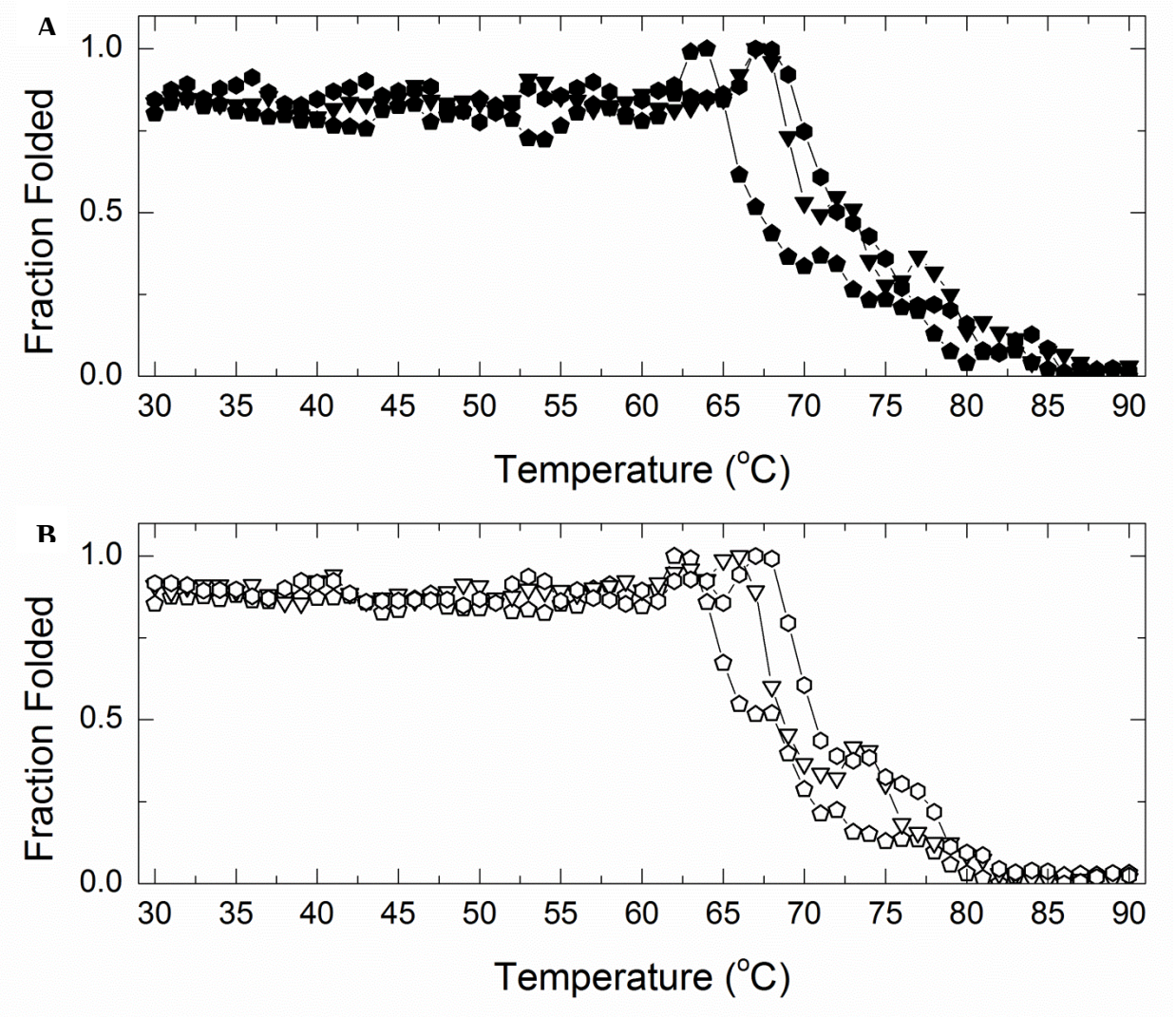

Figure C1: CD determined melting temperatures of the glycosylated (A) and aglycosylated (B) antibodies from Chapter 5. Melts were run in 200 mM ionic strength solutions containing perchlorate (pentagon), chloride (▼), and sulfate (hexagon).

Pertaining to data from Chapter 6:

DLS temperature ramps were run from 35 to 92 ^{0}C at a ramp rate of 1 ^{0}C/min using a Malvern ZS90 Zetasizer (Worchestershire, U.K.). Two 30 second acquisitions were collected and averaged at each temperature. The melting temperature was determined as the temperature where the DLS diameter spiked. Figures C2 show representative DLS protein melts in (A) buffer and (B) sucrose.

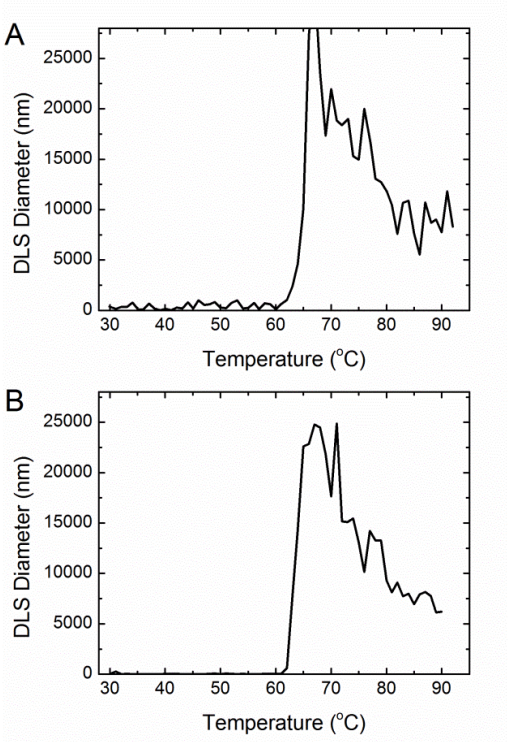

Figure C2: DLS temperature ramps performed in (A) buffer and (B) sucrose. The temperature at which the Z-average diameter spikes is the melting temperature.

All melts performed showed a fairly steady baseline diameter followed by a large spike in the DLS diameter upon melting. Overtime the DLS diameter decreases due to aggregates precipitating and leaving the DLS's field of vision.

This set of experiments was performed to study the unfolding intermediate using a different protein melting technique; however, DLS is insensitive to changes in protein secondary and tertiary structure, so the intermediate was not captured. Further, we found that DLS could not distinguish between different sugar solutions (see Table C1). The difference in melting temperature between these results and CD melting temperatures reported are due to difference in convention in determining T_m. The DLS results do confirm that sugars stabilize the IgG1 compared to buffer alone.

Table C1: Collection of DLS melts for selected sugars and other excipients. $\Delta T_m = T_{m,\,Excipient} - T_{m,Buffer}$.

Excipient	**Onset of melt (°C)**	**ΔT_m (°C)**
Buffer	60	-
Trehalose	64	4
Sucrose	64	4
Glucose	64	4
Sorbitol	63	3
Mannitol	65	5
Glycerol	63	3
Glycine	54	-6

APPENDIX D

PALEONTOLOGY STUDY

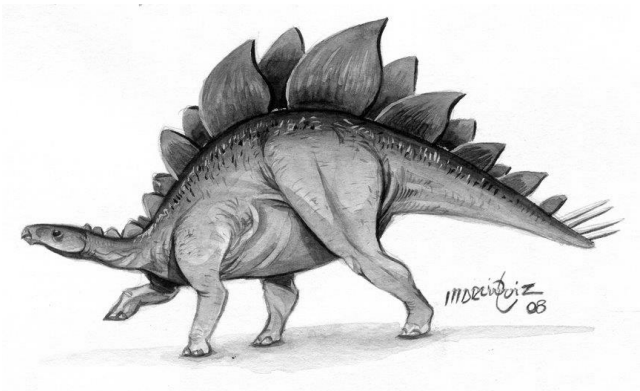

Figure D1: Stegosaurus, meaning "covered lizard." These are plant eaters that can grow up to 30 feet long and 4.5 metric tons. They have a single, tiny brain (previously thought to have second brain in their tail). They lived in the late Jurassic period. This is my favorite dinosaur. Image taken from < http://www.wikidino.com/wp-content/uploads/Stegosaurus-marciolcastro.jpg >, accessed on February 7, 2013.

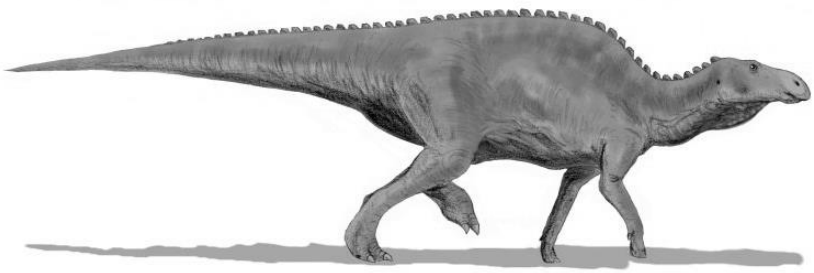

Figure D2: Edmontosaurus was a 4.0 metric ton, small brained, biped herbivore that used to live in Alberta, Canada during the late Cretaceous period. They are thought to run at speeds of up to 28 mph. These animals lived in herds and were likely prey for by T. Rex. Image taken from <http://en.wikipedia.org/wiki/File:Edmontosaurus_BW.jpg>, accessed on February 6, 2013.

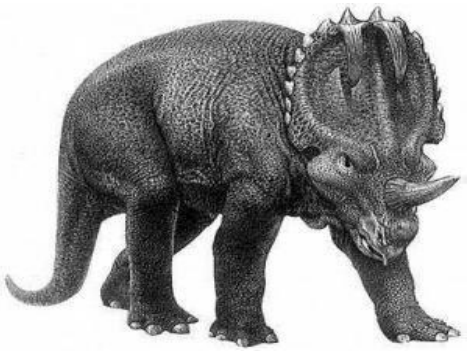

Figure D3: Monoclonius were 6 foot long, herding herbivores. They lived during the late Cretaceous period. Current thinking suggests that Monoclonius are improperly classified as a unique species, rather they are simply juvenile Centrosaurus; however, no one can tell for sure so the taxonomical distinction remains. Image taken from <http://www.kidsdinos.com/dinosaurs-for-children.php?dinosaur=Monoclonius>, accessed on February 6, 2013.

APPENDIX E

REFRCATIVE INDICES OF SALINE AND SACHHARIDE SOLUTIONS AND VISCOSITY OF SACCHARIDE SOLUTION

Data pertaining to Chapter 4's saline solutions:

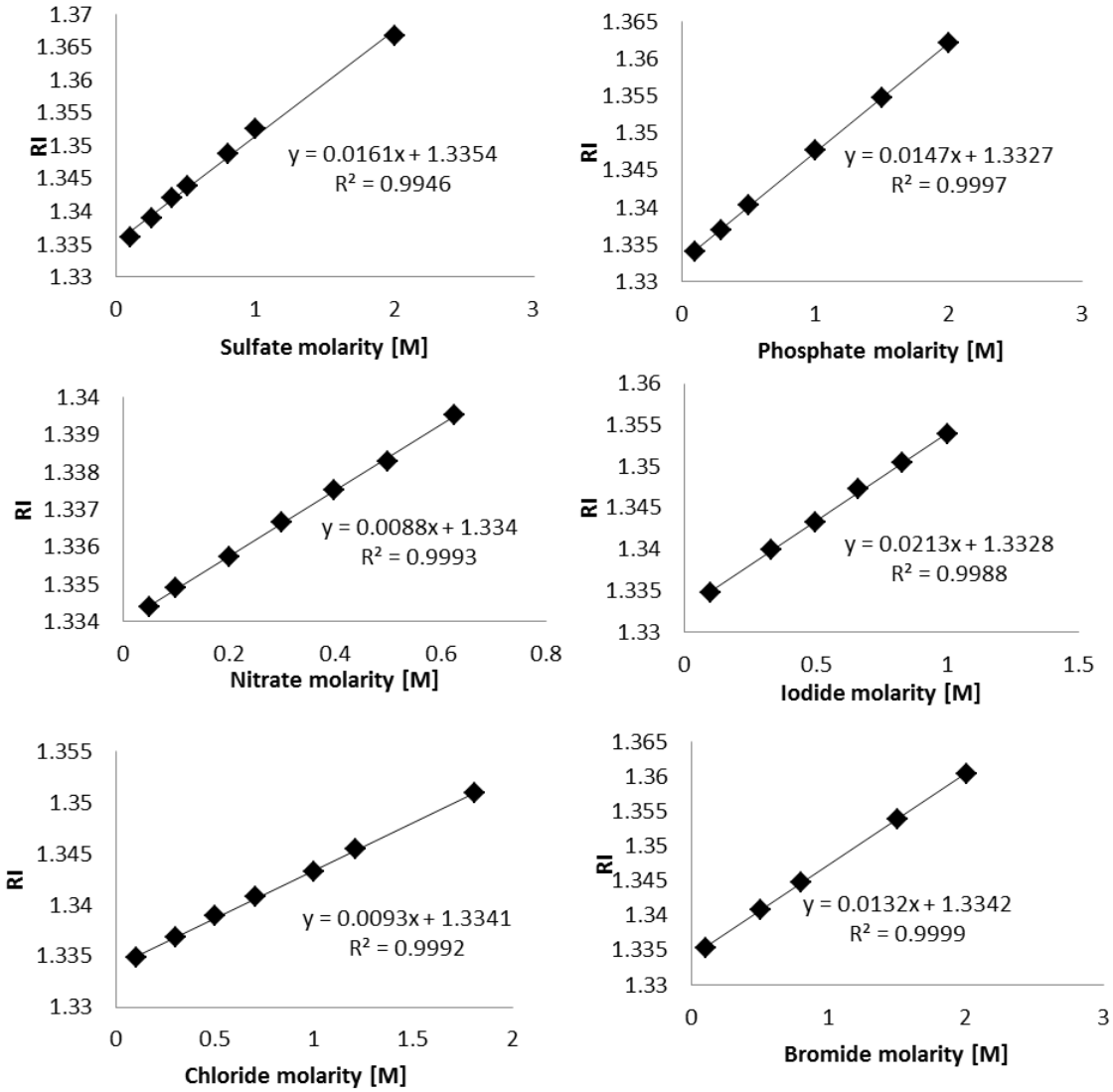

Figure E1: Refractive index values measured and used for this work using a digital Libby Refractometer at 25°C. 100 mM sodium acetate at pH 4.5 was the background buffer for all measurements.

Data pertaining to Chapter 6 and saccharides:

Refractive index measurements were conducted at 20 °C using a digital Libby refractometer (Figure S1). The buffer alone gave a refractive index of 1.3342 (y-intercept).

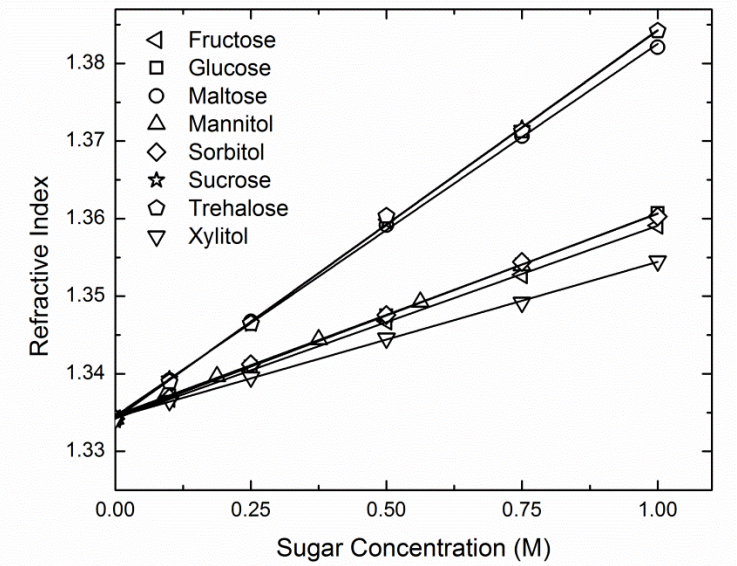

Figure E1: Refractive index measurements of a variety of sugars in buffer (25 mM acetate, 150 mM sodium chloride, pH 5.5)

Table E4: Presented are the slopes of the curves shown in Figure S1 and the refractive index at 500 mM of each sugar. The y-intercept for all curves was 1.3342 (i.e. buffer).

Sugar	***dn/dc*** **(M^{-1})**	**RI @ 500 mM**
Fructose	0.0248	1.3468
Glucose	0.0263	1.34752
Maltose	0.048	1.35915
Mannitol	0.026	1.3472
Sorbitol	0.0262	1.34757
Sucrose	0.05	1.35955
Trehalose	0.05	1.36034
Xylitol	0.02	1.34457

The viscosities η of 500 mM sugar solutions were inferred using 200 nm standard polystyrene (PS) particles (Bangs Laboratories Inc., Fishers, Indiana). The actual hydrodynamic radius of the particle will not change in different saccharide solutions; however, if viscosity is not entered accurately, the dynamic light scattering (DLS) instrument will output an R_h larger than the real size. The Einstein-Stokes equation relates R_h and η:

$$R_h = \frac{k_B T}{6\pi\eta D} \qquad \text{(Equation E1)}$$

where k_BT is the thermal unit and D is the mutual diffusion coefficient. Using this relation, we can determine η if we know the actual R_h and measure the spuriously high apparent hydrodynamic radius $R_{h,\,app}$.

The PS particles' R_h in buffer was determined using a Malvern Zetasizer ZS90 (Worcestershire, UK) to be 205 nm. In sucrose, for example, $R_{h,\,app}$ was 337 nm. DLS directly measures D, so this value is accurate and constant regardless of the inputted viscosity. Dividing $R_{h,\,app}$ by R_h:

$$\frac{R_{h,app}}{R_h} = \frac{\left(\frac{k_B T}{6\pi\eta_{actual} D}\right)}{\left(\frac{k_B T}{6\pi\eta_{input} D}\right)} = \frac{\eta_{input}}{\eta_{actual}} \qquad \text{(Equation E2)}$$

Using equation E2 we determined the viscosities in Table E2.

Table E5: Viscosity of 500 mM sugar solutions at 25 °C

Sugar	η **[mPa*s]**
Buffer	0.89
Glucose	1.11
Maltose	1.46
Mannitol	1.19
Sorbitol	1.11
Sucrose	1.46
Trehalose	1.58
Xylitol	1.06

VITA

JONATHAN RUBIN

Shimon Rubin immigrated to the United States from Israel in the mid 1970's to pursue a degree in Electric Engineering at West Virginia University. Soon after matriculating, Yehudit Rubin joined her husband in the United States and settled in Philadelphia, Pennsylvania. Jonathan was born in Wynnewood, Pennsylvania in 1985, the youngest of three accomplished brothers (eldest, Dr. Gabriel Rubin, professor of Justice Studies at Montclair State University, and middle brother, Ben Fox Rubin, a Dow Jones Newswire reporter). Jonathan attended private Jewish elementary school where Yehudit has taught for nearly three decades. He went on to attend Haverford Senior High School, where he graduated with honors in Social Sciences. After high school, he enrolled at McGill University (Montreal, Qc). Initially he pursued a degree in finance, but quickly found it not as challenging or alluring as the sciences. He transferred to chemical engineering and flourished. As an undergraduate researcher he worked under Drs. Viviane Yargeau and David G. Cooper from 2006-7, where he discovered his love for research. Upon graduating from McGill University in 2008, Jonathan migrated south for warmer weather and to pursue a doctorate in chemical engineering at the Georgia Institute of Technology. He joined Dr. Andreas S. Bommarius's lab in the fall of 2008. Over time, Jonathan collected additional advisors at Georgia Tech, Drs. Sven H. Behrens and Yury O. Chernoff. His passion for research led him to study yeast prion proteins and protein stability from a colloidal perspective. Jonathan received his doctorate on February 22, 2013. After acquiring his PhD, Jonathan moved to Athens, Georgia to work for the Department of Homeland Security and Merial Pharmaceutical.